Gesellschaft für Anlagen- und Reaktorsicherheit (GRS) mbH

Experimental Investigations on the Backfill Behaviour in Disposal Drifts in Rock Salt (VVS-Project)

Final Report

GRS - 173

Gesellschaft für Anlagen- und Reaktorsicherheit (GRS) mbH

Experimental Investigations on the Backfill Behaviour in Disposal Drifts in Rock Salt (VVS-Project)

Final Report

Johannes Droste
Hans-Karl Feddersen
Tilmann Rothfuchs

With contributions of
C. Lerch (DBE)

März 2001

Anmerkung:

Die diesem Bericht zugrundeliegenden Arbeiten wurden mit Mitteln des Bundesministeriums für Wirtschaft und Technologie (BMWi) unter dem Förderkennzeichen 02 E 8805 1 gefördert.

Die Arbeiten wurden von der Gesellschaft für Anlagen- und Reaktorsicherheit (GRS) mbH durchgeführt.

Die Verantwortung für den Inhalt dieser Veröffentlichung liegt allein bei den Autoren.

GRS – 173
ISBN 3-931995-40-2

Deskriptoren:
Endlager, Hochaktiver Abfall, Langzeitsicherheit, Salz, Technische Barriere, Thermomechanik

Foreword

In the Federal Republic of Germany, two emplacement concepts have been developed for the disposal of heat generating waste from nuclear power plants. The drift emplacement concept comprises the direct disposal of spent fuel assemblies by packaging the fuel rods in self shielding Pollux casks which are emplaced in the drifts of a repository in rock salt. The remaining volume of the drifts will be backfilled with crushed salt immediately after the emplacement of the casks. The borehole emplacement concept provides the disposal of vitrified high-level waste in canisters which are stacked in vertical boreholes beneath repository drifts. The upper part of the boreholes and the annulus around the canisters will be backfilled with crushed salt.

The "Thermal Simulation of Drift Emplacement" (TSDE) large-scale test was performed in the Asse salt mine to demonstrate the technology of drift emplacement and to study the thermomechanical effects of the direct disposal of spent fuel. The test was carried out by the Forschungszentrum Karlsruhe GmbH (FZK), the Gesellschaft für Anlagen- und Reaktorsicherheit (GRS) - Repository Safety Research Division, the Bundesanstalt für Geowissenschaften und Rohstoffe (BGR), and the Deutsche Gesellschaft zum Bau und Betrieb von Endlagern für Abfallstoffe (DBE).

The work was funded by the Bundesministerium für Bildung, Wissenschaft, Forschung und Technologie (BMBF) of the Federal Republic of Germany. The test was started in 1985 within the framework of the R&D-programme “Direct Disposal of LWR-Fuel Elements” which ended in December 1995. Since 1996, the GRS work in the TSDE project was continued under the contract number 02-E-8805-1. From August 1994 until April 1995, the investigations on backfill compaction and gas release were funded by the European Commission under contract number FI2W-CT94-0127. From January 1996 to December 1998, the project was funded by the European Commission as part of the BAMBUS (“Backfill and Material Behaviour in Underground Salt Repositories”) project under the contract number FI4W-CT95-0009.

Planning and test performance of the TSDE project were divided in several tasks comprising project co-ordination, in-situ investigations, laboratory experiments, and model calculations. Within the framework of the project, the partners realized different tasks. Project co-ordination was done by the FZK – Projektträger für Entsorgung (FZK-PTE), since January 1, 2000, Projektträger für Wassertechnologie und Entsorgung (FZK-PtWT+E). In the preliminary phase of the in-situ experiment, DBE was

responsible for heater cask emplacement and backfilling. Test field instrumentation was carried out by BGR and the GSF - Forschungszentrum für Umwelt und Gesundheit GmbH - Institut für Tieflagerung (IfT) which was taken over by GRS in July 1995. During the in-situ experiment, GRS (until June 30, 1995: GSF-IfT) was responsible for test operation and most geotechnical in-situ measurements while main topic of BGR in-situ investigations were stress measurements. During the heating phase, DBE was subcontractor of GRS and responsible for the heater operation and the testing of measuring techniques for a final repository.

Laboratory investigations on crushed salt material were carried out by BGR, FZK-INE and GRS. Numerical calculations were performed by BGR, FZK-INE, GRS (with DBE as subcontractor), ENRESA-CIMNE / Spain, G.3S / France and NRG / Netherlands within the framework of the BAMBUS project.

This report presents the in situ measurement results of the final heating phase and the cool-down phase obtained by GRS during the last project period from January 1996 until March 2000. For comprehension reasons, it was indispensable to summarize also the results obtained over the whole project since the beginnings in 1985. A detailed description of the in-situ investigations until 1995 is given in the report:

GRS-127 The TSS Project: Thermal Simulation of Drift Emplacement, Final Report Phase 2.

Table of Contents

1 Introduction

In a repository in rock salt, waste isolation from the biosphere is provided by a multi-barrier system which comprises technical barriers like canisters, backfill, and seals, and natural barriers like the host rock.

As the host rock is the most important barrier, the thermomechanical effects of heat generation on the host rock are of primary importance for the long-term safety of a repository. In rock salt, all excavations respond initially by elastic deformation due to stress redistribution, and subsequently by inelastic deformation due to deviatoric stresses. Because of this time-dependent rheologic behaviour, which is called creep, the surrounding rock mass moves slowly into the openings. As a result of heat input, the creep deformations of rock salt are accelerated leading to a faster closure of excavations. However, accelerated deformations may increase the permeability of the host rock by fracturing. To avoid fracture development and to support the host rock around excavations, repository drifts and boreholes will be backfilled as soon as possible.

In the multi-barrier concept, the backfill is an important component because of its supporting and sealing functions, but also due to its ability to conduct the decay heat from the waste into the host rock. Crushed salt, which is directly available from excavation activities, has been selected as the most suitable backfill material for a repository in rock salt because of its similar behaviour to the surrounding host rock.

In the beginning, the sealing capacity of crushed salt backfill is low even if it contributes to the retention of radionuclides. The required compaction of the backfill is achieved by the gradual closure of the backfilled drifts which is accelerated by the heat input from the radioactive waste. By this process, the porosity and permeability of the backfill are decreased continuously to very small values almost equal to solid rock salt. Finally, the compaction process terminates in the complete sealing of the waste canisters in the host rock. According to present planning, crushed salt as received by drift excavation, which is a coarsely grained material with a maximum grain size of 60 mm, will be used as backfill material in emplacement drifts.

In the past, the behaviour of crushed salt was investigated mainly by laboratory studies to obtain specific material parameter values required for the development of constitutive material models. Most investigations focused on the compaction behaviour,

but permeability and thermal properties were studied, too /STÜ 95/, /KOR 96/. Basing on different laboratory results, several constitutive models were developed to predict the thermomechanical behaviour of the backfill /SPI 88/, /HEI 91/, /OLI 93/, /ZHA 93/, /CAL 95/. However, comparison between numerical predictions and experimental results indicated the requirement of further studies.

Due to the limited experimental dimensions in the laboratory, a smaller grain size was used for the investigated crushed salt material being not directly representative for the coarse grained backfill material in a repository. Furthermore, only single processes were studied as the coupling of several processes is difficult in small-scale laboratory tests. Therefore, large-scale in-situ experiments were started in the early 1990s to investigate the behaviour of representative crushed salt backfill under complex full-scale repository conditions, i.e., with regard to the effects of heat input, rock stress, backfill compaction, and room closure. These studies aimed at the confirmation and further refinement of the existing codes for predicting the thermomechanical performance of backfill and host rock in a repository in rock salt. The in-situ investigations were backed by laboratory experiments. In the GRS laboratory in Braunschweig, a comparatively large triaxial compression cell was used for this purpose.

The "Thermal Simulation of Drift Emplacement" (TSDE) test was the first large-scale in-situ experiment which investigated the safety of drift emplacement by studying the behaviour of backfill material and surrounding rock salt under heat and pressure. Heating was started on September 25, 1990 and terminated on February 1, 1999. After switching-off the heaters, the in-situ investigations were continued in the cool-down phase. In a post-test investigation phase following from August 2000 until April 2003, one test drift will be uncovered to perform a validation programme of the data obtained during the in-situ experiment. Backfill removal and post-test investigations will be part of the project BAMBUS II.

The final years of the heating phase of the TSDE test were included in the BAMBUS project in which for the first time full-scale in-situ experiments were combined with laboratory tests and modelling studies /BEC 99/. The modelling studies comprised a benchmarking exercise "Comparative Study on Crushed Salt" $(CS)^2$ which was conducted to assess and refine the predictive capability of different numerical models by comparing calculation results with the data obtained from laboratory and in-situ experiments.

A fundamental subject in the safety assessment of a final repository are gases that are generated by corrosion of the waste canisters and by thermal and radiolytical decomposition of backfill and host rock. The most important gas component is hydrogen generated by the corrosive reaction of water with the cask material. Corrosion of canisters and waste matrix may release radionuclides. Gas production can result in a significant increase in gas pressure after the sealing of the repository. Increasing compaction of the backfill may cause an increase in gas pressure, too. Furthermore, the generation of inflammable gas mixtures has to be taken into account.

Investigations on gas generation and transport in a repository in rock salt have been performed both in situ and in the laboratory. The state of knowledge was presented at a GRS-Workshop in May 1996 /MLY 97/.

In the TSDE experiment, gas measurements were carried out to determine the chemical conditions around the heater casks where corrosion samples had been installed. The gas release from the backfill was determined by measuring gas concentrations and gas diffusivity in the backfill pore space. Furthermore, the water content in the backfill was determined by humidity measurements.

2 Objectives

The TSDE project was performed to demonstrate the feasibility of drift emplacement and to provide the data base for repository performance assessments. The project comprised in-situ investigations, laboratory experiments, and model calculations. The in-situ experiment was carried out under conditions almost representative for a repository for heat generating radioactive waste in rock salt.

The work of GRS focused on in-situ measurements of the thermomechanical effects of drift emplacement. During the heating phase, the main objectives of the investigation programme of GRS were the following:

- Study of thermomechanical processes in backfilled emplacement drifts and in the surrounding host rock.
- Study of backfill compaction behaviour in emplacement drifts.
- Study of interactions between backfill and surrounding rock salt.
- Providing data for the confirmation of thermal and thermomechanical computer codes.
- Study of water and gas release from the backfill material due to heating.
- Testing of measuring techniques for the safety monitoring of a repository.
- Numerical calculations and laboratory experiments on crushed salt behaviour.

In the cool-down phase, the geotechnical in-situ measurements of GRS were continued with the following objectives:

- Study of cooling effects on the backfill and the surrounding host rock.
- Determination of actual temperature and stress values being important parameters for laboratory investigations on backfill samples under in-situ conditions in the post-heating investigation programme.

- Determination of extent and permeability of the excavation disturbed zone around the test drifts at the end of the heating phase.

- Determination of volatile organic compounds which were released from the installations by heating and might affect working conditions during the drift excavation.

3 Test Design

3.1 Test Field

The TSDE test field is located in the Asse salt mine in the north-eastern part of the anticlinal core of the salt dome (Fig. 3.1). On the 800-m level, the test field was excavated inside the undisturbed Staßfurt Halite (Na2ß) of the Zechstein Series which is dipping to the north-east in this part of the anticline. The Staßfurt Halite is built by a monotonous series of alternating halite (NaCl) and sulphate layers. The thin sulphate intercalations are mainly composed of anhydrite ($CaSO_4$) and polyhalite ($K_2SO_4 \cdot MgSO_4 \cdot 2CaSO_4 \cdot 2H_2O$).

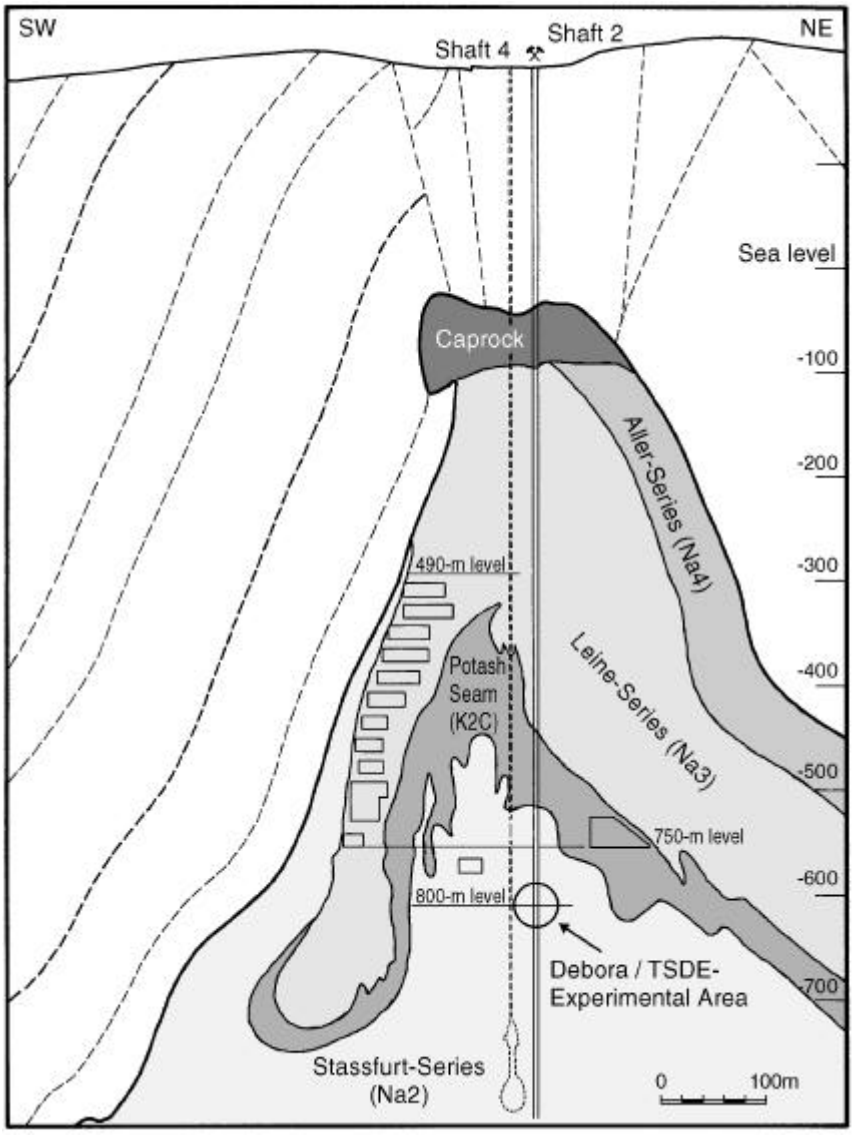

Fig. 3.1 Cross section of the Asse salt mine

On the 800-m level of the Asse salt mine, several in-situ experiments were carried out in a part of the salt anticline which had not been significantly disturbed by former mining activities. The different test fields on the 800-m level are shown in Figure 3.2.

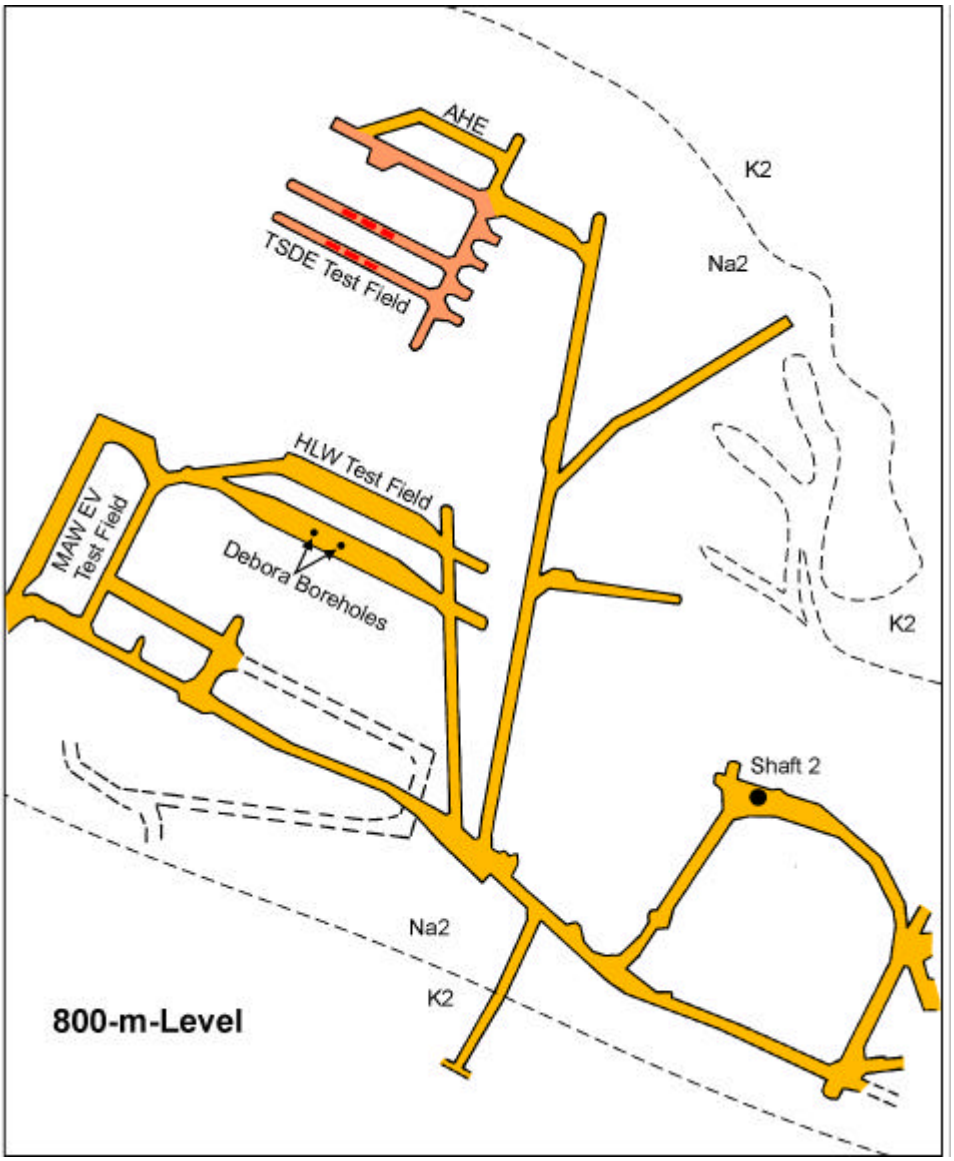

Fig. 3.2 General plan of the 800-m level in the Asse salt mine: location of the TSDE test field and other test field areas

The TSDE test field was designed to simulate reference repository conditions for spent fuel. A general view of the entire test field is given in Figure 3.3. Two parallel test drifts were excavated on the 800-m level. The test drifts were 70 m long, 3.5 m high, and 4.5 m wide, and separated by a 10 m wide pillar. In each test drift, three electrically heated casks were deposited.

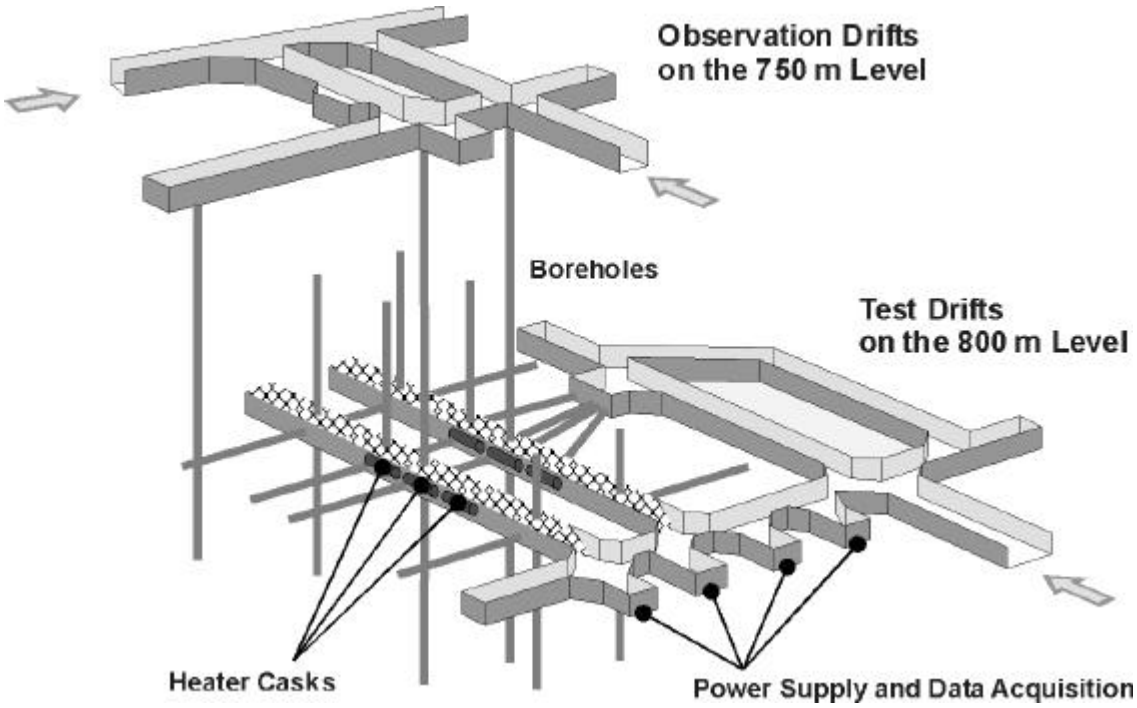

Fig. 3.3 General view of the TSDE test field

The layout of the heater casks was based on the data of a POLLUX cask for 8 PWR fuel elements and on the test boundary conditions as follows:

- Length: 5.50 m
- Outside diameter: 1.542 m
- Total weight: 65 t
- Maximum thermal power per heater: 10 kW, 100 % adjustable
- Design service power per heater: 6.4 kW
- Heater lifetime: 60,000 h at full load (design basis)
- Redundancy: in duplicate including all cables for energy supply and the heater control system
- Cask and lining strength: against 18 MPa rock pressure
- Distance between the casks: 3 m

Each heater cask consisted of seven bolted ring-shaped segments and contained two electric heaters (Fig. 3.4). For redundancy reasons, each electric heater contained three heating circuits (4 kW power per heating circuit) with separate conductor to the

heater control system. In case of interruption, the heater control system switched over to the next heating circuit. The heater cask layout provided the requested heat power of 6.4 kW per cask with a safety factor 2.

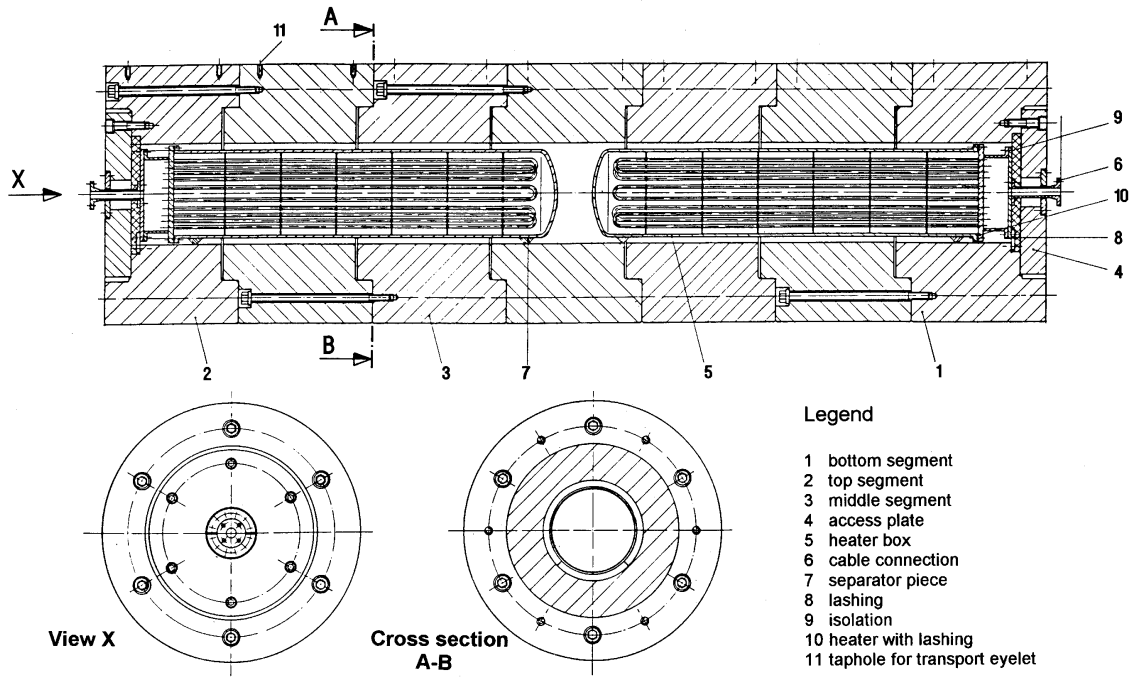

Fig. 3.4 Schematic view of a heater cask

In addition to the two test drifts, the test field included several observation and access drifts on the 800-m level and on the 750-m level (Fig. 3.3). Measuring niches along the observation and access drifts contained the power supply and the data acquisition systems.

A large number of boreholes had been drilled from the observation drifts into the vicinity of the test drifts and from the test drifts into the surrounding rock salt. In total, more than 200 boreholes had been realized. The total length of all boreholes was approximately 2700 m. The boreholes were equipped with various measuring gauges to determine the thermomechanical reactions of the rock. Other devices had been installed in the backfill and at the surface of the heater casks.

The measuring instruments were installed in selected monitoring cross sections (Fig. 3.5). Most cross sections were located in the heated area around the casks and between the casks (sections A, B, C, D, F, G, H, I, J, and K). Additional cross sections

(E1, E2, and L1) were located in the non-heated regions farther away from the casks. Additional indices, like $D1^{-1}$ or $E1^{+1}$, specify the distance of a measuring section from the respective cross section with the index numbers indicating the distance in meters. Plus index gives the distance in western direction, and minus index the distance in eastern direction.

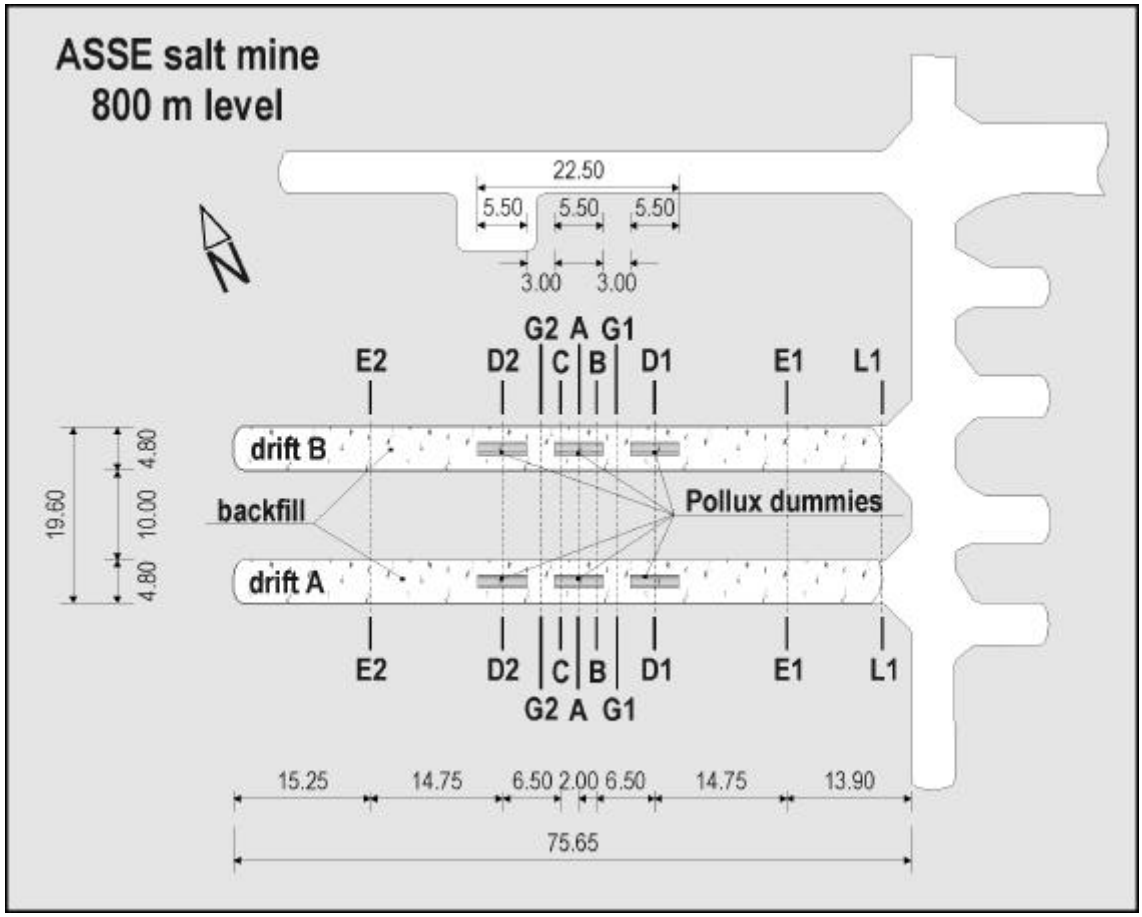

Fig. 3.5 Test drifts on the 800-m level with monitoring cross sections

After the installation of the heaters and the measuring equipment, the test drifts were backfilled in slinger technique with crushed salt material /TEST 93/. The crushed salt used for the backfilling was derived from the excavation of the test drifts by means of a continuous miner. The oversized grain fraction was removed by sieving, leaving crushed salt material with a grain size of less than 45 mm. This backfill material was re-emplaced in the test drifts using a slinger truck. From the total mass of crushed salt material emplaced and the test drift volume, an initial backfill porosity of about 35 % was determined, corresponding to an initial density of 1400 kg/m^3.

3.2 Investigation Programme

The geotechnical investigation programme involved temperature, deformation, and stress measurements.

Temperatures were recorded by nearly 800 resistance thermometers at the surface of the heater casks, in the backfill, and in the surrounding rock salt. The sensors consisted of a temperature dependent platinum resistor PT 100 with a nominal resistance of 100 Ohms (Ω) at a temperature of 0°C. In order to compensate temperature influences on the cable resistance, the sensors were fabricated in four-wire technique. The sensor measuring range was from 0°C to +250°C for type I used in the heated area and from 0°C to +80°C for type II used in the non-heated area. The maximum measuring uncertainty was ± 0.01°C at 0°C, ± 0.07°C (type I) and ± 0.05°C (type II) at 100°C, and ± 0.15°C (type I) and ± 0.07°C (type II) at 250°C.

In order to determine backfill compaction, both drift closure and backfill settling were measured by means of stationary measuring equipments which had been specially designed for the TSDE test.

Horizontal and vertical convergence measurements were carried out both in the heated zone (cross sections B^{+1}, $D1^{-1}$, G1, and G2) and in the non-heated area (sections $E1^{-1}$ and E2). Each device was fixed to the rock and consisted of a displacement transducer and a measuring rod for transmitting the rock deformation to the displacement transducer. The maximum measuring range of the measuring devices was 400 mm at temperatures up to 200°C. Displacement transducers and measuring rods were protected against mechanical impact by telescopic steel tubes. Additionally, drift closure of the observation drifts on the 750-m level was recorded manually in section D1 and D2, and automatically by permanent devices in section D1 in the southern drift and section D2 in the northern drift.

Backfill settling was monitored by equipments which were installed in the heated sections B^{+1}, $D1^{-1}$, and $G2^{+}$, and in the non-heated sections $E1^{+1}$ and $E2^{-1}$ (Fig. 3.5). With each equipment, the settling was measured at three levels. At each level, a measuring rod was coupled to a metal plate at a telescopic steel tube. The distance between each plate and the roof was monitored by an electric transducer. Generally, one gauge was installed at the floor to measure the drift convergence, another one in the middle of the backfill, and the uppermost one on the top of the backfill to monitor the opening and

closing of the gap between drift roof and backfill. This gap results from the primary settling of the backfill due to gravity. In the cross sections $G2^{+}$ and $E1^{+1}$, where separate convergence measurements were carried out, two gauges were installed in the lower and upper third of the backfill in order to determine the vertical distribution of backfill settling.

Rock deformations around the test drifts were recorded by extensometer and inclinometer measurements in boreholes registrating the axial and radial borehole displacements, respectively.

Axial borehole displacements were monitored by multiple point glass fibre rod extensometers which were installed in the sections A and D1 in the heated area and in the non-heated sections E1 and E2 (Fig. 3.5). Boreholes in the floor, in the walls, in the pillar, and in the roof of the test drifts were equipped with a set of four extensometers each. From the observation drifts on the 750-m level, further extensometers had been installed in the pillar and above the test drifts. The accuracy of the measuring system depended on the extensometers' length. According to the manufacturer, the accuracy was 0.02 mm up to a length of 20 m, 0.1 mm up to 50 m length, and 0.3 mm up to a length of 100 m.

In section A^{+1}, the rock deformations were additionally recorded by inclinometer measurements. From the 750-m level, five boreholes had been equipped with access guide tubes. Two boreholes ended above the test drifts, and the other ones were located in the pillar and beside the test drifts. Since December 1988, displacements perpendicular to the borehole axis were measured regularly with a mobile inclinometer probe, the resolution of which was 0.02 mm per meter measuring depth. The accuracy of the whole inclinometer measuring system was 0.1 mm per meter measuring depth.

Hydraulic Glötzl type pressure cells were used to measure the pressure between backfill and surrounding rock. The pressure cells were installed at the floor, at the roof, and at the walls of the test drifts. Measurements were carried out in the heated sections B, D1, D2, and G1 as well as in the non-heated section E1 (Fig. 3.5). The accuracy of the pressure cells was ± 0.02 MPa.

To observe long-term stress changes in the host rock induced by drift excavation and by heating, more than fifty stress monitoring probes were installed in a number of boreholes. Most probes were operated by BGR. Additional measurements were carried

out by GRS in cross section B. From the observation drifts on the 750-m level, two boreholes ending above the test drifts and three boreholes extending into the pillar were equipped with monitoring probes. Two additional boreholes were located below each test drift. The probes consisted of seven Glötzl type hydraulic pressure cells which had various orientations for measuring the vertical component, three horizontal components perpendicular, parallel, and at an angle of 45° to the drift axis, and two subvertical components with an incline of 45° perpendicular and parallel to the drift axis. The accuracy of the pressure cells was ± 0.02 MPa. In 1995, almost all gauges had failed, but were replaced by probes of the same type in July 1995. According to the most frequent probe configuration of BGR, four-component probes were used for these replacements in section B^{+1} measuring the vertical component, two horizontal components perpendicular and parallel to the drift axis, and a subvertical component with an incline of 45°.

For gas measurements, 24 glass filters were attached to the surface of the central casks and to the drift roof above these casks in zones with different temperatures. In the northern drift, four additional glass filters were installed at the floor next to the central cask. From the glass filters, gas samples were taken periodically via Teflon tubes and analyzed by gas chromatography.

All measuring lines in the heated area were designed for a maximum temperature of 200°C. From the gauges in the boreholes and in the backfill, the measuring lines were led into slots around the drift walls which were subsequently filled with insulating material and protected with metal plates against mechanical damages during backfilling. Close to the roof, the cable slots led into a cable duct which was also protected by metal plates. Via this cable duct, the cables were led to the drift entrance and to the data acquisition systems in the measuring niches.

3.3 Data Acquisition

The data acquisition in the TSDE test was carried out by local front end processors which were operating independently. The measurements around the test drifts and from the observation drifts were registrated by two units on each level with one unit (FEP) recording the electrical readings and the other one (MFA) the hydraulic measurements (Fig. 3.6). Generally, the measuring sensors were scanned every twelve hours.

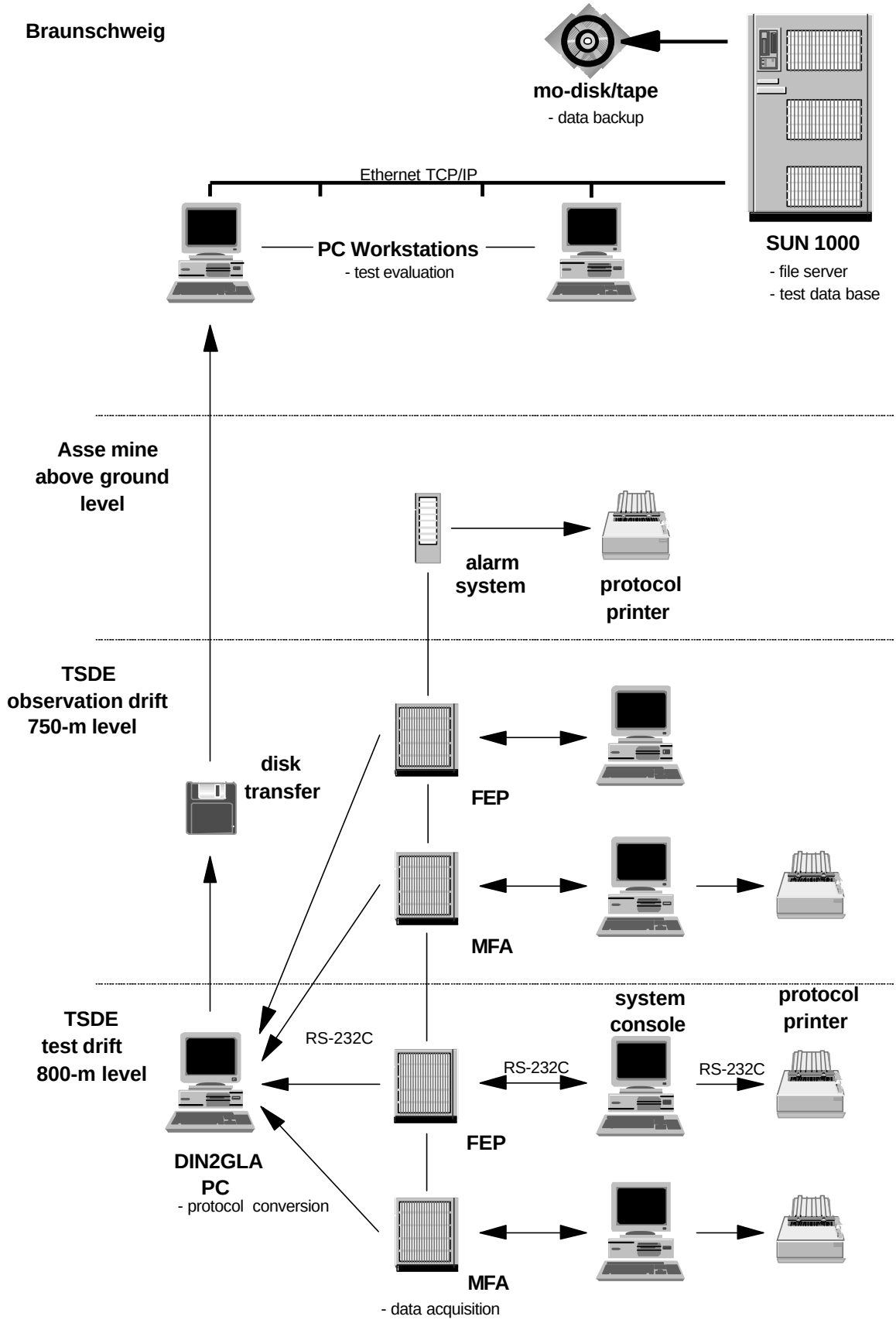

Fig. 3.6 Synoptic view of the TSDE data acquisition system

A central PC (DIN2GLA-PC) was installed on the 800-m level which received the data from all front end processors via RS-232C interfaces (Fig. 3.6). The data were converted into a standardized temporary format and stored on hard disk. Once a week, the data on the DIN2GLA-PC were transferred by disk to the archiving and evaluation computer in Braunschweig. The DIN2GLA-PC operated since March 1994. The system replaced the former ERMEDA and VEMEDA program on a VAX computer which had been shut down due to a system change. In Braunschweig, an archiving of the data was carried out by a local TCP/IP network on a hard disk of the central file server SUN 1000. The hard disk was saved regularly on DAT-tapes or MO-disks (Fig. 3.6).

Different precautions had been taken against loss of data and unauthorized access. Additionally, an alarm system was registrating different fault messages in the test field. The coded fault messages were transmitted above ground to the service facilities where they were shown on a display and recorded as print-out.

Further details of the data acquisition system are described in /DRO 96/.

4 Project Performance

Planning and preliminary work for the TSDE test were started in 1985. Excavation of the observation drifts on the 750-m level was done in 1987, followed by drilling and instrumentation of the measuring boreholes in 1988. Mining of the test drifts on the 800-m level was carried out in spring of 1989. Excavation effects on the surrounding rock were already recorded by the measuring devices on the 750-m level. After that, drilling of the boreholes and instrumentation of drifts and boreholes took place as well as emplacement of the dummy casks, step by step walking along with the backfilling of the drifts. With the whole measuring equipment being connected to the data acquisition system, the test field was ready for operation in August 1990.

Heating started on September 25, 1990. Since then, the heater casks were operated with a thermal power output of 6.4 kW each. The total power output in each drift was about 19.2 kW (Fig. 4.1). The electrical heaters operated satisfactorily for more than 73,000 hours until the end of the heating phase on February 1, 1999. Several short interruptions had no significant impact on the thermomechanical behaviour of rock and backfill. No heating circuits failed although their designed lifetime was exceeded by over 20 %. None of the redundant second heating circuits had to be used. Without exception, the observed interruptions were caused by overvoltages.

In March 1993, a continuous registration of the thermal power output was installed allowing the continuous monitoring of the total sum of power output. For each test drift, the percentage of deviation of the recorded power output from the design value of 19.2 kW is shown in Figure 4.2.

In 1994, problems at the heater control system caused a higher thermal power output resulting in temporarily increasing temperatures in the heated area /DRO 96/. The deviation from the design value of 19.2 kW reached up to 18 % (Fig. 4.2). After the replacement of several electronic components, the designed power output was achieved again. In November 1995, a renovation of the whole heater control system was carried out. The problematical power controllers and signal converters were completely replaced by solid-state relays and different signal converters. The analog setpoint potentiometers were substituted by a digital preset. The improved system operated with higher precision.

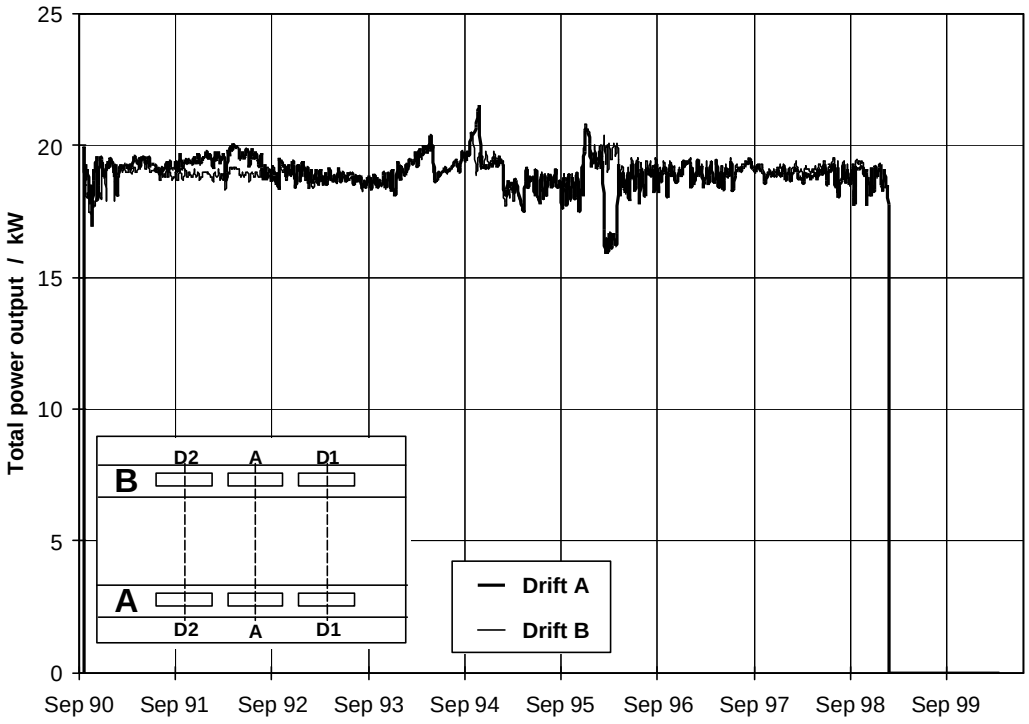

Fig. 4.1 Thermal power output in each test drift

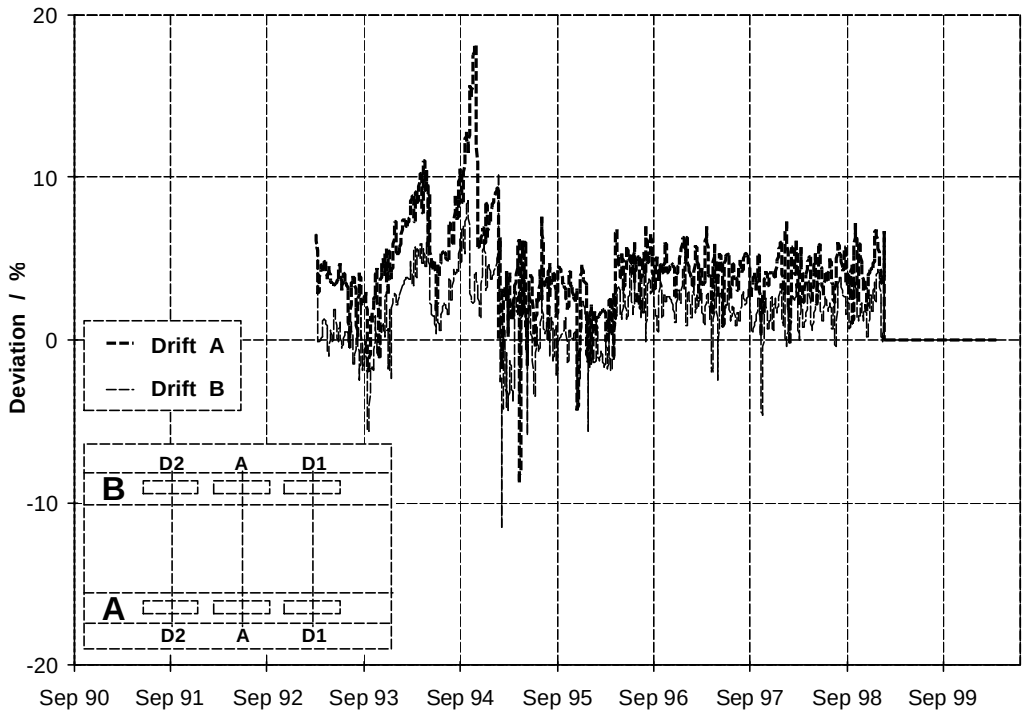

Fig. 4.2 Percentage of deviation of the thermal power output from the design value of 19.2 kW in each test drift

On February 1, 1999, the heating phase was terminated by switching-off the heaters. In the following cool-down phase, the in-situ investigations were continued until the end of March 2000. To enable post-heating studies and the performance of a validation programme, one test drift will be opened within the framework of the project BAMBUS II what is discussed in chapter 8.

Since the start of heating, the measuring systems in the test field were operated under conditions similar to a repository in rock salt, i.e., high temperatures, stresses, and deformations. Due to these conditions, an increasing part of the measuring equipment was damaged and failed. A detailed description of instrument performance and failure reasons will be given in chapter 8. Several replacement measures were carried out to compensate for the failed gauges. In the years 1994 and 1995, seven new boreholes in the heated area were equipped with additional extensometers. In July 1995, five boreholes were drilled from the observation drifts on the 750-m level to replace the failed stress monitoring probes of GRS. Finally, four failed convergence measuring gauges in horizontal direction were replaced in the heated area in the end of 1996.

5 In-situ Investigations

5.1 Temperature

Prior to heating, the ambient temperature in the test drifts on the 800-m level and in the surrounding rock salt was about 36°C. After the start of heating on September 25, 1990, the temperatures in the heated area increased rapidly.

5.1.1 Backfill Temperature

The temperature development in the backfill is shown in Figures 5.1.1 to 5.1.4.

At the surface of the heater casks, a maximum temperature of 210°C was reached within five months (Fig. 5.1.1). Subsequently, the temperatures decreased slowly due to the increasing thermal conductivity of the compacting backfill. Temporary drops in temperature were caused by short-term interruptions in heating, but temperatures always increased again immediately. Although these heater breakdowns had no significant thermomechanical impact, short-term effects were observed in the backfill pressure development (see chapter 5.5.1). Higher temperatures at the surface of one cask in 1991 and the disturbed temperature development in 1994 were caused by troubles at the heater control system /DRO 96/. At the end of the heating phase, almost steady state temperatures between 159°C and 169°C were measured at the surface of the heater casks (Fig. 5.1.1).

In the heated backfill, the temperatures increased rapidly, too, but the temperature increase was lower. After three to five years of heating, the backfill temperatures around the heaters had reached steady state conditions (Fig. 5.1.2 and 5.1.3). Farther away from the casks, backfill temperatures increased until the end of the heating phase. When heating ended in February 1999, temperatures at the drift floor ranged between 117 - 130°C near the heaters and 91 - 102°C near the walls (Fig. 5.1.2). Temperatures at the drift walls ranged between 93 - 102°C at the pillar wall and 86 – 96°C at the opposite wall. As the pillar was being heated on both sides, pillar temperatures were always 5 – 10°C higher (Fig. 5.1.2). At the roof, temperatures of 84 – 96°C were recorded. Temperatures at different positions in the test drifts are shown in Figure 5.1.3 revealing the temperature gradient in the heated backfill with increasing distance from the heaters.

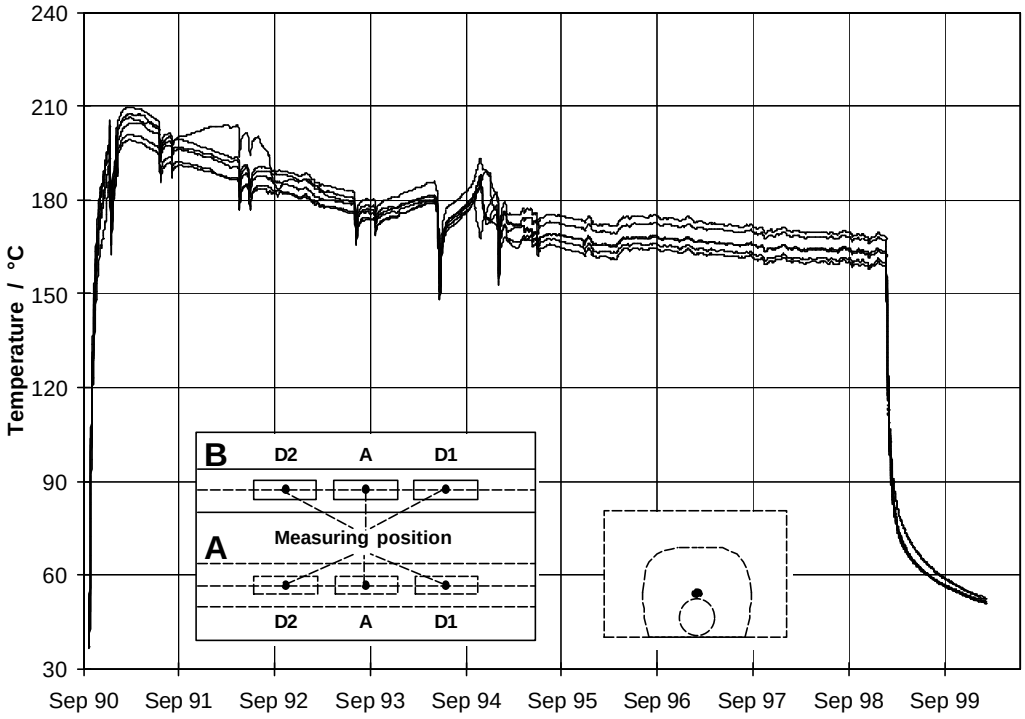

Fig. 5.1.1 Temperatures at the heater surface

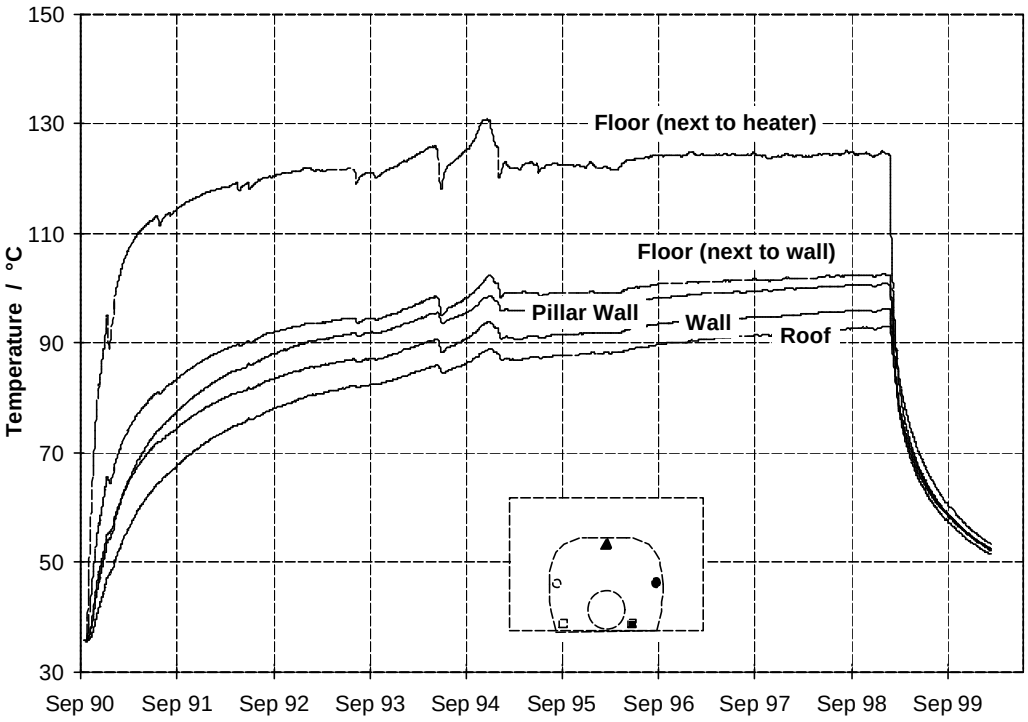

Fig. 5.1.2 Drift temperatures around a central heater (section B)

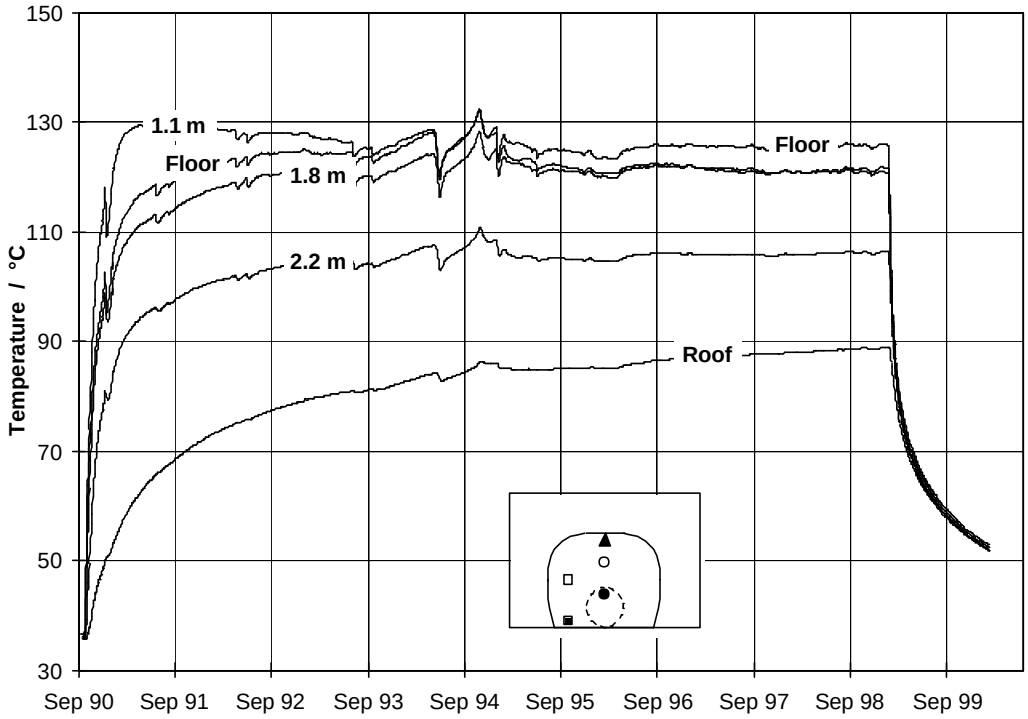

Fig. 5.1.3 Backfill temperatures around a central heater (sections B^{+1} and $G2^{+}$)

After 8.35 years, heating was terminated on February 1, 1999. After the heaters had been switched off, the temperatures in the heated area decreased rapidly (Fig. 5.1.1 to 5.1.3). Six weeks later, almost uniform temperatures of about 80°C were recorded all over the heated area. Subsequently, the temperatures decreased continuously reaching 50 – 52°C at the end of March 2000.

Warming up of areas further away from the heaters started with some delay. In the sections E1 and E2 at a distance of 12 m to the next heater cask, the temperatures began to rise about three months after the heaters had been switched on. Up to the end of the heating phase, the temperatures increased to 47 - 50°C (Fig. 5.1.4). However, the temperatures in the cold backfill had not reached a steady state when heating was terminated. After switching-off the heaters, the temperature decrease in the sections E1 and E2 started again with a delay of three months. Subsequently, the temperatures decreased continously, but less pronounced than in the heated area to 44 – 46°C at the end of March 2000 (Fig. 5.1.4).

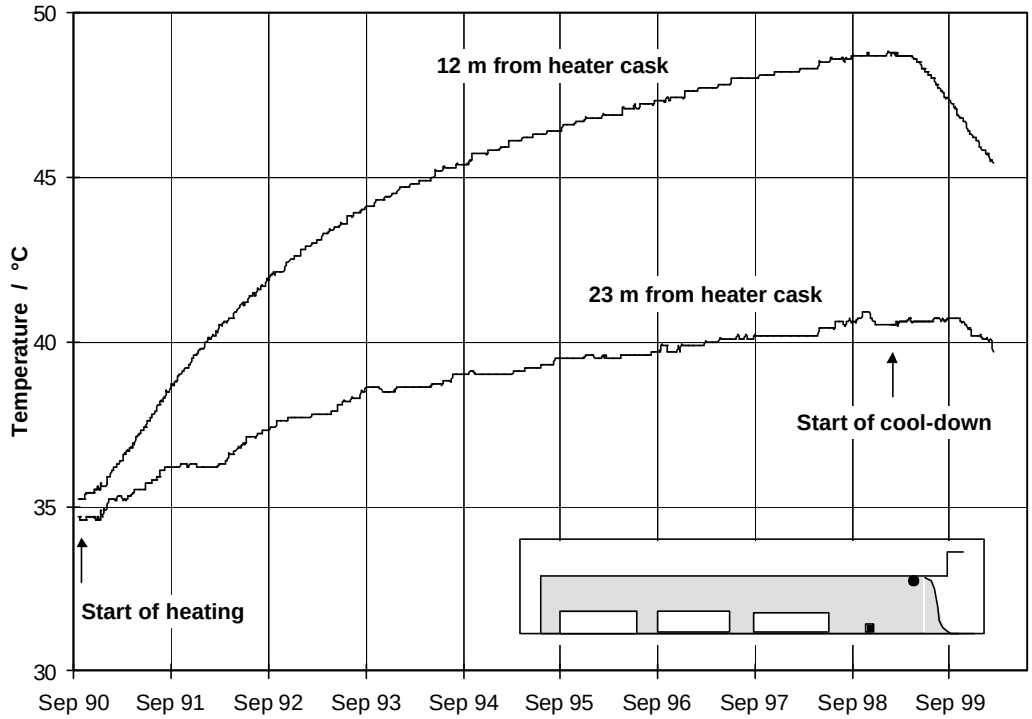

Fig. 5.1.4 Backfill temperatures in the cold area (sections $E2^{-1}$ and L1)

Far away from the heaters in section L1 at a distance of 23 m to the next cask, the temperatures increased up to 41°C until the end of the heating phase. The increase started about half a year after the beginning of heating and took a seasonal course with stagnating temperatures in winter time (Fig. 5.1.4). This phenomenon was caused by the influence of the mine ventilation, as cross section L1 was located very close to the exit of the test drifts. In the cool-down phase, no further temperature increase was observed in summer 1999, but it was not until nine months after the heaters had been switched off that temperatures decreased in section L1, too. Until the end of March 2000, the temperatures decreased slightly to 39°C (Fig. 5.1.4).

5.1.2 Rock Temperature

From the heater casks, heat was transferred to the surrounding rock salt both via the backfill and directly over the drift floor at the cask/rock-interface. The temperatures measured at various locations in the surrounding rock display the heat transfer paths (Fig. 5.1.5 to 5.1.8).

Temperatures resulting from direct heat transfer to the rock are shown in Figure 5.1.5. At the interface between cask and rock salt, the temperature increase was lower than at the cask surface, but steady state conditions were reached already one year after the start of heating indicating an equilibrium between heat generation and heat conduction. At the surface of the heater casks, however, where heat transfer took place via the backfill, an equilibrium had not been reached until several years of heating. At the end of the heating phase, the temperature difference between cask surface and cask/rock-interface was about 20°C.

Within the rock, temperatures decreased with increasing depth. The temperature development directly below the drifts was comparable to the backfill temperatures near the casks reaching steady state conditions after three to five years of heating. In greater depths, however, the temperature increase was much lower and started delayed. Moreover, these areas were hardly affected by the disturbed temperature development in 1994 /DRO 96/. Temperatures increased until the end of the heating phase without reaching an equilibrium.

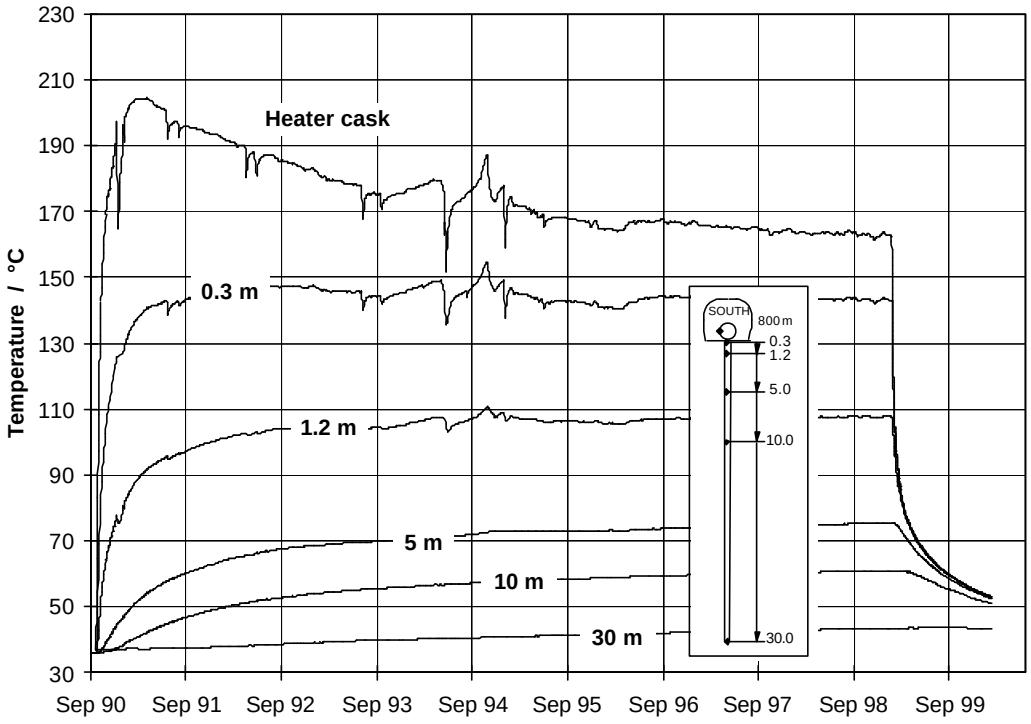

Fig. 5.1.5 Rock temperatures beneath the heated drifts (section A)

At the lowest measuring points 30 m beneath the heated drifts, the initial temperature of 37°C remained almost constant during the first year of heating. Since 1991, the temperature increased gradually up to 43°C at the end of March 2000 (Fig. 5.1.5).

Rock temperatures beside and above the heated drifts, which resulted from heat transfer through the backfill, are presented in Figures 5.1.6 to 5.1.8. In the beginning, the thermal conductivity of the backfill was low. Therefore, temperature increase started later and was lower than beneath the heated drifts. Though thermal conductivity of the backfill increased during heating, an equilibrium between heat generation and heat conduction had not been reached yet at the end of the heating phase as indicated by still increasing rock temperatures.

While a comparable temperature development was observed in the walls and above the drifts, temperatures in the pillar were higher as the pillar was being heated on both sides. In the inner part of the pillar, rock temperatures were almost identical. At the end of the heating phase, temperatures reached from 86°C in 2.5 m depth to 83°C in the pillar centre (Fig. 5.1.8). In the opposite walls, only 74°C and 64°C were recorded at the same time in corresponding depths (Fig. 5.1.7).

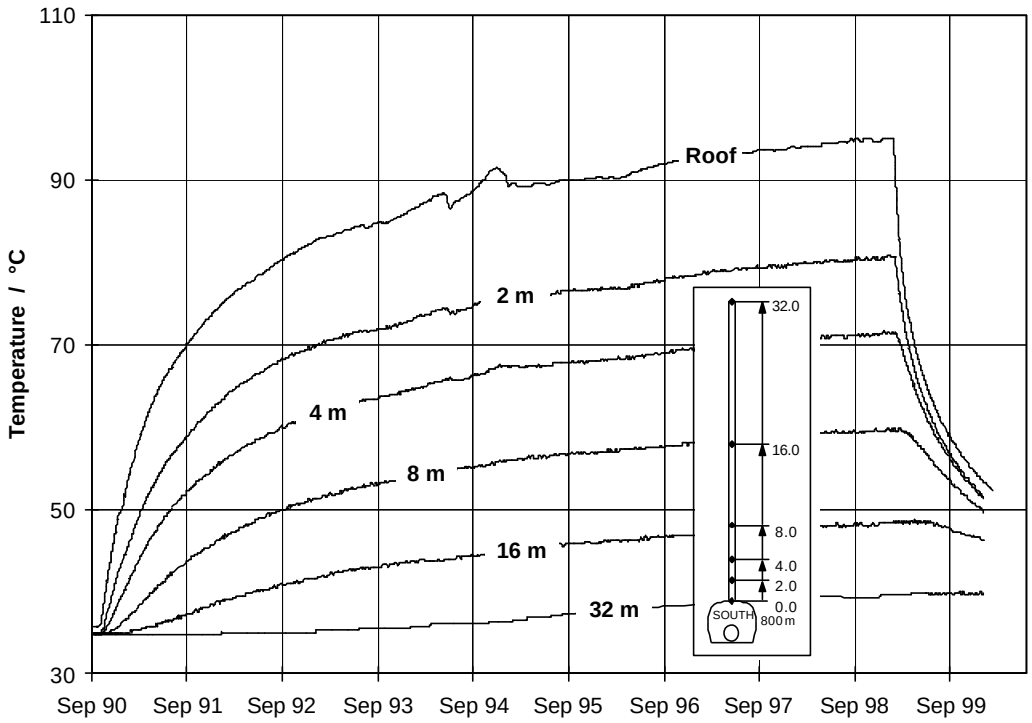

Fig. 5.1.6 Rock temperatures above the heated drifts (section A)

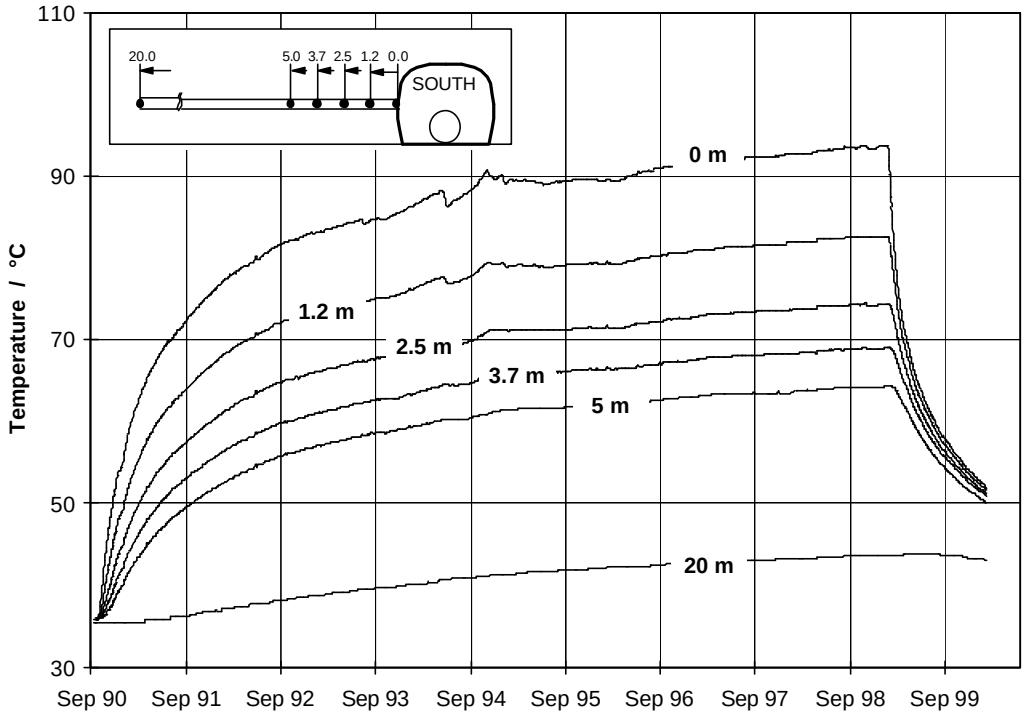

Fig. 5.1.7 Rock temperatures beside the heated drifts (section A)

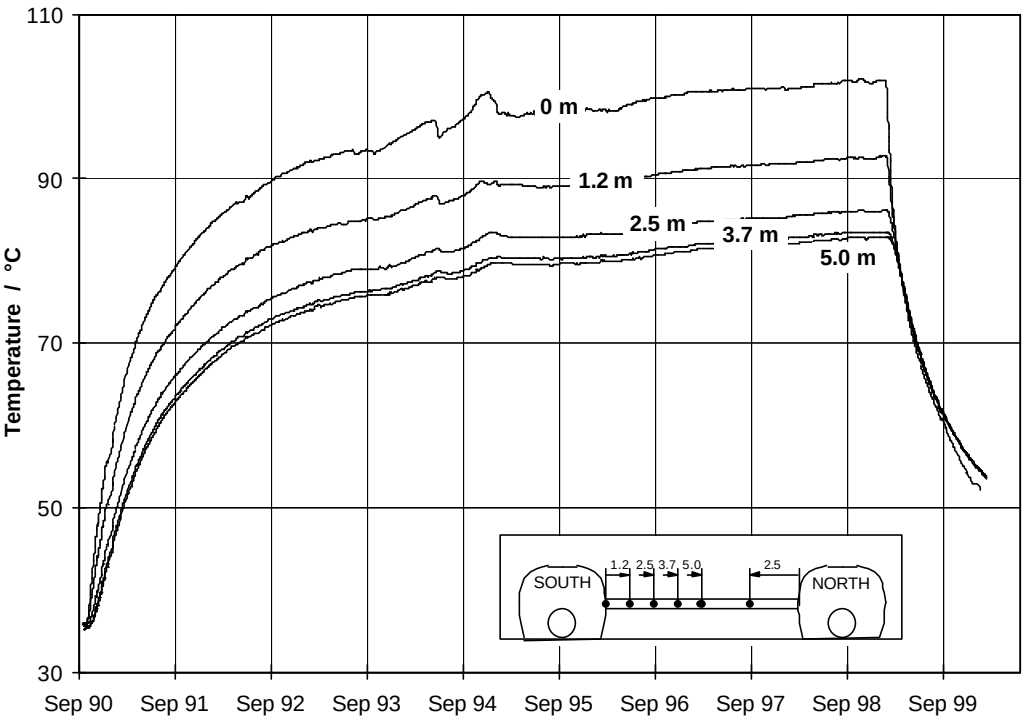

Fig. 5.1.8 Rock temperatures between the heated drifts (section A)

After heating was terminated, rock temperatures around the drifts decreased corresponding to the distance from the heater casks (Fig. 5.1.5 to 5.1.8). Up to 2.5 m beneath the drift floor and in the whole pillar, temperatures decreased immediately after the heaters had been switched off (Fig. 5.1.5 and 5.1.8). After six weeks, almost uniform temperatures of about 80°C were recorded in these areas. Above the heated drifts and in the walls, the temperature decrease started delayed, but after three months, rock temperatures up to 10 m depth decreased all over the heated area (Fig. 5.1.5 to 5.1.8). In 20 m depth, rock temperatures decreased not until half a year after the heaters had been switched off. At a distance of 30 m from the test drifts, however, the surrounding rock salt was not affected by cooling yet. At the end of March 2000, almost uniform temperatures of about 52°C were recorded in the whole pillar and up to a depth of 5 m below the drifts, and 48 – 50°C up to the same depth above the drifts and in the walls.

In the non-heated sections E1 and E2, rock temperatures took the same development in all directions. Exemplarily, the temperatures beneath the test drifts are shown in Figure 5.1.9. Steady state conditions had not been reached when heating ended.

Up to a distance of 5 m from the test drifts, temperature increase started about three months after the heaters had been switched on. Rock temperatures increased continuously up to 45 - 48°C at the end of heating. Generally, rock temperatures below the drifts were about 1– 2°C higher than beside and above the drifts. The highest values were recorded in the pillar with an uniform temperature increase all over the pillar up to 48°C at the end of heating (Fig. 5.1.10). After the heaters had been switched off, temperatures began to decrease slightly within three months. Up to the end of March 2000, temperatures decreased by 2 – 4°C to 43 – 45°C.

Farther away from the drifts, the temperature increase due to heating started later. At a distance of 10 m from the drifts, the delay was up to half a year. Temperatures of 43 - 45°C were reached until the end of heating (Fig. 5.1.9). Temperature decrease in the cool-down phase started with a delay of half a year, too, but was only 1 – 2°C until March 2000. In 20 m beneath the drifts, the first effects of heating were recorded after half a year. Temperatures increased up to 43°C until the end of the heating phase (Fig. 5.1.9). At the same distance beside and above the drifts, increasing temperatures were recorded after one year and temperatures increased up to 41°C. During the cool-down phase, the temperatures in 20 m depth kept almost constant (Fig. 5.1.9).

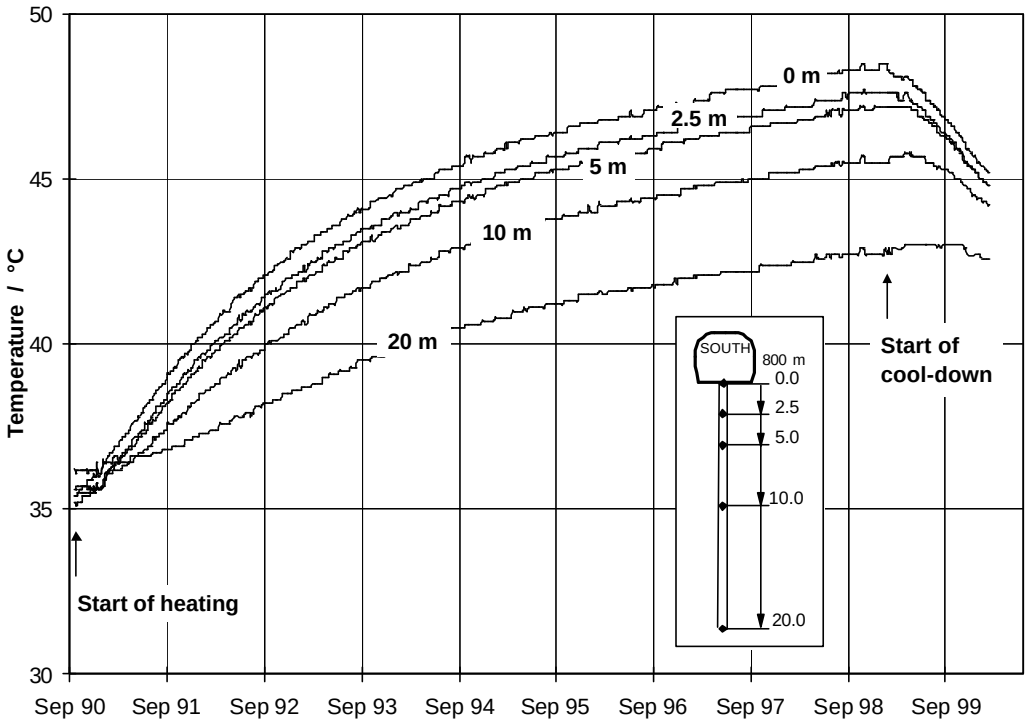

Fig. 5.1.9 Rock temperatures beneath the cold drifts (section E1)

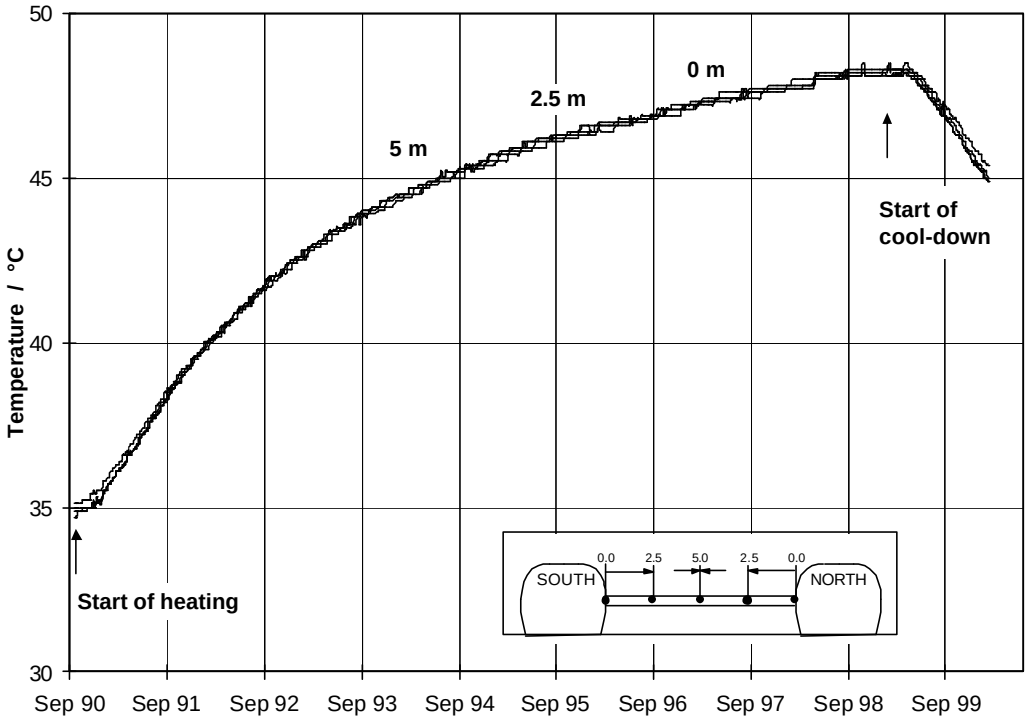

Fig. 5.1.10 Rock temperatures between the cold drifts (section E1)

5.2 Drift Closure

Drift closure measurements started immediately after test drift excavation. Prior to heating, closure rates averaged 0.25 %/a in horizontal direction and 0.3 %/a in vertical direction. The differences were mainly caused by the local stress field.

With the start of heating, the closure rates in the heated area accelerated considerably up to twelve times the amount (Fig. 5.2.1 and 5.2.2). Three months later, the rates decreased again due to the beginning support by the backfill. As a result of the higher thermal power output in 1994, drift closure remained almost constant over a year. But since 1995, closure rates were further reduced as the support by the backfill increased with its increasing density and rigidity (Fig. 5.2.2). At the end of the heating period, the rates were 0.4 %/a in horizontal direction and 0.5 %/a in vertical direction. These rates were still about one and a half times of the initial closure rates.

After the heaters were switched off, drift closure rates in the heated area decreased rapidly due to relaxation of thermally induced rock stress (see chapter 5.5.2). While closure rates in vertical direction dropped immediately, a short-term increase was observed in horizontal direction, but three months later, drift closure rates in horizontal direction decreased, too. In the end of March 2000, only 0.02 – 0.08 %/a were recorded, i.e., drift closure in the heated area had been almost stopped (Fig. 5.2.1 and 5.2.2).

In the non-heated sections, the closure rates remained unchanged at first. Three months after the start of heating, drift closure accelerated to double the amount for about two years (Fig. 5.2.1 and 5.2.2). The increase was caused by the gradual temperature increase in sections E1 and E2 starting at that time (see chapter 5.1.1). Subsequently, the rates were almost constant until the end of heating ranging between 0.25 - 0.35 %/a in horizontal direction and 0.25 - 0.55 %/a in vertical direction. These rates were nearly the initial closure rates and about two thirds of the rates observed in the heated area.

With switching-off the heaters, drift closure rates in the non-heated area accelerated temporarily by 30 – 50 % reaching up to 0.4 %/a in horizontal direction and 0.7 %/a in vertical direction (Fig. 5.2.2). The increase was a thermoelastic effect. The relaxation of thermally induced rock stress in the heated area (see chapter 5.5.2) caused an

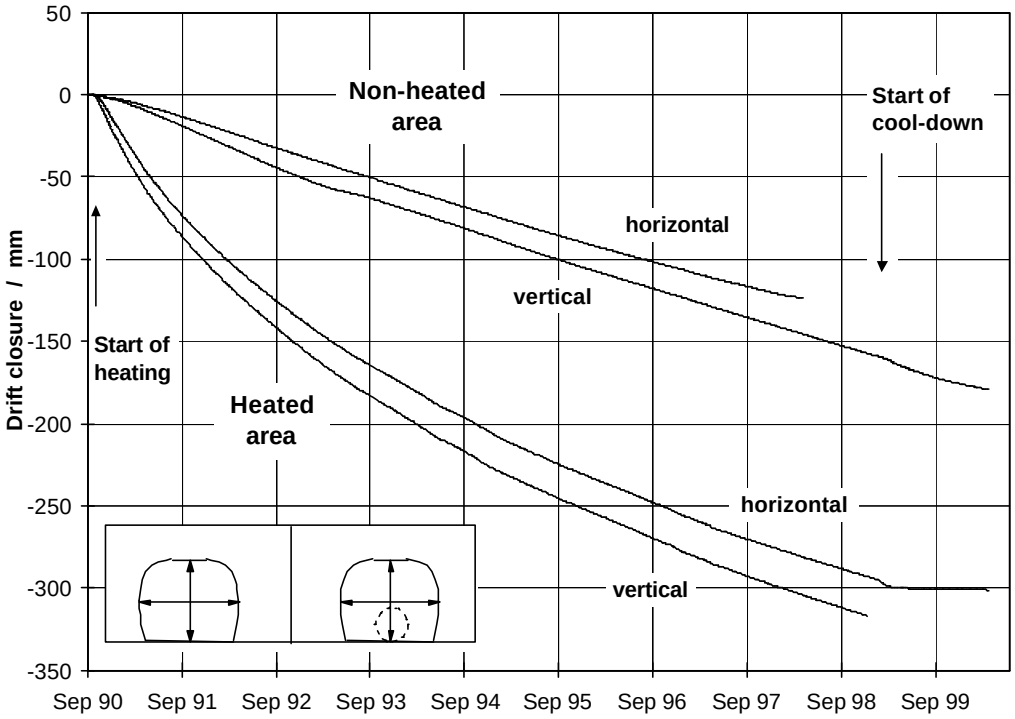

Fig. 5.2.1 Drift closure in the heated area (section G1) compared to the non-heated area (section E2)

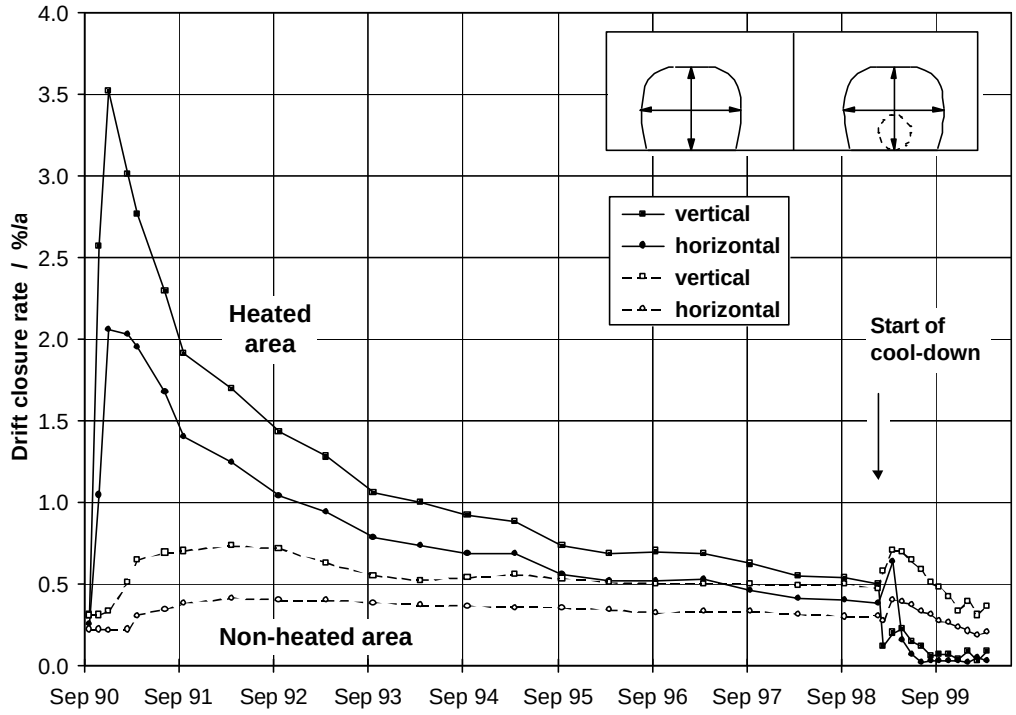

Fig. 5.2.2 Drift closure rates in the heated area (section G1) compared to the non-heated area (section E2)

immediate elastic reaction with an increase in effective rock stress in the non-heated area resulting in a temporary acceleration of drift closure. After two to three months, the drift closure rates decreased again. At the end of 1999, the initial closure rates were achieved with 0.2 %/a in horizontal direction and 0.3 %/a in vertical direction. These rates kept almost constant until the end of March 2000.

Vertical drift closure reached maximum values in the centre of the drifts. In 1 m distance from the walls, drift closure rates were lower (Fig. 5.2.3). Due to higher rock temperatures in the pillar, drift closure rates were always higher on the pillar side as compared with the opposite wall (Fig. 5.2.3). In the heated section G2, the difference was 5 - 10 %, and even 10 - 15 % were observed in the non-heated section $E1^{-1}$.

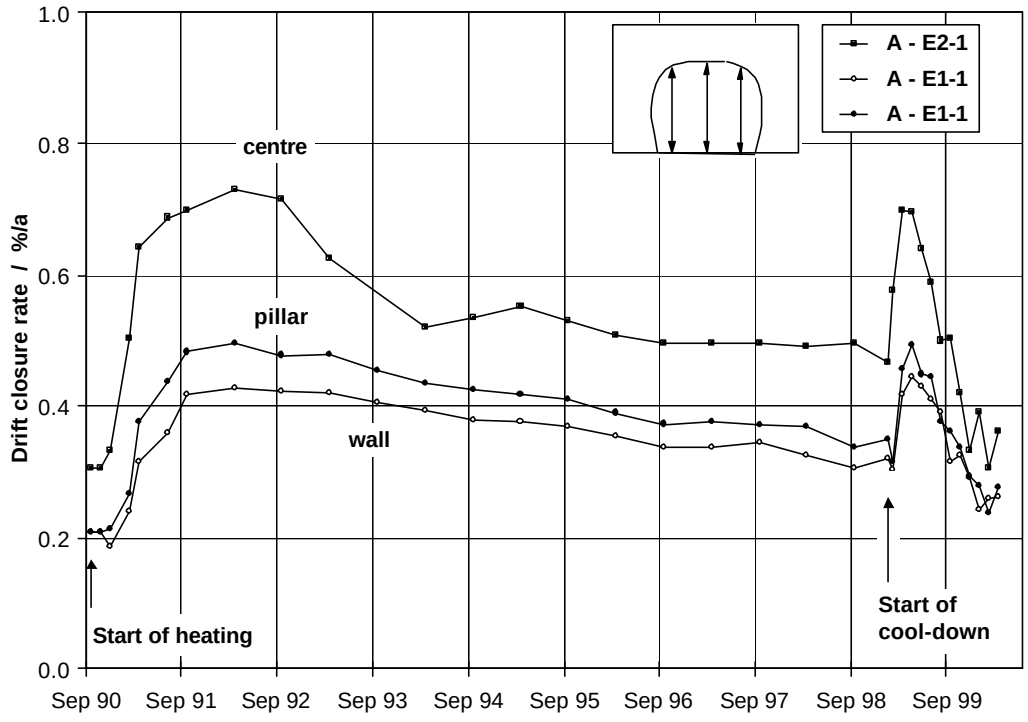

Fig. 5.2.3 Vertical drift closure rates in the non-heated area (sections $E1^{-1}$ and $E2^{-1}$)

Generally, drift closure rates in the southern drift were higher than in the northern drift. In the heated area, a difference of up to 10 % was recorded after the start of heating, but after two years, the rates in both drifts were approximately the same. In the non-heated area, however, differences of up to 20 % were observed during the whole experiment. The reasons are not understood yet, but may be identified during post-test drift excavation.

Drift closure measurements in the observation drifts on the 750-m level started already in 1987 in cross sections D1 and D2 /DRO 96/. Two years after drift excavation, nearly constant closure rates of 0.07 – 0.1 %/a in horizontal direction and 0.1 – 0.14 %/a in vertical direction were reached (Fig. 5.2.4). Some higher values were recorded in section D2 of the southern drift due to a measuring niche close by. These closure rates kept unchanged during the first years of heating.

Four years after the heaters had been switched on, drift closure in the observation drifts was affected by heating, too. Drift closure rates were accelerated by 20 – 35% reaching 0.11 – 0.13 %/a in horizontal direction and 0.13 – 0.16 %/a in vertical direction (Fig. 5.2.4). One year later, the rates decreased again to the previous values which were almost the same until the end of the heating period. With switching-off the heaters, vertical closure rates dropped immediately by 50 % to 0.05 – 0.08 %/a due to thermal stress relaxation in the host rock below. Horizontal drift closure rates, however, were less concerned and decreased slowly to 0.05 %/a (Fig. 5.2.4).

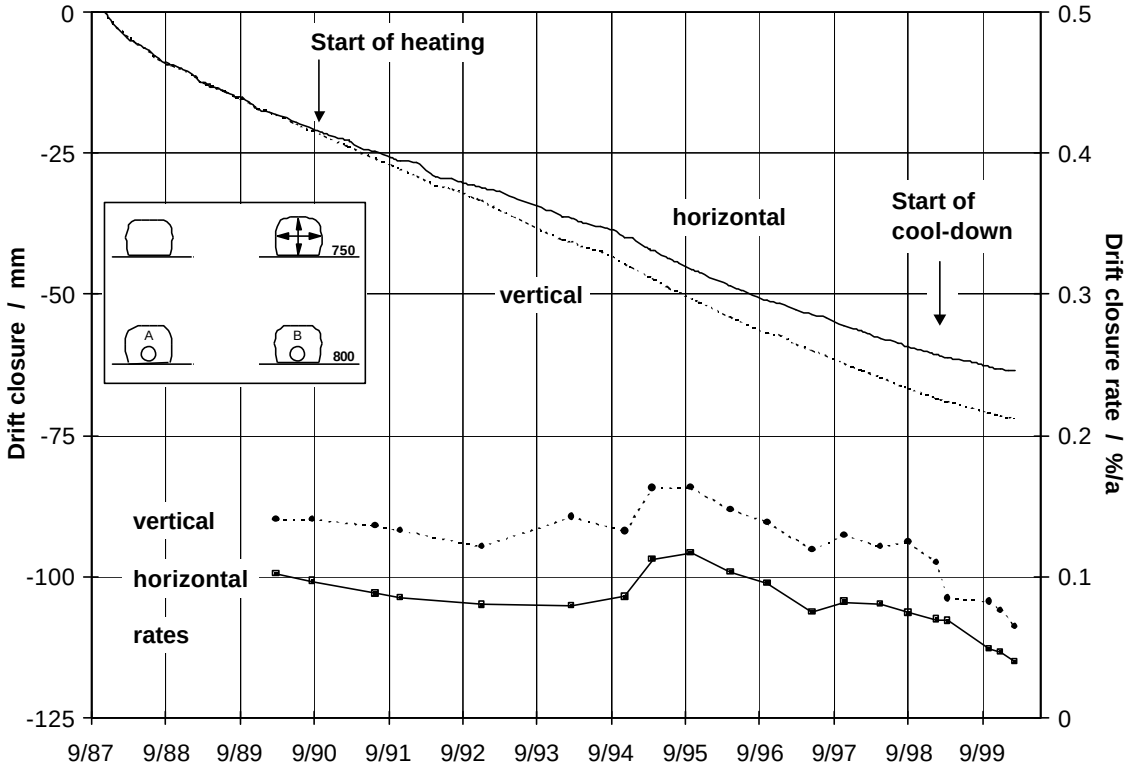

Fig. 5.2.4 Drift closure and drift closure rates in the observation drifts on the 750-m level (section D2)

5.3 Backfill Behaviour

5.3.1 Roof Gap

In the backfilled test drifts, the distance between the top of the backfill and a respective reference point at the roof was monitored in several cross sections since the backfill had been emplaced. After backfilling, primary gravitational backfill settling induced the opening of a gap between drift roof and the top of the backfill which is shown in Figures 5.3.1 and 5.3.2 for different sections of the heated and the non-heated area. An opening of up to 25 mm was recorded, but in most sections, primary backfill settling had not ended when heating started.

After the heaters had been switched on, accelerated drift closure induced the closing of the gap. Closing started as soon as backfill settling was exceeded by drift closure. Thus, the opening of the roof gap was counteracted by drift closure which acted both by roof sinking and by lifting the backfill as a whole due to floor uplifting. Closing of the gap terminated as contact was reached between roof and backfill which was indicated by suddenly dropping closing rates.

In the heated area, the gap was closed very rapidly within four to seven weeks (Fig. 5.3.1). In the non-heated sections, closing of the gap began several months after the start of heating. In these regions, the gap was closed after one to two years (Fig. 5.3.2). Subsequently, further distance changes of 1 – 4 mm were caused by the compression of the disturbed zone at the drift roof.

In contrast to the TSDE experiment, in which some time had passed between backfilling and heating, a roof gap will probably not appear in a final repository. In the repository, heat output from the spent fuel will accelerate drift closure immediately even before backfilling. Therefore, primary settling of the backfill will already be exceeded by accelerated drift closure.

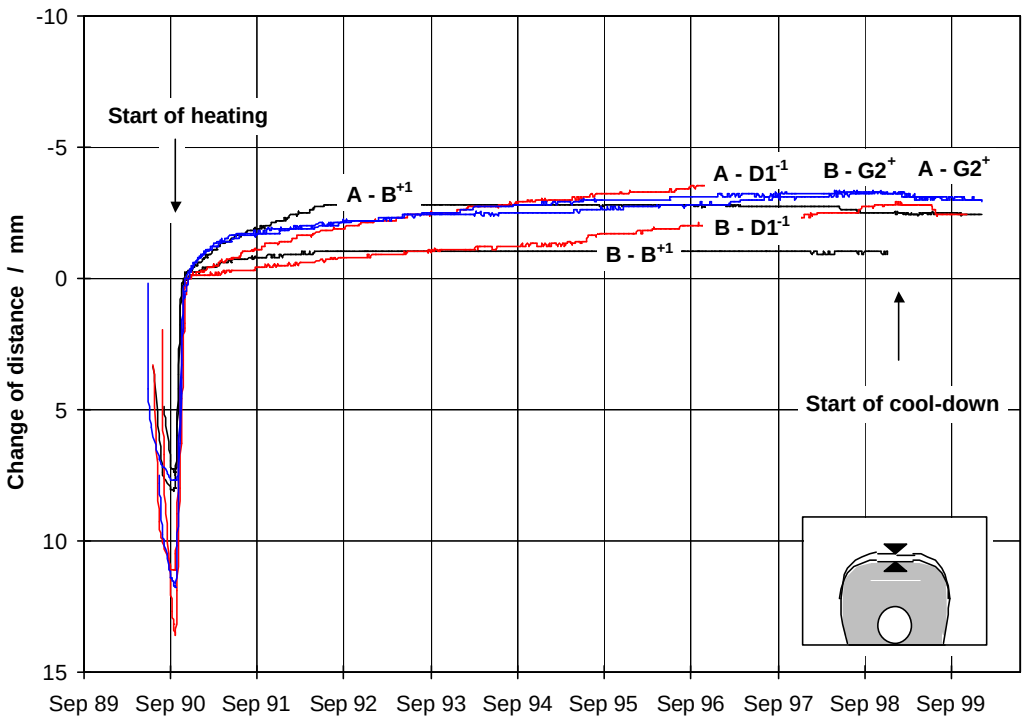

Fig. 5.3.1 Opening and closing of the roof gap in the heated area (sections B^{+1}, $D1^{-1}$, and $G2^{+}$)

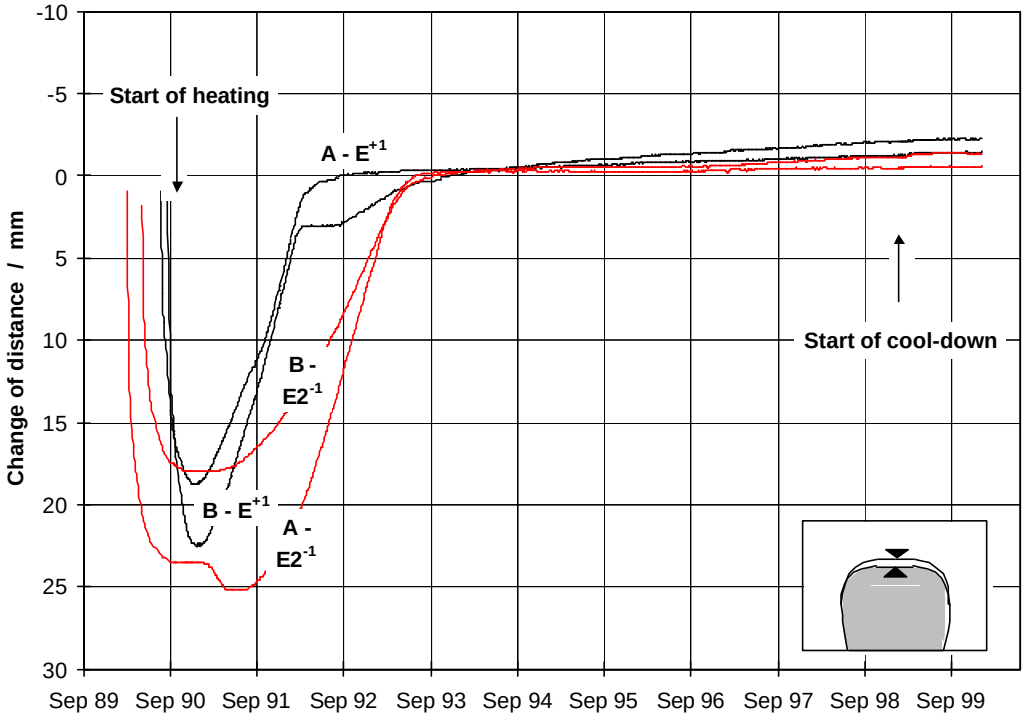

Fig. 5.3.2 Opening and closing of the roof gap in the non-heated area (sections $E1^{+1}$ and $E2^{-1}$)

5.3.2 Backfill Compaction

Backfill settling and vertical distribution of backfill compaction were determined at various levels in the backfill by recording the change of distance between a reference point at the drift roof and the measuring points in the backfill.

Backfill compaction in the heated area is being presented exemplarily in Figures 5.3.3 and 5.3.4 with the start of heating being reference point zero for the backfill settling curves in Figure 5.3.3. After the start of heating, the backfill was being lifted up as a whole at first due to the acceleration of drift closure and related floor uplifting. Backfill compaction started immediately after the roof gap had been closed. During the first months, about 70 % of backfill compaction was taking place in the upper third of the backfill (Fig. 5.3.4). Then, the central and the lower part were increasingly compacted. After two years of heating, the vertical distribution of backfill compaction was approximately balanced with an almost constant ratio of about 40 % in the upper third and 30 % in the central and lower parts (Fig. 5.3.4). Due to the failure of the respective drift closure measuring gauges in section G2, the calculations in Figure 5.3.4 could only be presented until 1995. But other cross sections revealed that vertical distribution of backfill compaction in the heated area hardly changed up to the end of the heating phase.

In the end of 1996, the backfill settling rates in sections B^{+1} and $G2^{+}$ increased temporarily (Fig. 5.3.3). But this was only a short-term effect caused by the drilling of two boreholes into the backfill for the replacement of failed drift closure measuring gauges.

Up to the end of the heating phase, the total backfill compaction in the heated zone reached up to 290 mm, being composed of 90 mm in each of the lower thirds and 110 mm in the upper third. Backfill compaction curves showed an almost identical development in both test drifts. The highest backfill compaction was recorded around the central heaters (section B^{+1}). Compaction decreased with increasing distance from the central heaters, being about 10 % to 15 % lower around the heaters in section $D1^{-1}$, 8.5 m away from section B^{+1}. Accordingly, non-homogeneous backfill compaction has to be assumed both in vertical and axial direction of the test drifts.

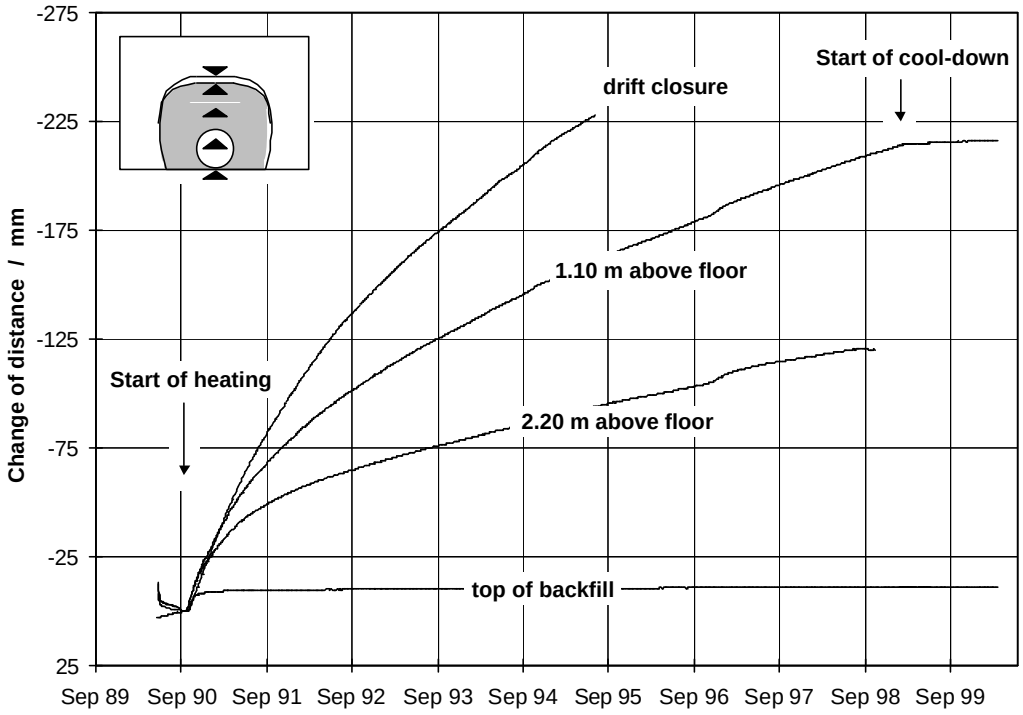

Fig. 5.3.3 Drift closure and backfill compaction between roof and different levels in the heated backfill (section G2^{+})

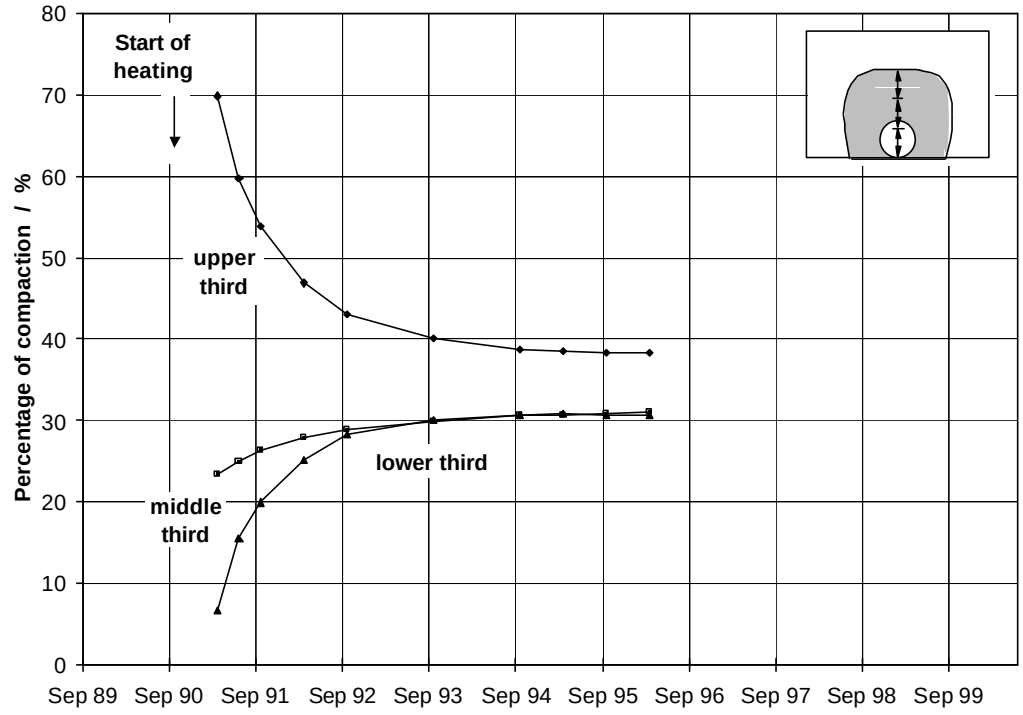

Fig. 5.3.4 Vertical distribution of backfill compaction in the heated backfill (section G2^{+})

In the cool-down phase, backfill compaction in the heated area almost stopped and backfill settling rates approached zero as a result of the rapidly decreasing drift closure rates (Fig. 5.3.3).

The development of backfill compaction in the non-heated area is shown in Figures 5.3.5 and 5.3.6. Again, the start of heating was reference point zero for the backfill settling curves in Figure 5.3.5. Primary backfill settling continued after the heaters had been switched on, mainly affecting the lower part of the backfill (Fig. 5.3.6). As a result of the acceleration of drift closure in the non-heated area in 1991 (Fig. 5.2.2), backfill settling rates were exceeded by drift closure rates which is indicated by the reversing slope of the backfill settling curves in Figure 5.3.5. While the roof gap was closing, the central part of the backfill was increasingly compacted (Fig. 5.3.6).

Compaction in the upper part started when the roof gap had been closed. Subsequently, most of the backfill compaction occurred in the upper part. Since 1993, the percentage of backfill compaction in the lower third increased again (Fig. 5.3.6). In the cool-down phase, backfill compaction in the lower part was even accelerated by up to 30 % (Fig. 5.3.5 and 5.3.6). But total backfill compaction was considerably lower than in the upper parts reaching only about 20 mm up to the end of March 2000 compared to about 40 mm in each of the upper thirds. Accordingly, total backfill compaction in the non-heated area was about 100 mm and compaction proved to be non-homogeneous.

Compared to the non-heated sections, total backfill compaction in the heated area was almost three times higher in the upper part of the backfill and over four times higher in the lower part. But at the end of heating, compaction rates were almost the same 0.5 %/a over the whole drift length.

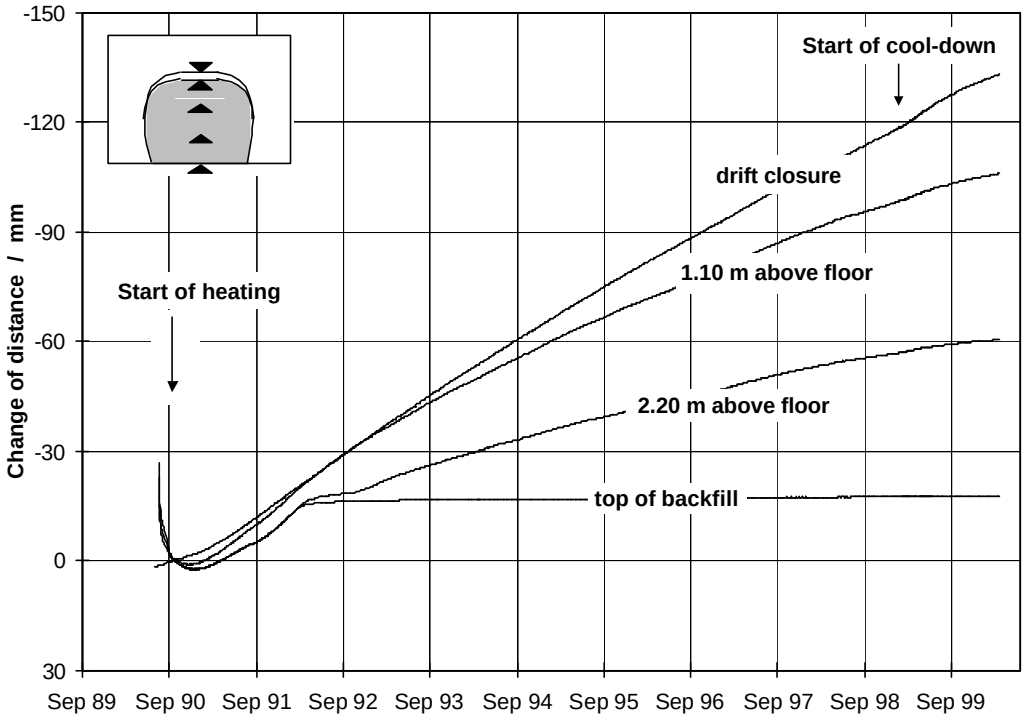

Fig. 5.3.5 Drift closure and backfill compaction between roof and different levels in the non-heated backfill (section E1^{+1})

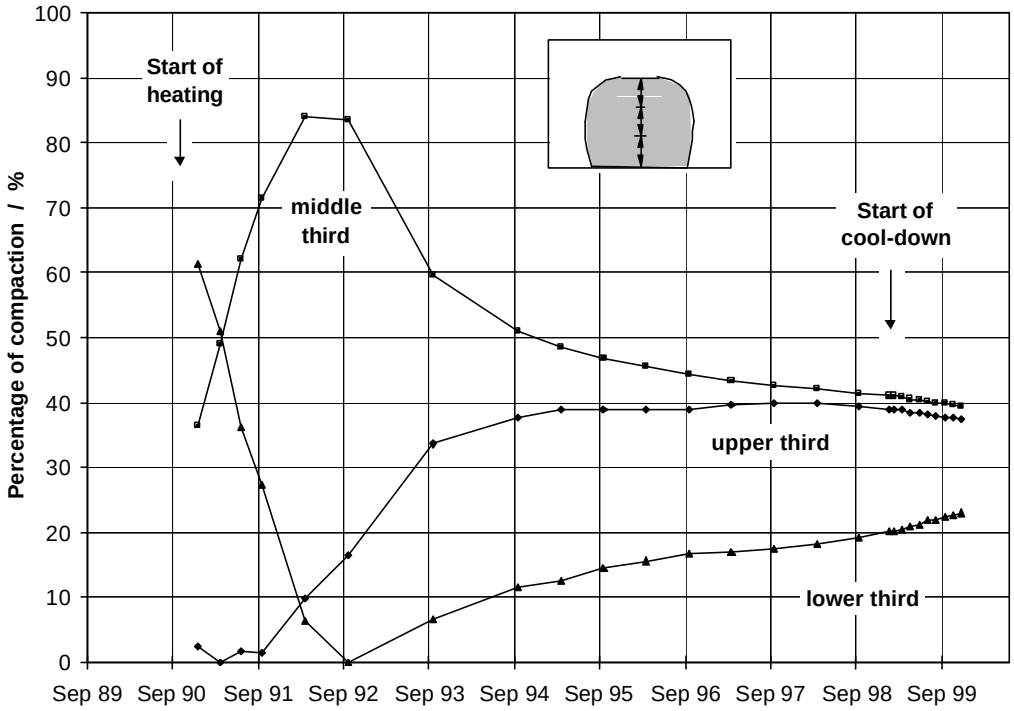

Fig. 5.3.6 Vertical distribution of backfill compaction in the non-heated backfill (section E1^{+1})

5.3.3 Backfill Porosity

For the determination of backfill porosity, different methods were used. The most reliable results were received from drift closure measurements by calculating the ratio of backfill mass and actual drift volume. However, the obtained porosities were only mean values over the respective cross sections basing on a limited number of measuring gauges. Non-homogeneous backfill compaction, which was probably caused by thermal gradients within the backfill, could not be determined with this measuring equipment. During test drift excavation, the local porosity will be determined on backfill samples from different areas to check the obtained porosity values and to verify that backfill porosity can be derived from drift closure measurements.

In the beginning of the experiment, attempts had been made to determine the backfill density additionally by geophysical methods /DRO 96/. Sonic measurements and gravimetry, however, showed no reliable results. Only the radiometric γ-γ-method was successfully applied in several boreholes even if absolute density values could not be determined due to calibration problems. But measured density changes were in the same range as the results from drift closure measurements. Moreover, the radiometric borehole measurements showed a non-homogeneous vertical density distribution in the backfilled drifts with an increasing density towards the roof. This general trend was attributed to the slinger technique which caused a segregation of different grain fractions during backfilling. The initial non-homogeneous backfill density distribution, which could be demonstrated around the borehole casings, was conserved during ongoing compaction.

After backfilling, an initial backfill porosity of about 35 % was determined from the total mass of crushed salt material and the test drift volume. With increasing drift closure, backfill porosity decreased accordingly. At the end of the heating phase, the porosity had been reduced to 23.5 – 25 % in the heated area (Fig. 5.3.7). In the non-heated sections, backfill porosity ranged between 30 – 32 %.

In the cool-down phase, backfill porosity in the heated area kept nearly unchanged as drift closure had been almost stopped after the heaters had been switched off (see chapter 5.2). In the non-heated area, backfill porosity decreased further reaching 29.5 – 31.5 % at the end of March 2000 (Fig. 5.3.7).

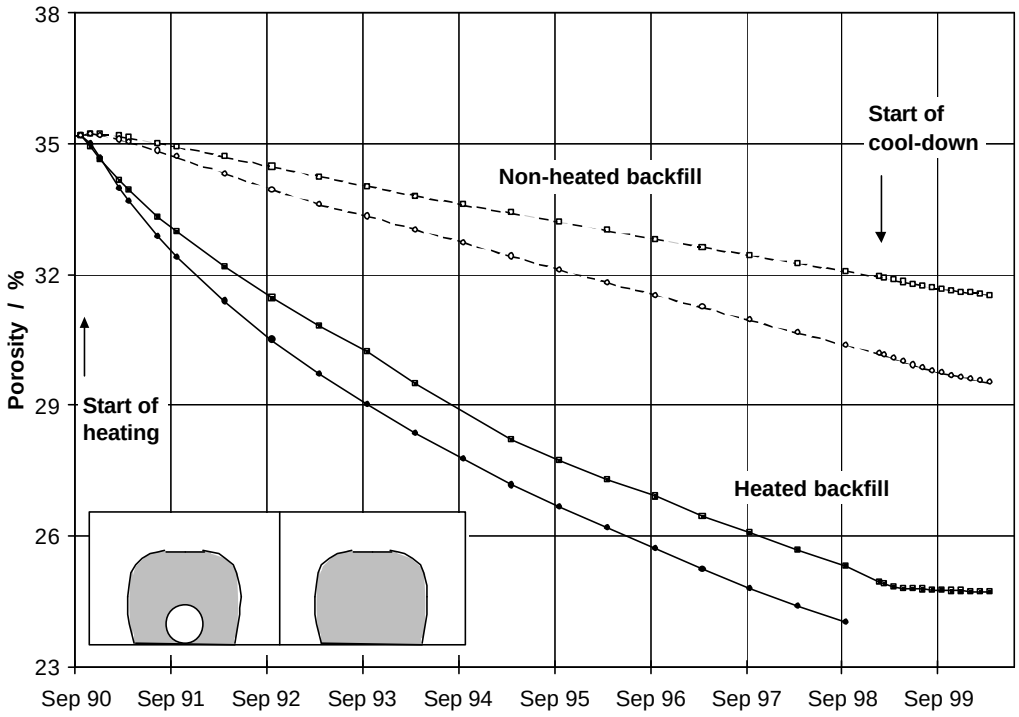

Fig. 5.3.7 Range of backfill porosity in the heated and the non-heated area

5.3.4 Backfill Permeability

Attempts were made to determine the backfill permeability by using the time delay of the air pressure pulse running through the backfill when the mine ventilation was switched on and off. The air pressure was measured in the access drift and at different locations in the backfill. However, no measurable time delay could be recorded. Obviously, the cable duct close to the drift roof acted as a bypass to the backfill impeding a direct permeability determination.

But from the pressure increase which was measured when the mine ventilation was switched off, the permeability of the backfilled drift could be estimated on the basis of finite-difference calculations. The boundary conditions were selected taking into account the bypass conditions. The cable duct was assumed as starting point. A "path length" of 3.04 m and a distance of 1.94 m between the "path entrance" and the measuring point in the backfill were chosen to simulate the conditions in the backfilled drift (Fig. 5.3.8). In 1998, a pressure increase of 8 hPa was measured. For the actual porosity of 25 %, the measurement results were best fitted by a permeability of at least 10^{-11} m^2 (Fig. 5.3.8).

During the DEBORA experiments, the backfill permeability decreased from $5 \cdot 10^{-12}$ m^2 to $7 \cdot 10^{-14}$ m^2 in DEBORA-1 and from $1 \cdot 10^{-10}$ m^2 to $4 \cdot 10^{-13}$ m^2 in DEBORA-2 /ROT 99/. The achieved permeabilities were still high compared to undisturbed rock salt. In-situ permeability measurements in the Asse salt mine indicated permeability values below 10^{-21} m^2 in rock salt /WIE 98/. To reach these low permeabilities in the backfill, a much longer testing period would be required which is not feasible within an in-situ experiment.

Basing on a large number of published laboratory data and the results of the DEBORA tests, an empirical relation between backfill porosity and permeability was derived by /MLY 99/. The estimated permeability value of the TSDE backfill fitted well into the range of the stated relation for dry crushed salt.

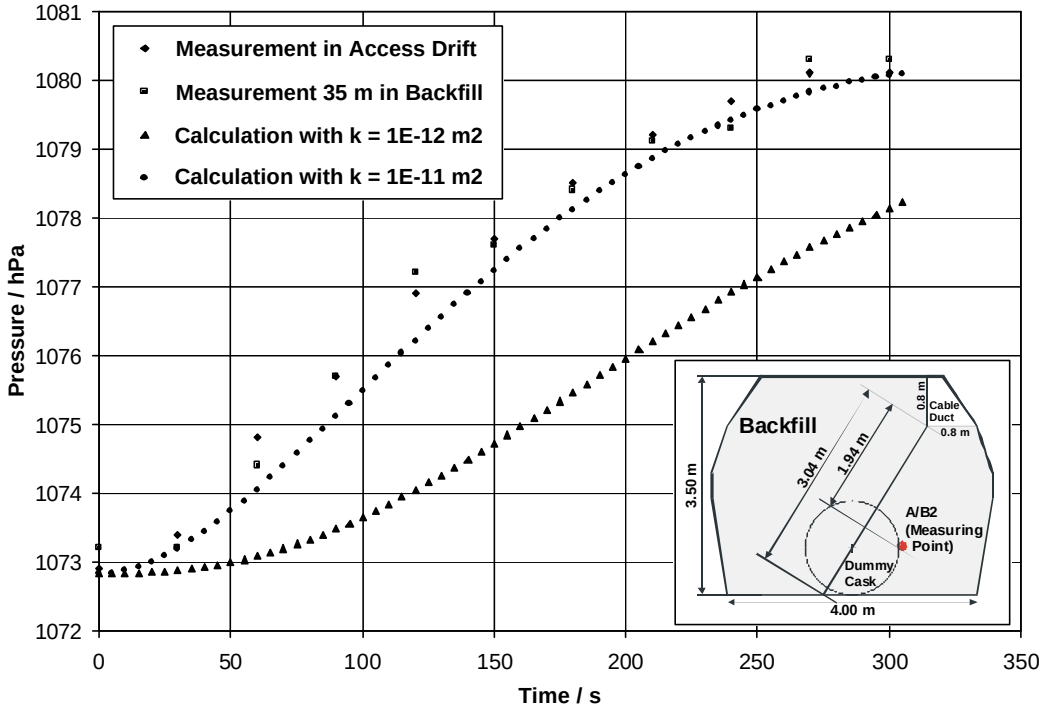

Fig. 5.3.8 Air pressure increase in the access drift and in a backfilled drift when switching-off the mine ventilation compared with calculational results for different backfill permeabilities (the model used for the permeability calculations is shown in the insert)

5.4 Rock Deformation

5.4.1 Extensometer Measurements

With the extensometer array which had been installed from the test drifts on the 800-m level, rock displacements were registered since September 1990. From the displacements in different borehole depths, the dilatations of the rock between the respective depths were calculated. For the determination of excavation-induced rock deformations, several extensometers had been installed earlier from the 750-m level in cross section A which recorded the vertical displacements in the pillar and above the test drifts since April 1989. The results are described in /DRO 96/. Deformations increased temporarily after the excavation of the test drifts, but had reached almost steady state conditions before heating started.

After the heaters had been switched on, rock deformations towards the test drifts were accelerated significantly. With increasing distance from the heaters, the acceleration of the displacements started later and was lower.

The first and largest rock deformations were observed below the heater casks (Fig. 5.4.1). Within one week after the start of heating, the dilatation rates accelerated between ten to twenty times up to 4 %/a in 0- 2.5 m depth (Fig. 5.4.2). Two months later, the rates decreased again due to the increasing support by the backfill. After two and a half years, 0.3 %/a were reached. In 2.5 m depth below the heater casks, the displacements were accelerated 2- 5 weeks later, whereas in 5m and 10 m depth the first effects of heating were recorded after several months (Fig. 5.4.1 and 5.4.2). The maximum dilatation rates between these depths were 1.4 %/a and 0.3 %/a, respectively. After the initial increase, all rates decreased. At the end of 1993, all floor extensometers in the heated area had failed.

In the drift walls, a complete deformation development could be obtained over the whole testing period. Though most wall extensometers in the heated area had failed until 1994, measurements were continued by replaced borehole gauges. Accelerated rock deformation in the drift walls started later and at lower deformation rates (Fig. 5.4.3). Near the drifts, maximum dilatation rates of 1.3 - 1.8 %/a were observed in 0 – 2.5 m depth (Fig. 5.4.4). Three months after the start of heating, the rates decreased approaching vertical displacement rates below the drifts after nine months.

In 1994, almost constant dilatation rates were recorded due to the higher thermal power output (Fig. 5.4.4 with wall extensometer values from the southern drift, which showed the same development, being added between 1992 and 1994). After drilling two boreholes for the replacement of failed drift closure measuring gauges, dilatation rates increased temporarily in 1996 and 1997, but decreased again subsequently. At the end of heating, dilatation rates in 0 – 2.5 m depth were below 0.1 %/a (Fig. 5.4.4). Dilatation rates decreased with increasing depth. In 2.5 - 5 m and 5 - 10 m depth, maximum dilatation rates of 0.7 %/a and 0.18 %/a were reached, respectively.

In the pillar, horizontal displacement rates were initially about 10 - 30 % higher than in the rock on the opposite side due to higher temperatures (Fig. 5.4.5). Maximum rates were reached after three months. After two years, the displacement rates approached the values of the corresponding wall extensometers. Differences were observed in the dilatation rates. In 2.5 - 5 m depth, dilatation rates in the pillar were twice as much reaching up to 1 %/a in the beginning (Fig. 5.4.6). In 1994, horizontal dilatation rates in the inner and outer part of the pillar were almost the same, before most pillar extensometers failed. Therefore, it can be concluded that the pillar was supporting homogeneously over its whole width. As the replacement of horizontal extensometers in the pillar was not feasible, measurements ended after the gauges had failed.

Vertical deformations in the roof area were different from the displacements below the drifts (Fig. 5.4.7). Dilatations above the drifts were smaller and more delayed. The rates were comparable to floor extensometer measurements which had been shifted by about 2.5 m (Fig. 5.4.8). The dilatation rates in section D1 are shown in Figure 5.4.8. They are in the same range as in section A where extensometers had been installed in different depths from the 750-m level (Fig. 5.4.9 and 5.4.10). Until 1993, all roof extensometers in section D1 had failed, but measurements were resumed in 1994 by additional gauges which were installed from the observation drifts on the 750-m level.

The dilatation rates around the heated drifts in 0 - 2.5 m depth are compared in Figure 5.4.11. Maximum rates were observed in the floor, but half a year after the start of heating, all rates were almost in the same range and kept decreasing until the end of heating. From these results it can be concluded that vertical drift closure in the heated area was by two thirds composed of floor uplifting and only by one third of roof sinking. In horizontal direction, however, an approximately uniform closure can be assumed from both sides of the test drifts, as the deformations on the pillar side were only slightly higher than on the opposite side.

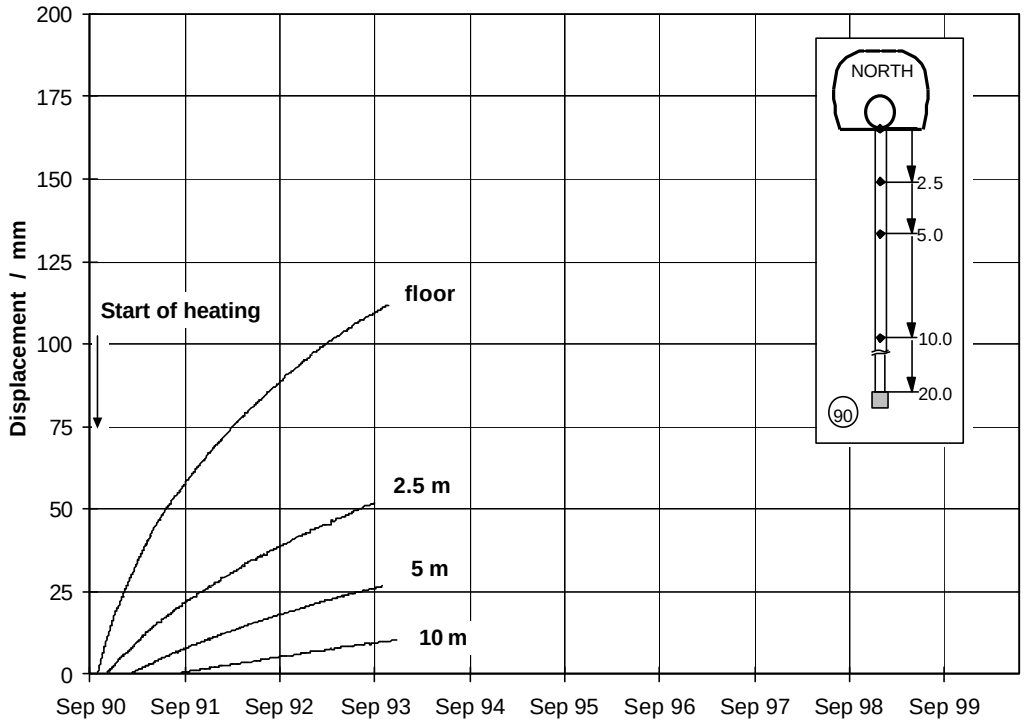

Fig. 5.4.1 Vertical displacements below the heated drifts (floor extensometer in section A)

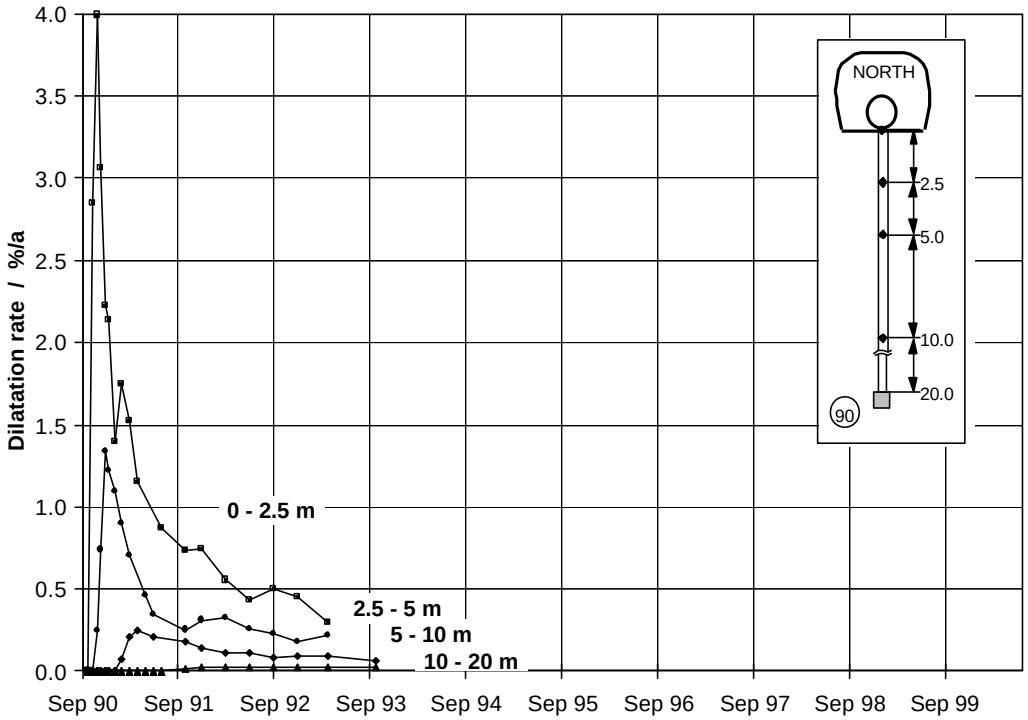

Fig. 5.4.2 Dilatation rates below the heated drifts (floor extensometer in section A)

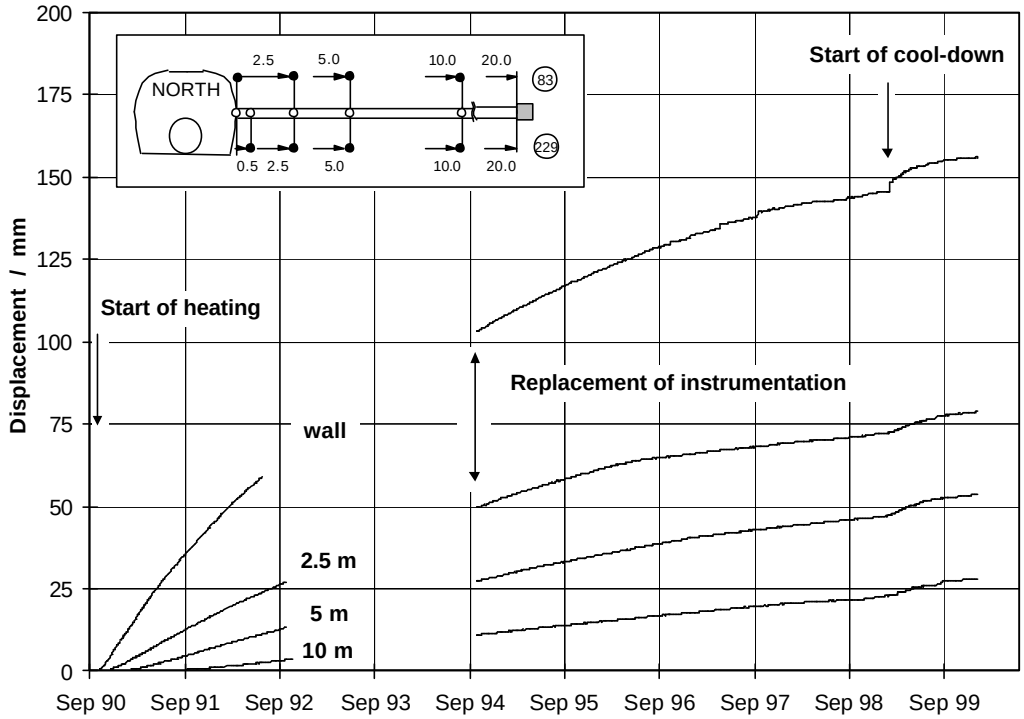

Fig. 5.4.3 Horizontal displacements beside the heated drifts (wall extensometer in section A)

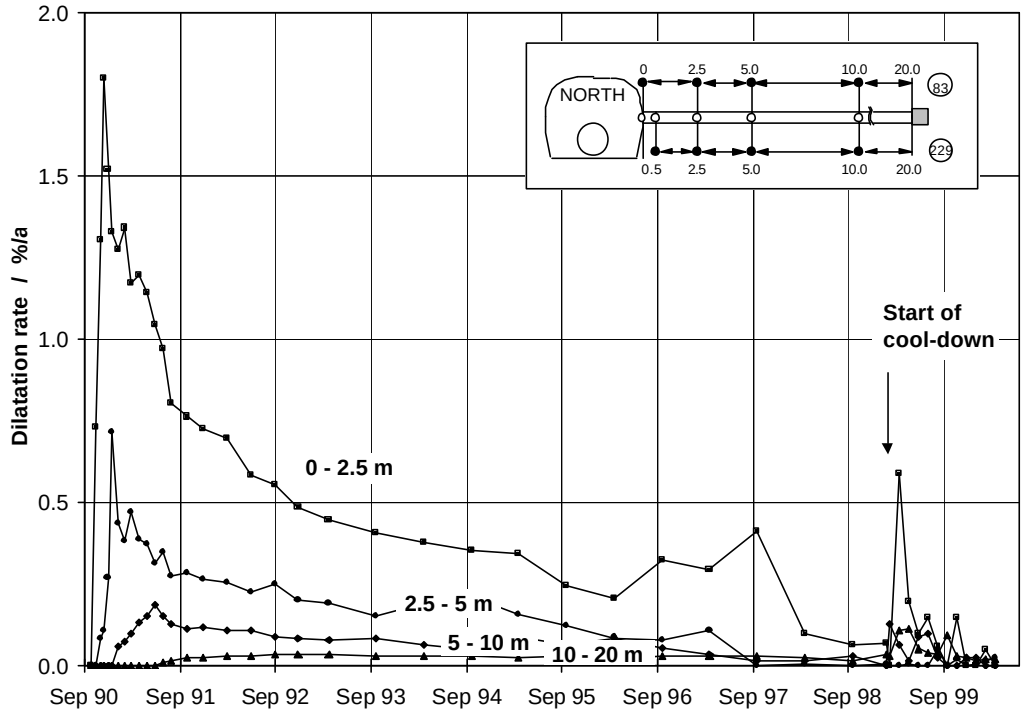

Fig. 5.4.4 Dilatation rates beside the heated drifts (wall extensometer in section A) with added values from the wall beside the southern drift from 1992 to 1994

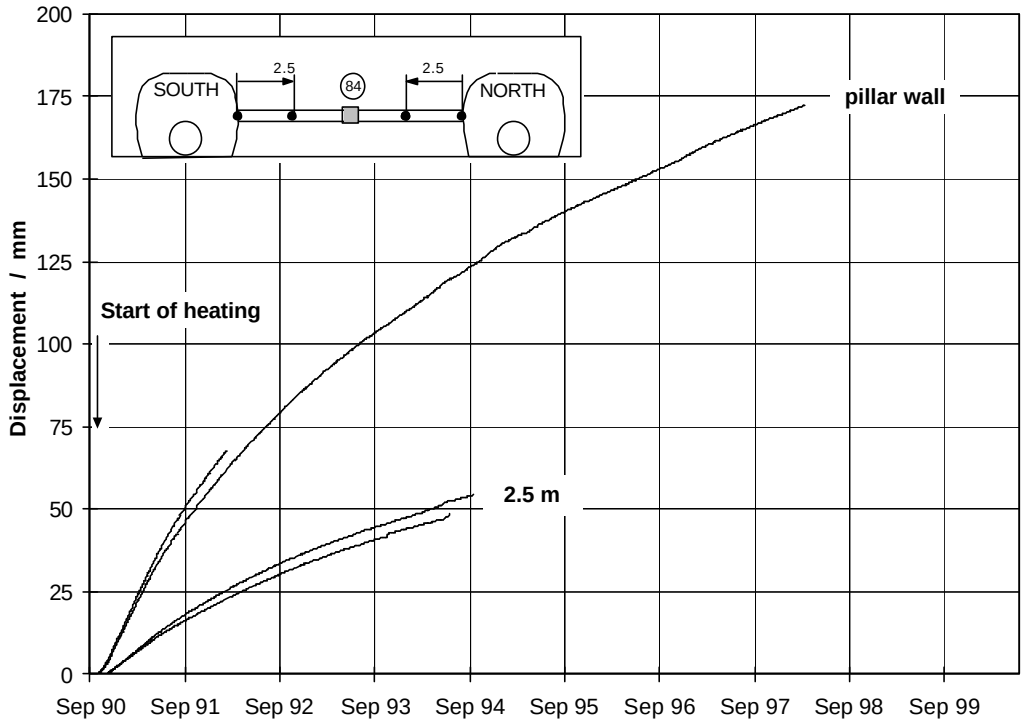

Fig. 5.4.5 Horizontal displacements between the heated drifts (pillar extensometer in section A)

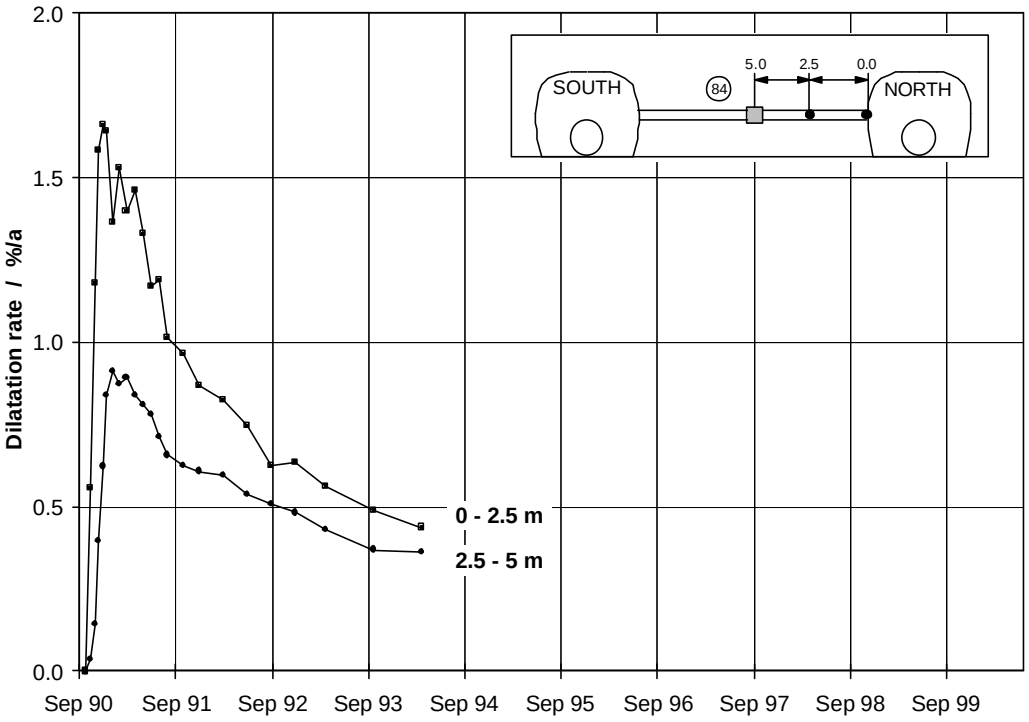

Fig. 5.4.6 Dilatation rates between the heated drifts (pillar extensometer in section A)

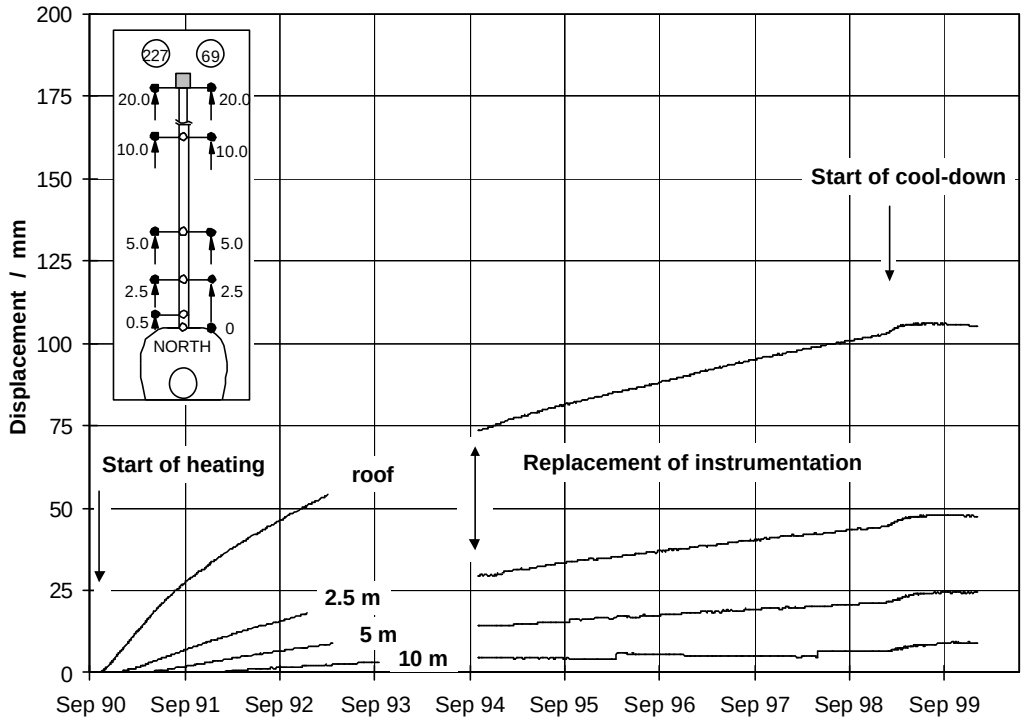

Fig. 5.4.7 Vertical displacements above the heated drifts (roof extensometer in section D1)

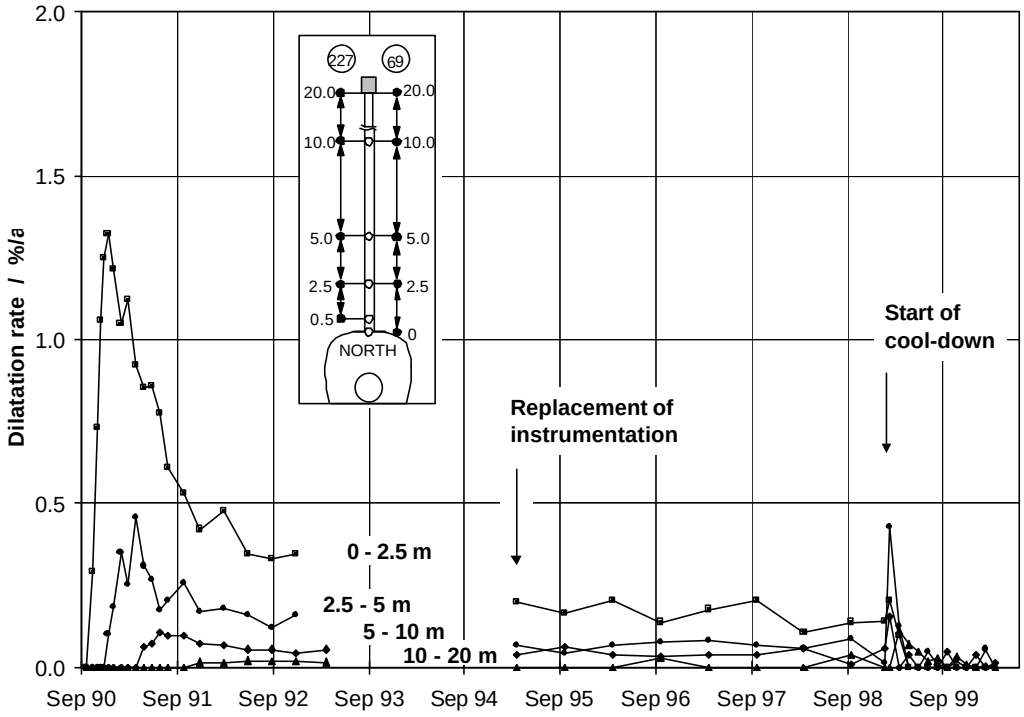

Fig. 5.4.8 Dilatation rates above the heated drifts (roof extensometer in section D1)

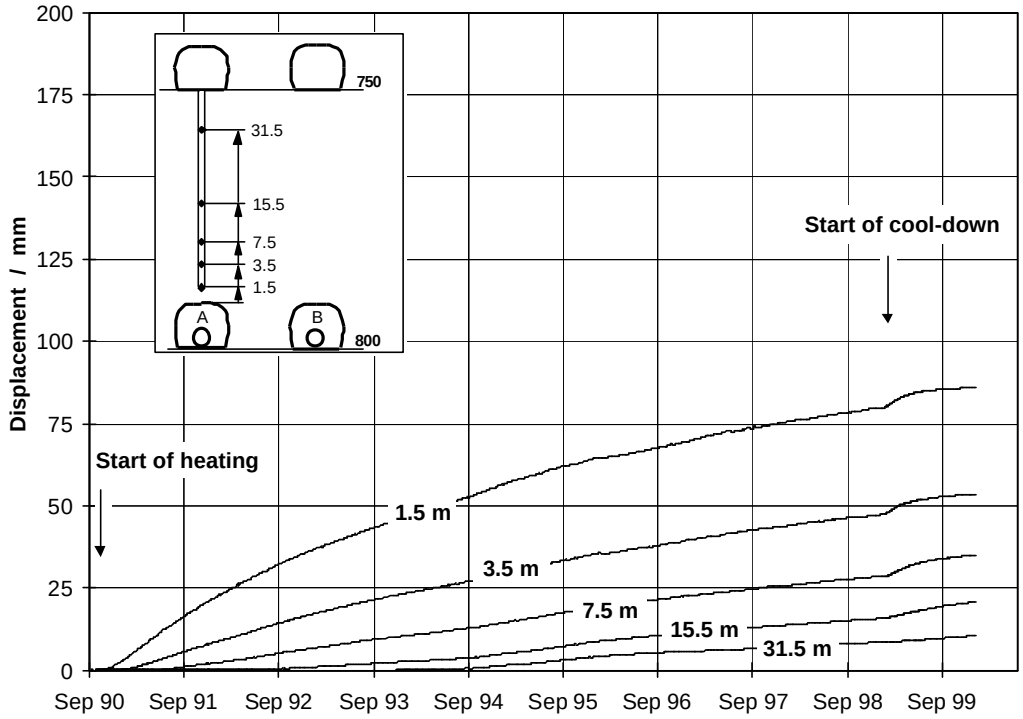

Fig. 5.4.9 Vertical displacements above the heated drifts (extensometer from the 750-m level in section A)

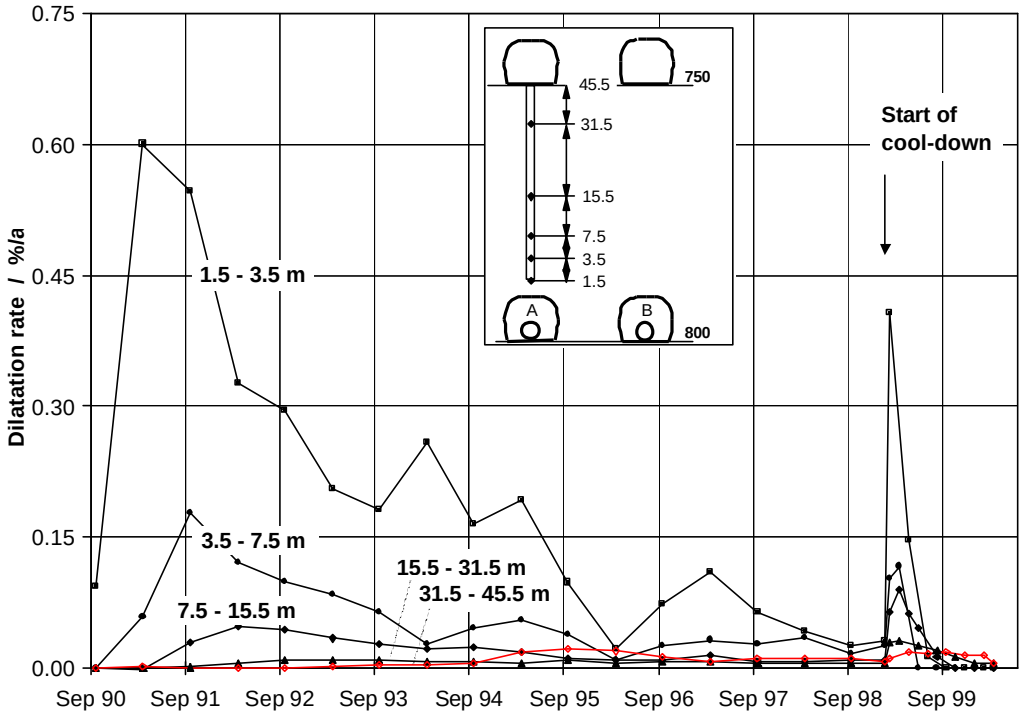

Fig. 5.4.10 Dilatation rates above the heated drifts (extensometer from the 750-m level in section A)

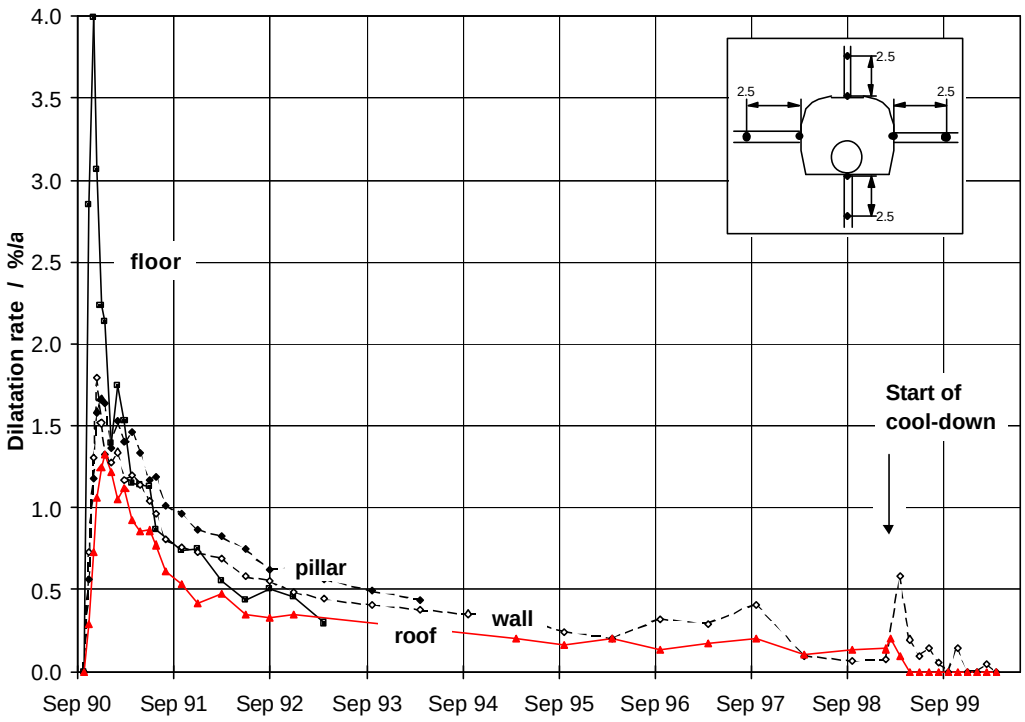

Fig. 5.4.11 Dilatation rates next to the heated drifts (0 - 2.5 m)

Vertical displacements in the pillar were recorded by extensometers which had been installed from the 750-m level in section A. Above the test drifts, rock deformations in the pillar were accelerated about half a year after the start of heating (Fig. 5.4.12). On the roof level of the test drifts, vertical displacements in the pillar were only half as much as the displacements directly above the test drifts. Higher above, however, rock deformations were comparable.

On the floor level of the test drifts, deformations were accelerated up to ten times immediately after the start of heating (Fig. 5.4.12). Maximum dilatation rates of 0.55 %/a were reached after one year (Fig. 5.4.13). Subsequently, the rates decreased continuously until the direction of rock displacement reversed in 1995 (Fig. 5.4.12). The initial uplifting in this part of the pillar changed into a downward movement which was observed until the end of March 2000.

Below the level of the test drift floor, the deformation rates increased with a delay of up to three months (Fig. 5.4.14). Maximum dilatation rates of 0.4 %/a were recorded directly below the drift floor level (Fig. 5.4.15). A comparison of vertical displacements

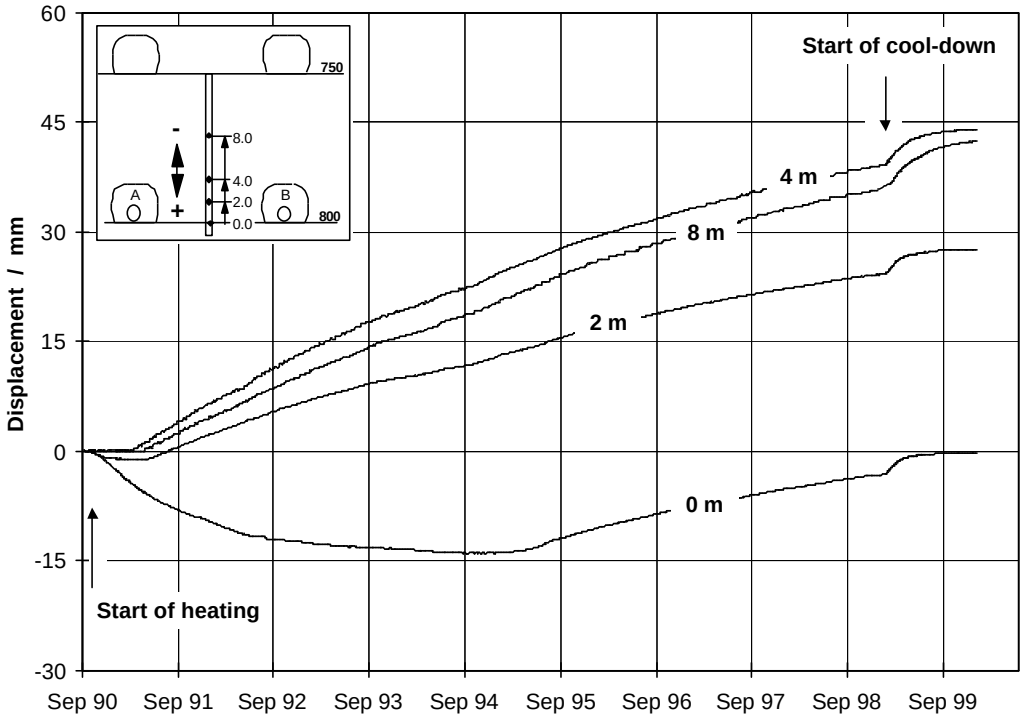

Fig. 5.4.12 Vertical displacements in the pillar beside and above the heated drifts (extensometer from the 750-m level in section A)

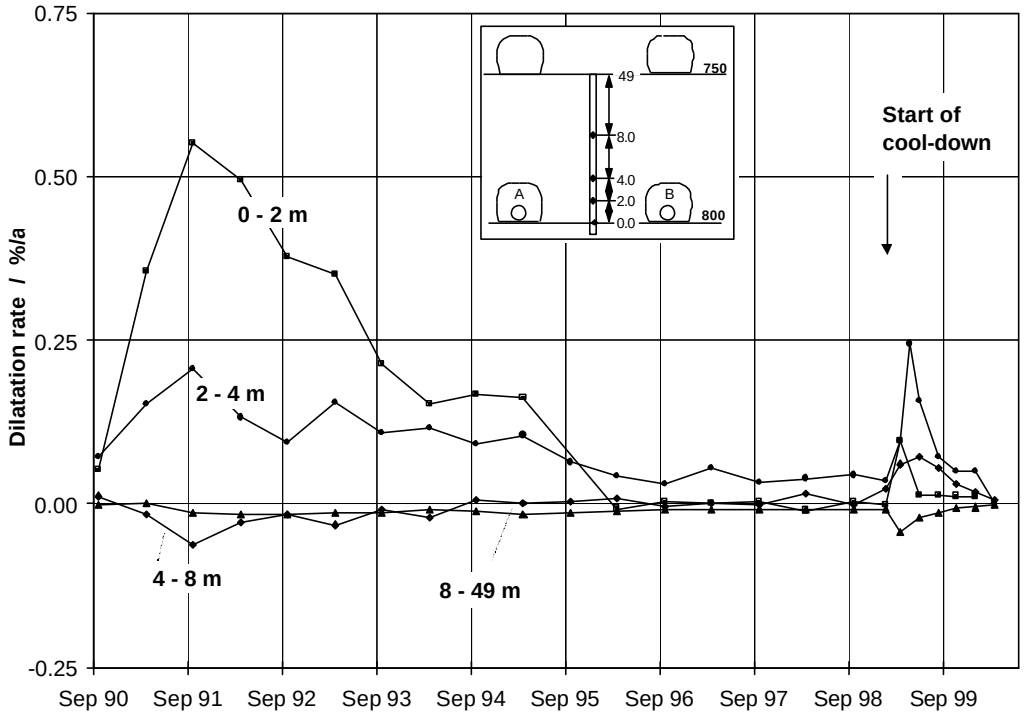

Fig. 5.4.13 Dilatation rates in the pillar beside and above the heated drifts (extensometer from the 750-m level in section A)

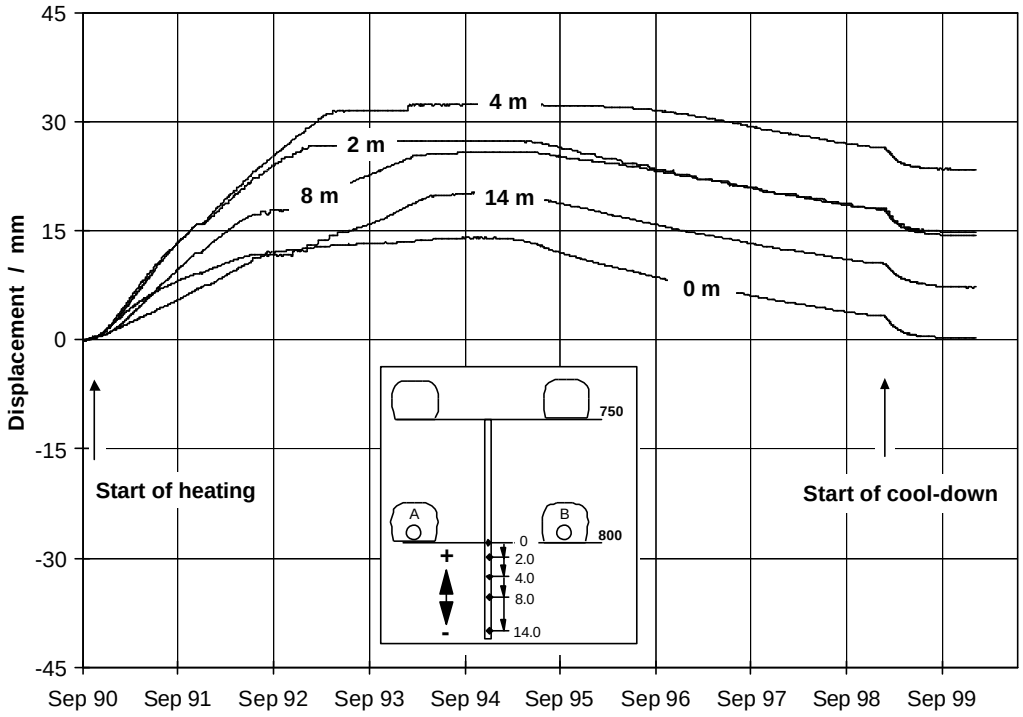

Fig. 5.4.14 Vertical displacements in the pillar below the heated drifts (extensometer from the 750-m level in section A)

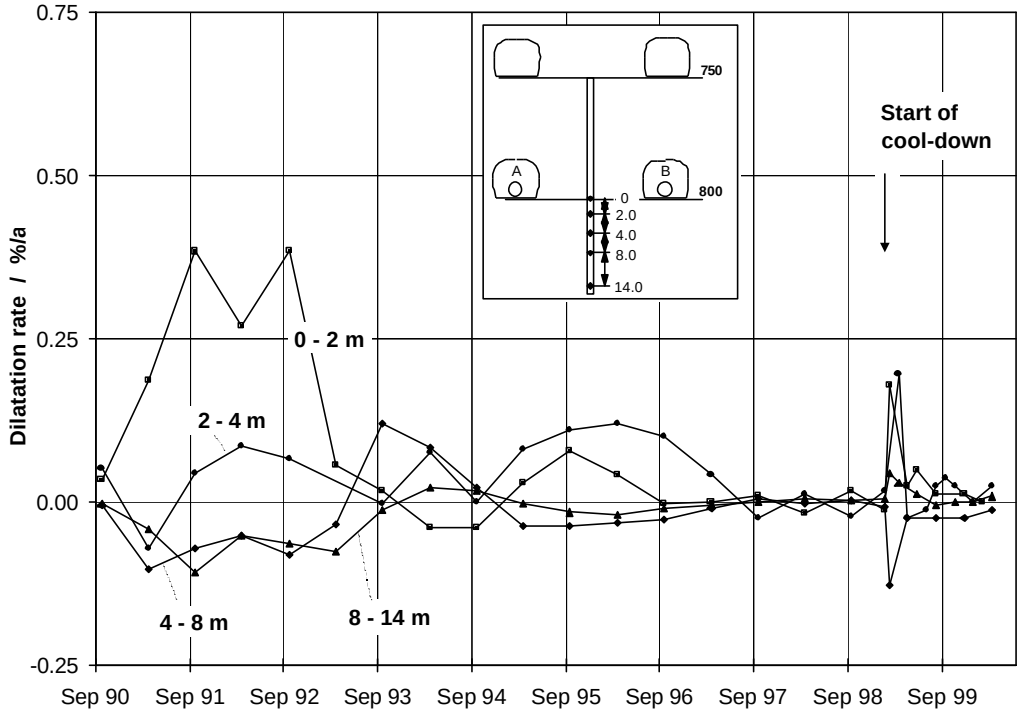

Fig. 5.4.15 Dilatation rates in the pillar below the heated drifts (extensometer from the 750-m level in section A)

in the pillar with rock deformations below the heated drifts was only possible until 1993 when all floor extensometers had failed. At that time, floor uplifting directly below the test drifts was up to eight times higher than in the pillar centre. In 2 m depth, floor uplifting was still twice as much, but in 5 m depth, displacements were in the same range. Further down, the vertical displacements in the pillar were even higher than below the heated drifts. Since 1993, the initial uplifting of the deeper part of the pillar suddenly stopped and displacements stagnated for one to three years (Fig. 5.4.14). Subsequently, rock movement in the deeper pillar changed into a downward direction, too, since 1995.

With switching-off the heaters, the deformation rates in the heated area increased significantly at first. The increase was caused by the pressure-drop in the cooling backfill (see chapter 5.5.1). Thus, its supporting effect decreased immediately leading to temporarily increased rock deformations towards the test drifts. Within a few weeks, the dilatation rates decreased again when the contact between backfill and surrounding rock was re-established. In the walls, the horizontal dilatation rates soon approached the rates which had been measured at the end of the heating phase (Fig. 5.4.3 and 5.4.4). Above the drifts and in the pillar, however, the vertical dilatation rates dropped almost to null (Fig. 5.4.7 to 5.4.15).

In the non-heated area, the total displacements reached only 30 % of those in the heated sections. Again, larger deformations were recorded by the floor extensometers, but dilatations in the corresponding measuring depths were almost similar in all directions. Contrary to the heated area, the proportions of floor uplifting and roof sinking were nearly the same. The deformation development is exemplarily shown for the roof (Fig. 5.4.16 and 5.4.17) and the pillar (Fig. 5.4.18 and 5.4.19).

Generally, the deformation rates increased gradually with the temperature increase in 1991 reaching maximum dilatation rates of 0.4 %/a in 0 - 2.5 m depth after one year of heating (Fig. 5.4-17). After that, the rates decreased continuously reaching the same dilatation rates of 0.1 - 0.2 %/a as in the heated sections after five years of heating. In 2.5 – 5 m depth, the acceleration of the displacements started later. At the end of the heating phase, dilatation rates were still lower than in the heated area (Fig. 5.4.17). Beyond 5 m depth, dilatation rates were only very small and hardly affected by heating. Further details are described in /DRO 96/.

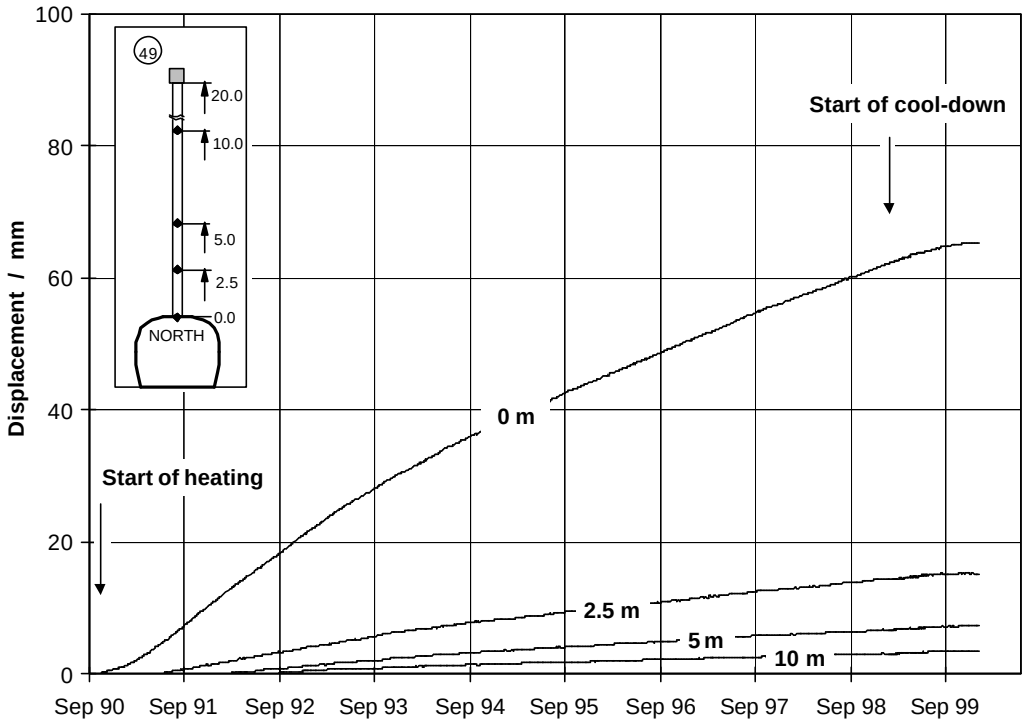

Fig. 5.4.16 Vertical displacements above the cold drifts (roof extensometer in section E1)

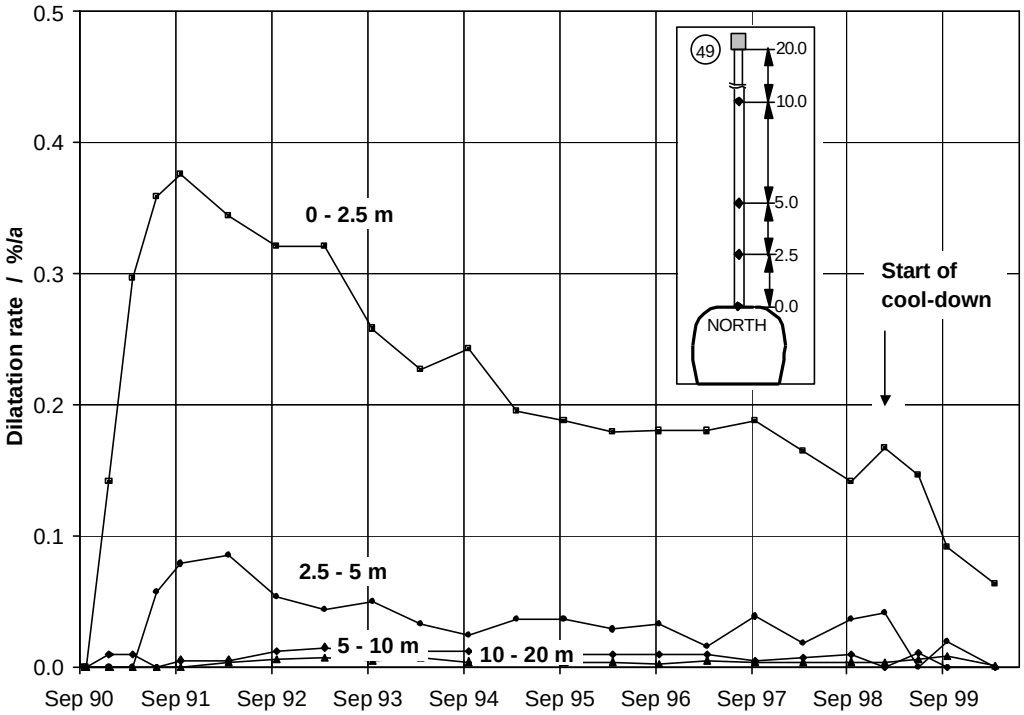

Fig. 5.4.17 Dilatation rates above the cold drifts (roof extensometer in section E1)

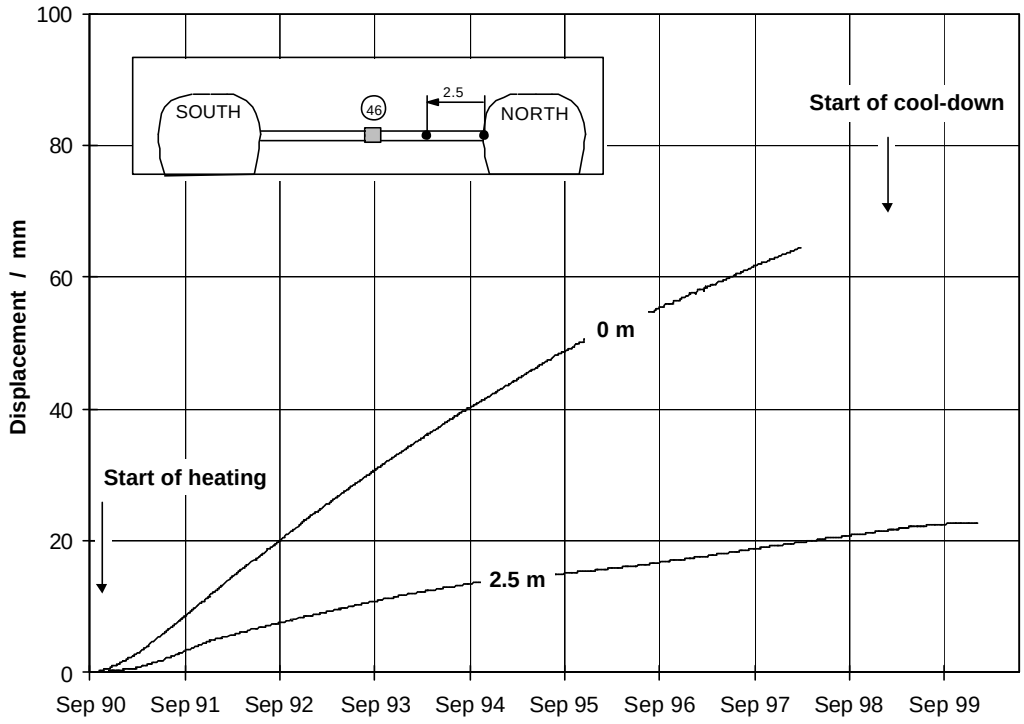

Fig. 5.4.18 Horizontal displacements between the cold drifts (pillar extensometer in section E1)

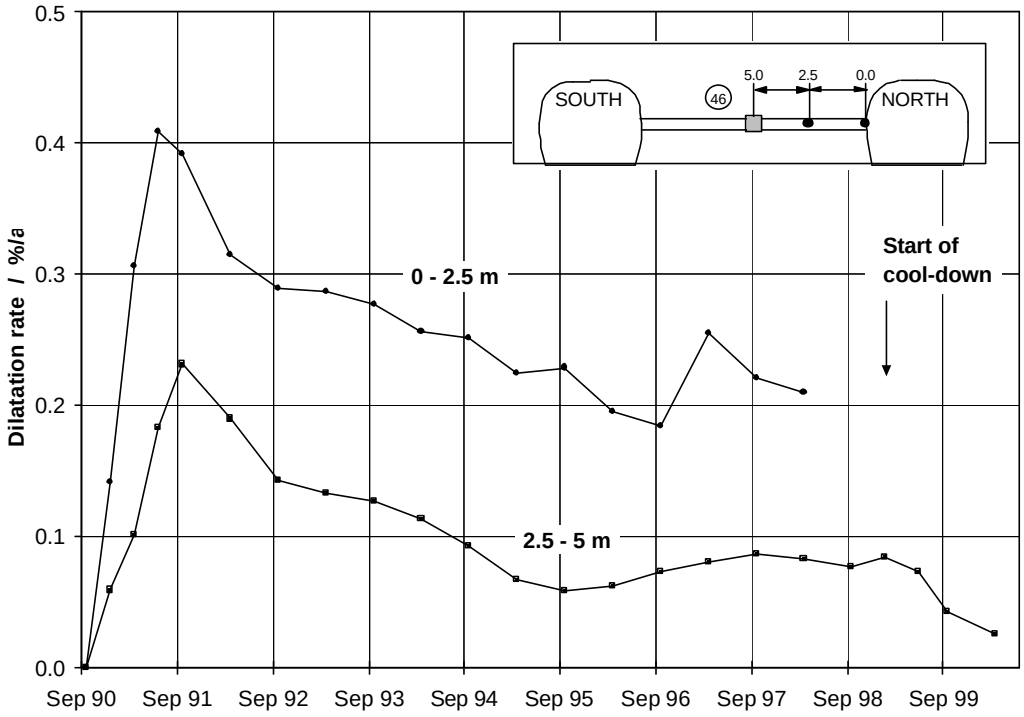

Fig. 5.4.19 Dilatation rates between the cold drifts (pillar extensometer in section E1)

In the pillar, dilatation rates in 2.5 – 5 m depth reached maximum values of 0.2 %/a after one year (Fig. 5.4.19). At the end of the heating phase, dilatation rates were still twice as much compared to the opposite side. Contrary to the heated area with almost similar rates over the whole pillar after two years of heating, dilatation rates in the non-heated pillar were still much higher in the outer part until the end of heating (Fig. 5.4.19).

After the heaters were switched off, the deformation rates in the non-heated area decreased continuously in the nearfield (Fig. 5.4.16 to 5.4.19). Beyond 5 m depth, however, the dilatation rates were not affected by cooling.

5.4.2 Inclinometer Measurements

In cross section A^{+1}, rock deformations in the test field area were additionally recorded by inclinometer measurements (Fig. 5.4.20). With these measurements, which covered a large area in the central heated section, the results of the extensometer measurements were confirmed.

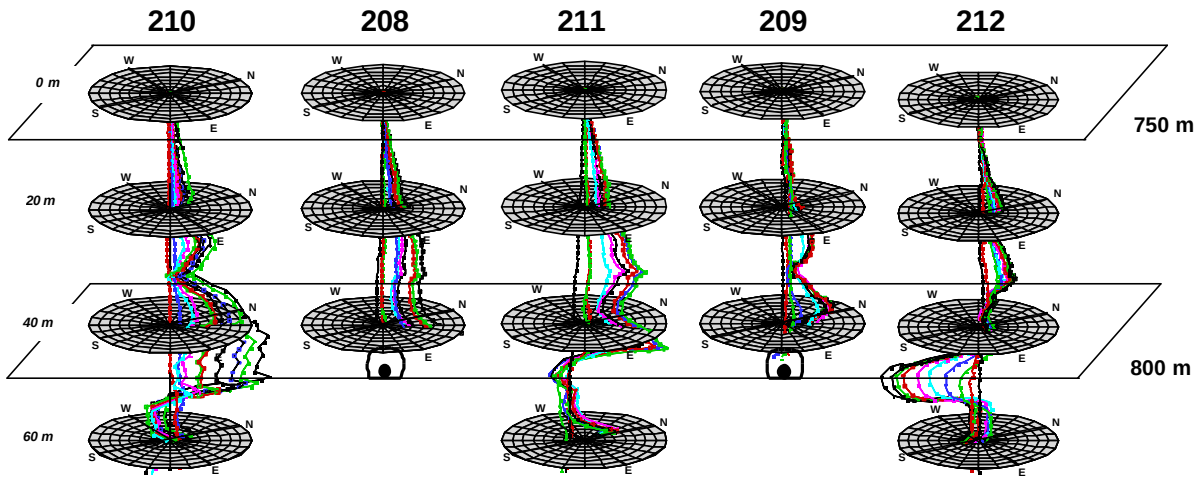

Fig. 5.4.20 Horizontal displacements in the test field area from selected inclinometer measurements from 1988 until 1999 (section A^{+1} with borehole numbers 208 - 212; each arc of the circles corresponds to a displacement of 5 mm)

Between the 750-m level and the 800-m level, a general tendency of horizontal rock displacements to the north-east was already recorded prior to the start of heating with displacement rates up to 2.5 - 5 mm/a. Probably, former potassium mining on the 750-m level, which had taken place north and north-east of the test field area, was the reason for these north-eastern movements. During the heating phase, trend and displacement rates were almost the same resulting in total displacements of up to 30 mm (Fig. 5.4.20). Obviously, the horizontal displacements above the test drifts were neither affected by heating, nor by cooling which started in February 1999.

On the level of the test drifts, however, horizontal displacements were significantly accelerated due to heating since January 1991. The increase was observed in all three boreholes extending beside the test drifts. Measurements in the external boreholes 210 and 212 revealed that movements turned towards the test drifts, with the total displacements reaching up to 35 - 45 mm at the end of heating (Fig. 5.4.20). Maximum values were recorded on the level of the test drift floor. During cooling, deformations continued showing the same displacement rates and the same direction of movement. Total displacements reached a maximum of 50 mm at the end of 1999.

In Figure 5.4.21, the displacement rates measured in borehole 212 on the test drift level (46 – 50 m borehole depth) are compared with the results of the horizontal extensometer measurements beside the test drifts in the corresponding depth of 5 m. Displacement rates in borehole 212 increased from a maximum of 5 mm/a prior to heating to a maximum of 9 mm/a in 1993. Subsequently, the rates decreased again to the initial rates which were reached in 1995. These results were consistent with the data of the wall extensometer measurements which were in the same range (Fig. 5.4.21). But, as inclinometer measurements were carried out periodically, the immediate acceleration of the deformations after the start of heating and cooling could not be recorded to the same extent as by the extensometer measurements.

A different behaviour was observed in the pillar (borehole 211). Directly above the roof level of the test drifts, displacements of up to 35 - 40 mm were recorded to the north-east, but on the level of the test drifts, the movements turned to the south-west with a total displacement of 18 mm at the end of heating (Fig. 5.4.20). During the cool-down phase, accelerated deformations were recorded above the roof level of the test drifts with total displacements reaching up to 45 mm at the end of 1999. Horizontal displacements in the other parts of the pillar, however, were less affected by cooling.

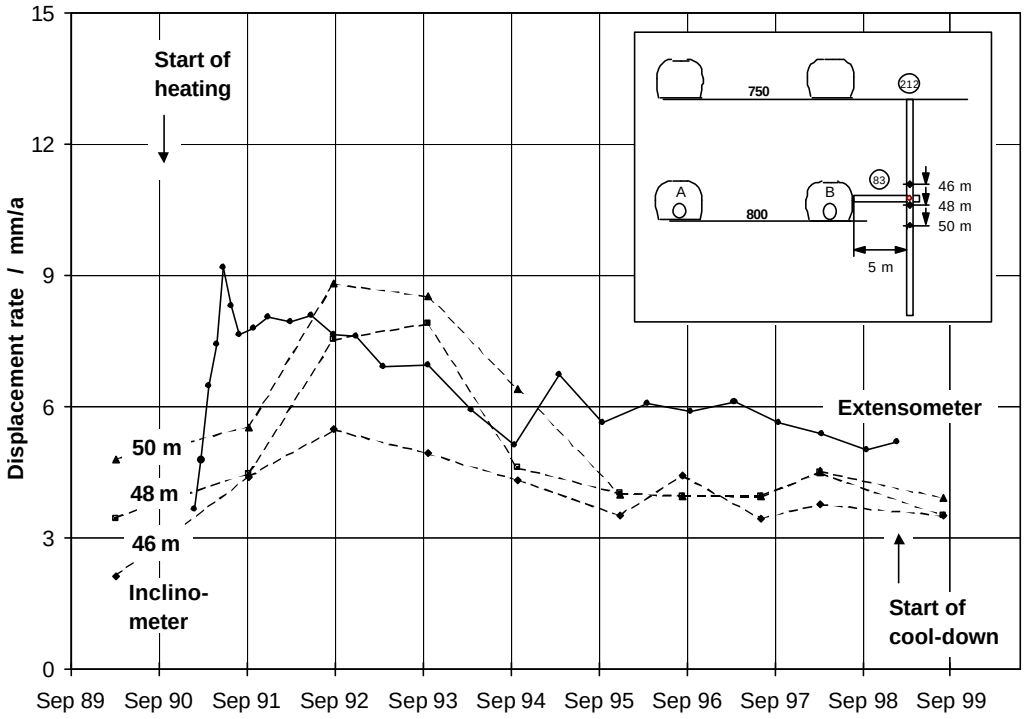

Fig. 5.4.21 Horizontal displacement rates 5 m beside the heated northern drift (wall extensometer in section A and inclinometer measurements in section A^{+1} on the level of the test drifts between 46 and 50 m borehole depth)

5.5 Pressure

5.5.1 Backfill Pressure

In the non-heated backfill, the pressure was nearly unchanged in the monitored cross section E1 during the first year of heating. Following the gradual temperature increase in the non-heated sections in 1991, the pressure began to rise slowly due to the beginning compaction of the backfill (Fig. 5.5.1). Since then, seasonal variations in pressure development were observed with stagnating or even decreasing pressure values during summer time. This phenomenon can be explained by variations in the air temperature of the mine ventilation. Since cross section E1 was located at a distance of 11 m from the ventilated access drift, the backfill showed a delayed reaction to the temperature variations. The lower winter air temperatures affected the backfill in cross section E1 some months later by stopping the pressure increase during summer time.

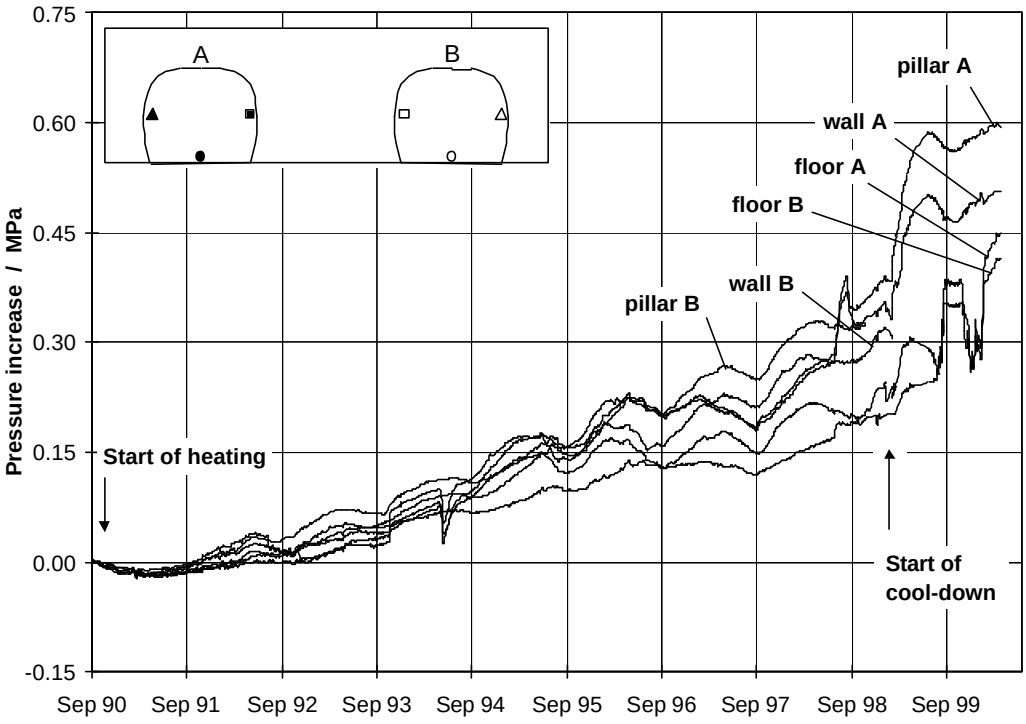

Fig. 5.5.1 Backfill pressure in the non-heated area (section E1)

At the end of the heating phase, the pressure in the non-heated backfill ranged between 0.20 – 0.25 MPa at the floor and 0.32 - 0.39 MPa at the walls. In the cool-down phase, a further pressure increase was recorded with a distinct increase immediately after the start of cool-down. This was a thermoelastic effect (see chapter 5.2) due to the relaxation of thermally induced rock stress in the heated area (see chapter 5.5.2) which caused an immediate elastic reaction with an increase in effective rock stress and hence in backfill pressure in the non-heated area. At the end of March 2000, 0.45 MPa were measured at the floor and 0.5 – 0.6 MPa at the walls (Fig. 5.5.1).

In the heated backfill, the pressure at the walls increased immediately after the beginning of heating (Fig. 5.5.2 and 5.5.3). At the roof, pressure increase started three months later indicating the beginning support by the backfill. This observation corresponded to decreasing drift closure rates about three months after the start of heating (Fig. 5.2.2). Pressure increase at the floor started not until six months after heating had begun.

Since 1991, all pressure gauges recorded a continuous rise in backfill pressure (Fig. 5.5.2 and 5.5.3). Sudden drops were caused by short-term heater breakdowns

resulting in a thermally induced relaxation of stress. The immediate response of the gauges to interruptions of heat input was a prove for their correct function. First reactions were observed at the roof and wall gauges, followed by the gauges at the floor. From the increasing sensitivity of the backfill to power failures, an increasing backfill rigidity can be derived starting from its upper part.

Further pressure changes were caused by replacement measures for failed measuring gauges. In March 1992, a sudden pressure increase was caused in the sections B, G1, and D1 (Fig. 5.5.2) by the overcoring of boreholes in section G1 /DRO 96/. In the end of 1996, the measurements were affected by further boreholes drilled into the heated backfill for the replacement of failed drift closure measuring gauges. Pressure decreases were recorded in the sections B, D2, and G1 with section B in the southern drift and section D2 in the northern drift being the most concerned (Fig. 5.5.3).

Generally, the highest backfill pressure was observed at the roof ranging between 3 - 4 MPa at the end of the heating phase (Fig. 5.5.4). Horizontal pressure values reached between 1.7 - 2.8 MPa at the walls (Fig. 5.5.5) and 1.8 - 3.5 MPa at the pillar walls (Fig. 5.5.6) being always somewhat higher at the pillar side. In section G1, even 4 MPa were recorded at the pillar wall in the southern drift (Fig. 5.5.6). Usually, the wall pressure reached only 50 - 80 % of the roof pressure. The pressure at the floor ranged between 1.6 - 2.7 MPa corresponding to 50 - 65 % of the roof pressure.

The pressure gradient between the bottom and the top of the backfill was probably caused by the heater casks which were hard inclusions in the less rigid backfill leading to a decrease in backfill pressure towards the drift floor. In the non-heated backfill, however, pressure increase at the floor was also lower than at the drift walls. For a final evaluation of the observed behaviour, the dismantling of the experiment is being required.

Usually, the backfill pressure in the northern drift reached only 70 % of the pressure in the southern drift probably due to lower drift closure rates (see chapter 5.2). In cross section D2, however, the backfill pressure in the northern drift was up to 50 % higher than in the southern drift. The different values may be ascribed to non-homogeneous backfill compaction leading to a varying local backfill rigidity. During the dismantling of the experiment, the reasons for different backfill pressures may be found by studying the local backfill density distribution.

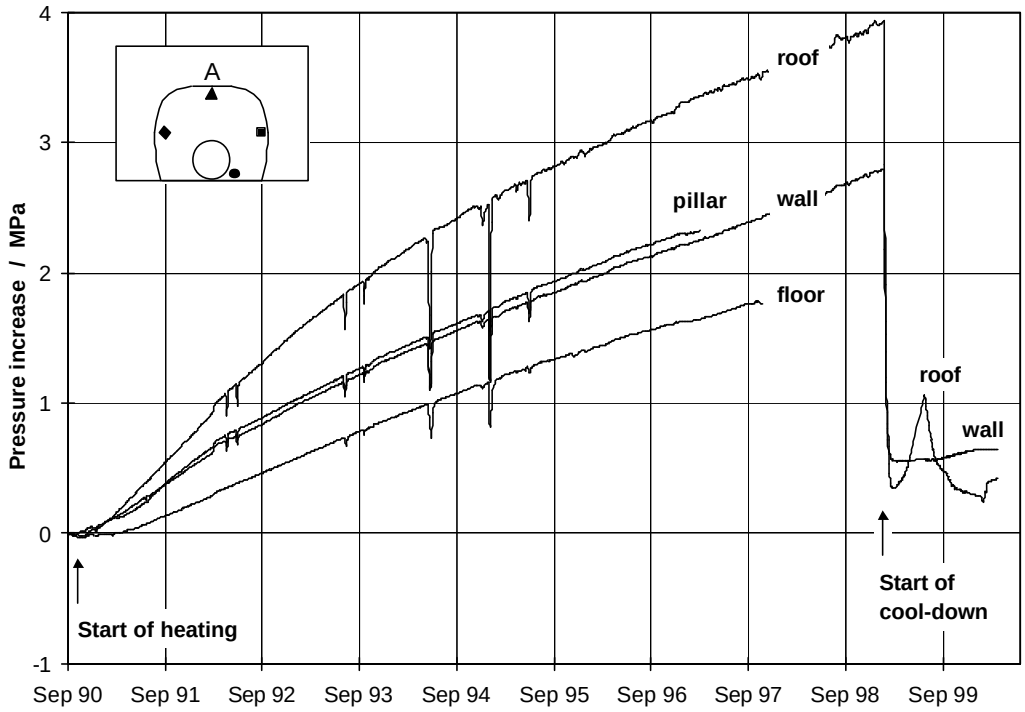

Fig. 5.5.2 Backfill pressure in the heated area (section D1)

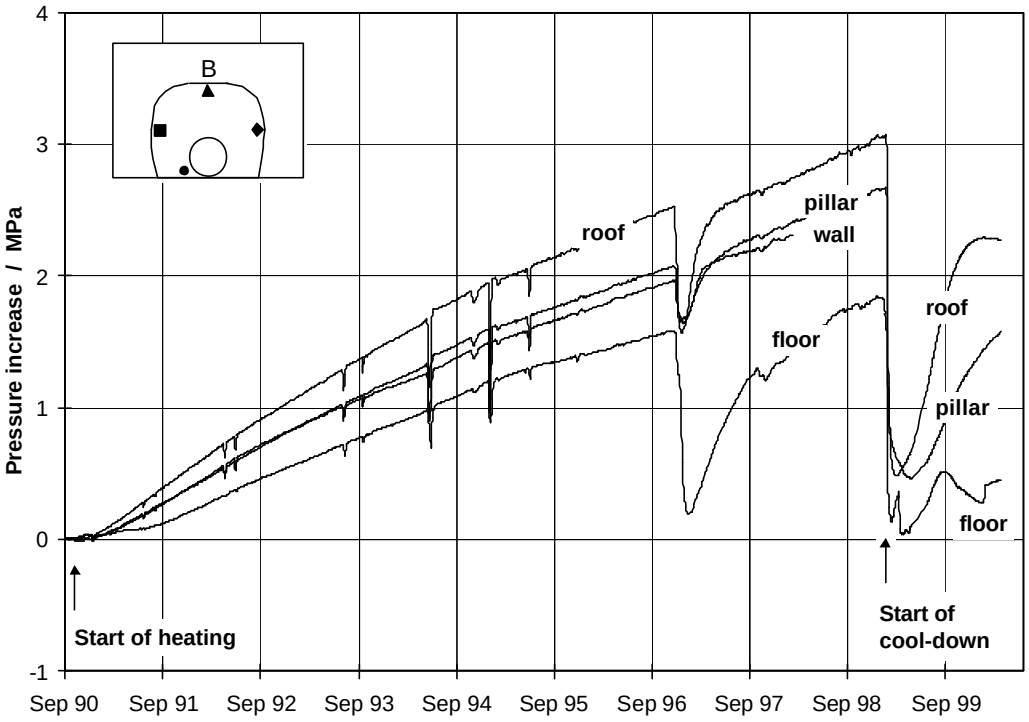

Fig. 5.5.3 Backfill pressure in the heated area (section D2)

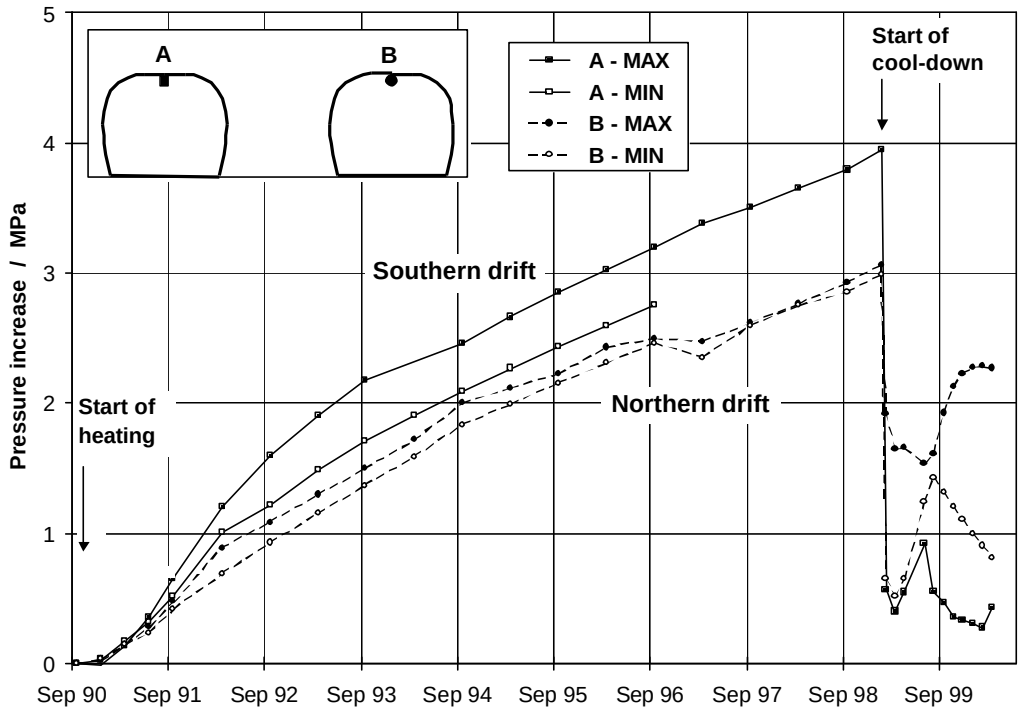

Fig. 5.5.4 Range of vertical backfill pressure at the roof in the heated area

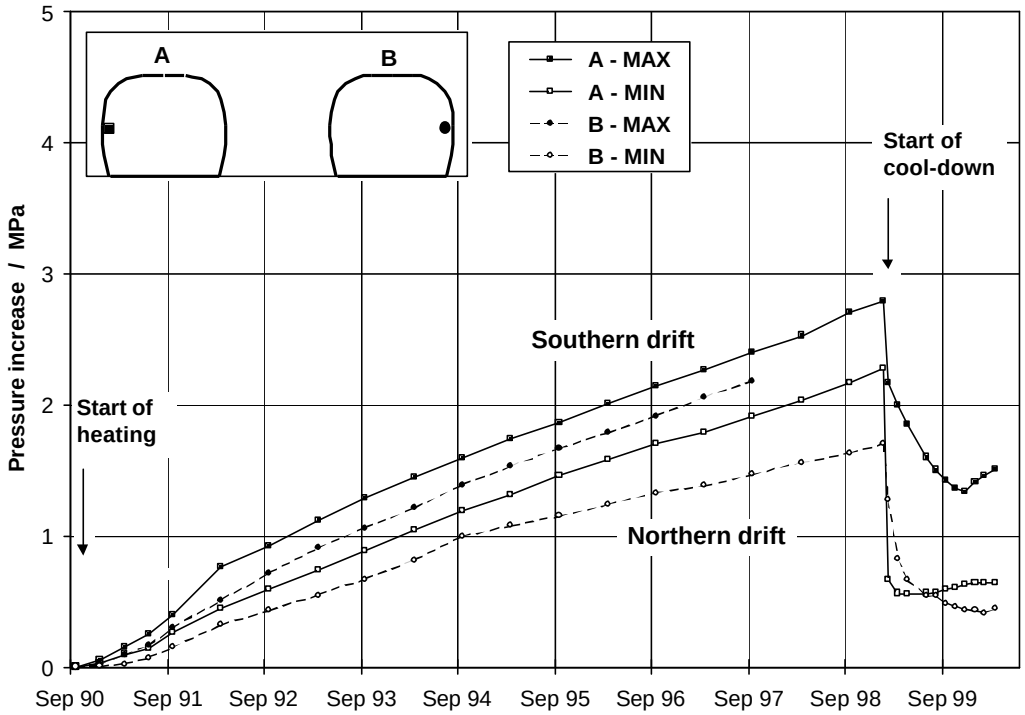

Fig. 5.5.5 Range of horizontal backfill pressure at the wall in the heated area

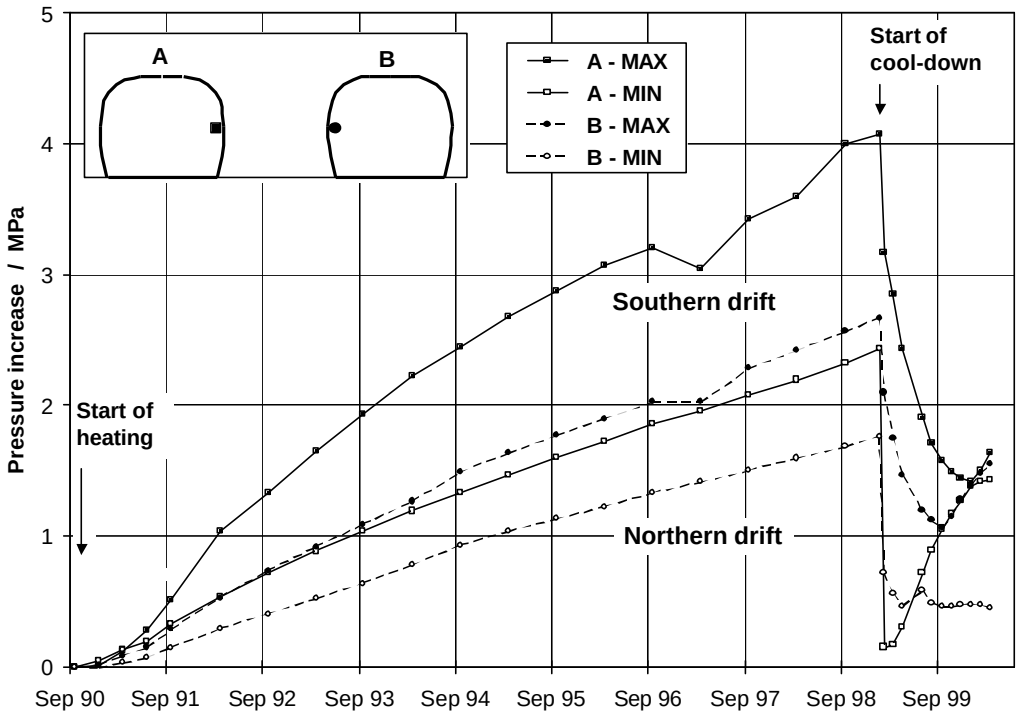

Fig. 5.5.6 Range of horizontal backfill pressure at the pillar in the heated area

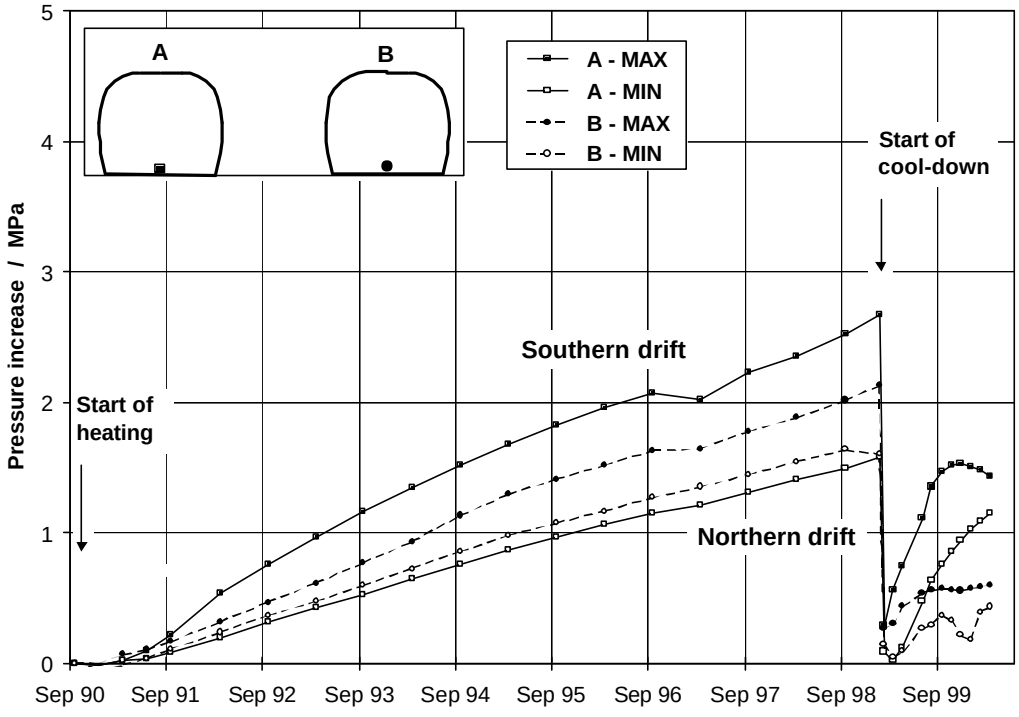

Fig. 5.5.7 Range of vertical backfill pressure at the floor in the heated area

At the end of the heating phase, the average backfill pressure had reached 3.3 MPa at the roof which was 27.5 % of the initial vertical stress estimation of 12 MPa in the test field /HEU 95/. Due to the overburden, a rock pressure of about 18 MPa had to be expected, but lithostatic stress had been reduced by the mining activities in the Asse salt mine (see chapter 5.5.2).

After the heaters were switched off, the backfill pressure dropped rapidly due to thermal contraction of the cooling backfill down to 0.3 –0.7 MPa at the roof and walls and even to 0.05 MPa at the drift floor (Fig. 5.5.2 to 5.5.7). Only in section G1 between the heater casks, pressure decrease was slower and kept decreasing until the end of March 2000. After its rapid decrease, the backfill pressure increased again at several locations as the contact between backfill and surrounding rock salt was re-established again. Especially in section D2, a significant pressure increase was recorded up to 2.3 MPa at the end of March 2000 (Fig. 5.5.3). In the other cross sections, the backfill pressure in the heated area was between 0.4 – 1.6 MPa at the end of March 2000.

5.5.2 Rock Stress

Generally, the techniques for measuring stress in a rock mass are classified into determination of absolute stress and measurements of stress variations. Absolute stress measurements were carried out by BGR to determine the initial state of stress in the test field. From the stress release in slot cutting tests and by means of the overcoring method, an initial stress of approximately 12 MPA was estimated /HEU 95/. The obtained lithostatic stress in the test field, however, was considerably lower than the expected lithostatic overburden pressure of about 18 MPa. The reduced rock stress in the test field was caused by far-field creep and stress relaxation around the large excavations in the Asse mine remaining from former salt mining. The results were confirmed by back-calculation of drift closure measurements which were recorded in the first 1.5 years prior to heating. Using the steady-state creep model of BGR /HUN 94/, best fit of finite-element calculations and measured drift closure was obtained with an initial rock stress of 12 MPa /HEU 95/.

In the heating phase, the actual total stress was again determined by BGR by hydrofracturing measurements in the heated host rock beside the northern test drift /BEC 99/. In March 1997, a minimum principal rock stress between 16 and 17 MPa was measured. This value was considerably higher than the initial rock stress due to the significant increase in thermally induced stress after the start of heating.

For the determination of stress variations, stress monitoring probes were installed in boreholes which recorded the stress changes throughout the testing period. Probe configuration and boreholes are described in chapter 3.2 and in /DRO 96/. To record already excavation-induced stress changes, a part of the probes was installed from the 750-m level prior to test drift excavation. The rigid inclusion stressmeters were bonded into the borehole to become an integral part of the rock mass, and as such responded directly to stress changes. Different types of concrete were tested for the embedding of the probes. Probe inclusion in the host rock was improved by subsequent injection of epoxy resin around the pressure cells leading to a pre-stressing of the gauges. The injection pressure was between 13 – 17 MPa, but decreased again as the resin shrank during hardening (Fig. 5.5.8 and 5.5.9).

The excavation of the test drifts on the 800-m level caused significant stress changes in spring 1989. The vertical stress above the excavated drifts was completely relieved as the vertical load was transmitted aside by arch action (Fig. 5.5.8). In the pillar, however, the vertical stress increased considerably (Fig. 5.5.9). Stress changes in horizontal direction depended on their direction. Above the excavated drifts, horizontal stress increased up to 11 MPa normal to the drift axis, but decreased distinctively parallel to the drift axis (Fig. 5.5.8). In the pillar, horizontal stress normal to the drift axis decreased considerably due to free expansion of the host rock, but increased parallel to the drift axis (Fig. 5.5.9).

After the excavation-induced stress redistribution, stresses changed only slightly until the start of heating. Backfilling of the test drifts caused only a small stress increase in summer 1990. Steady state conditions were not fully reached when heating started.

After the start of heating, the stress measurements showed a significant increase in rock stress by 1 to 5 MPa. In the floor below the heater casks, an increase of up to 7 MPa was measured. These thermo-elastic stress changes reached maximum values after a few months, but were only short-term effects. In the pillar, the maximum was reached after two months with the highest value of 13.5 MPa in horizontal direction parallel to the drift axis (Fig. 5.5.9). Above the test drifts, stress maxima were recorded three to five months after heating started with a magnitude of 15 MPa in horizontal direction normal to the drift axis (Fig. 5.5.8). Vertical stress above the test drifts, however, was hardly affected by heating.

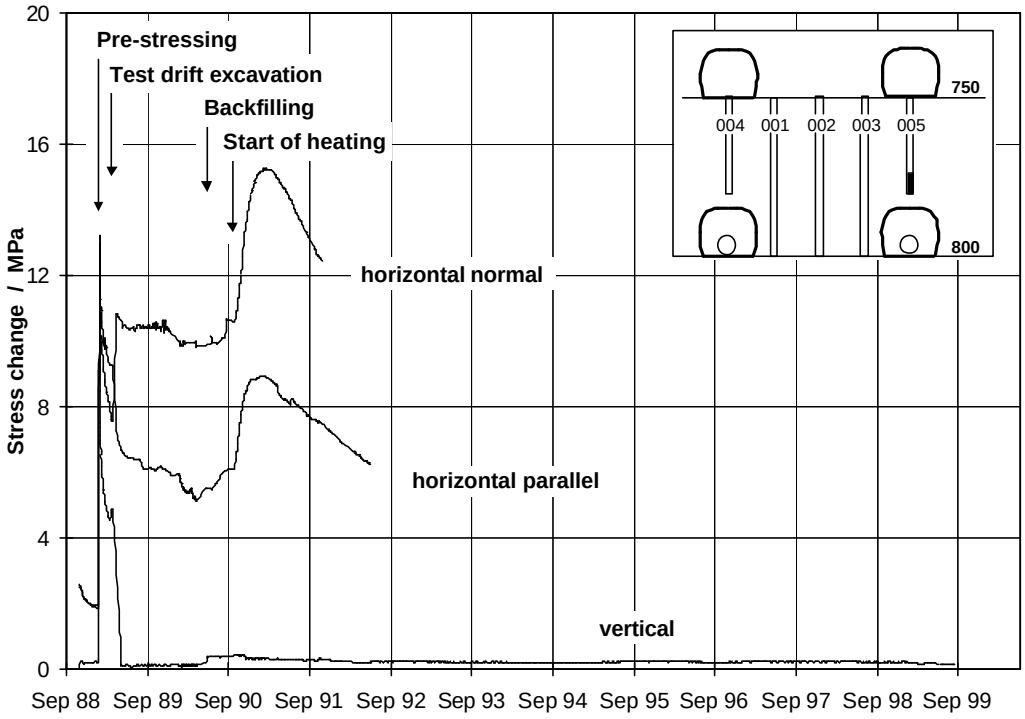

Fig. 5.5.8 Rock stress above the heated drifts (section B)

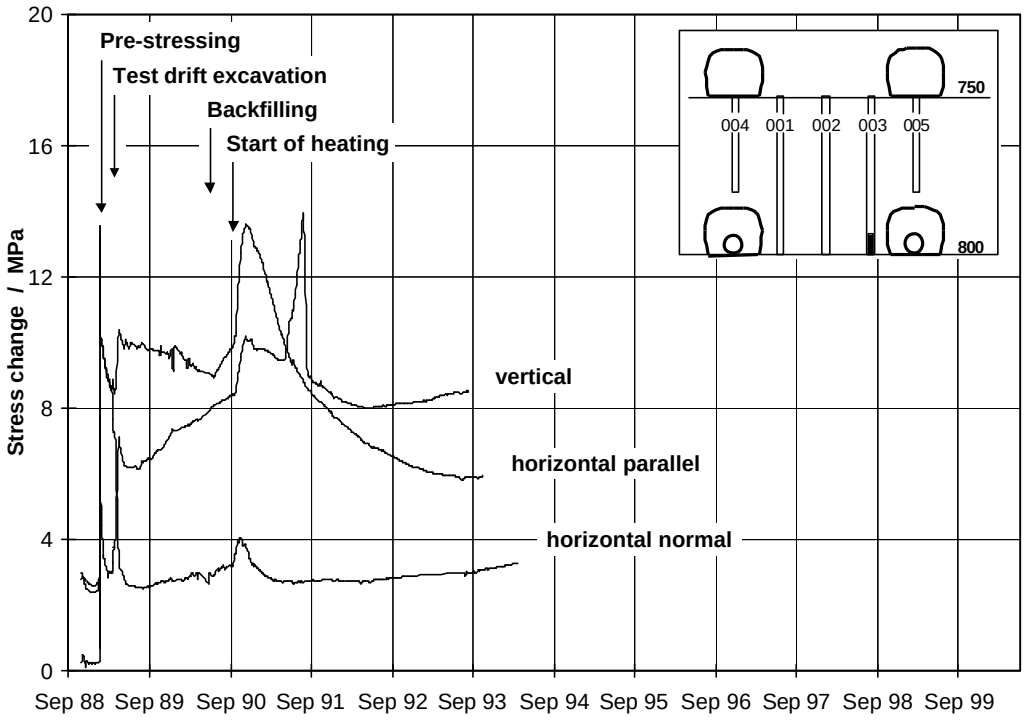

Fig. 5.5.9 Rock stress between the heated drifts (section B)

Due to relaxation of the thermally induced stress by creeping of the rock salt, rock stresses decreased again continuously reaching their original stress state prior to heating within two years. Occasionally, some gauges recorded an increase in rock stress in the relaxation phase (Fig. 5.5.9). Such pressure peaks, however, were only temporary phenomena. Due to the accelerated rock deformations around the heated drifts, most probes of GRS failed until 1995 what will be dealt with in chapter 8.2.3. But the monitoring probes of BGR showed a steady stress state in the pillar since 1994 /HEU 96/.

In the areas beside the test drifts farther away from the heater casks, a different stress development was observed by long-term stress measurements of BGR. With the start of heating, the stresses increased continuously over a long time and reached a maximum of up to 12 – 14 MPa after a couple of years /BEC 99/. Since 1996, the stresses were more or less constant until the end of the heating phase.

In July 1995, the failed gauges, which had been installed from the 750-m level, were replaced by probes of the same type which were embedded in special K-UTEC saltcrete. To improve probe inclusion in the host rock, the gauges were pre-stressed by epoxy resin injection in spring 1996. The injection pressure was between 8 – 12 MPa (Fig. 5.5.10 and 5.5.11). After the injection, the pressure decreased again rapidly due to resin hardening.

Subsequently, all replaced monitoring probes recorded increasing pressure values which approached the prevailing stress. In the pillar, steady state values were reached within one year with a magnitude of 5 – 7 MPa (Fig. 5.5.10). In the pillar centre, even 9 MPa were measured on the level of the test drift floor. Generally, vertical stress was definitely higher than horizontal stresses, and horizontal stress normal to the drift axis was slightly higher than parallel to the drift axis (Fig. 5.5.10).

Above the test drifts, the pressure increase was not as fast. Even after three years, steady state values had not been reached by all monitoring probes. Directly above the drifts, steady state conditions were achieved at magnitudes of 6 – 7 MPa in horizontal direction and 5 – 5.5 MPa in vertical direction (Fig. 5.5.11). Higher above, vertical stress approached the same value at the end of the heating phase, but horizontal stresses were still increasing (Fig. 5.5.11).

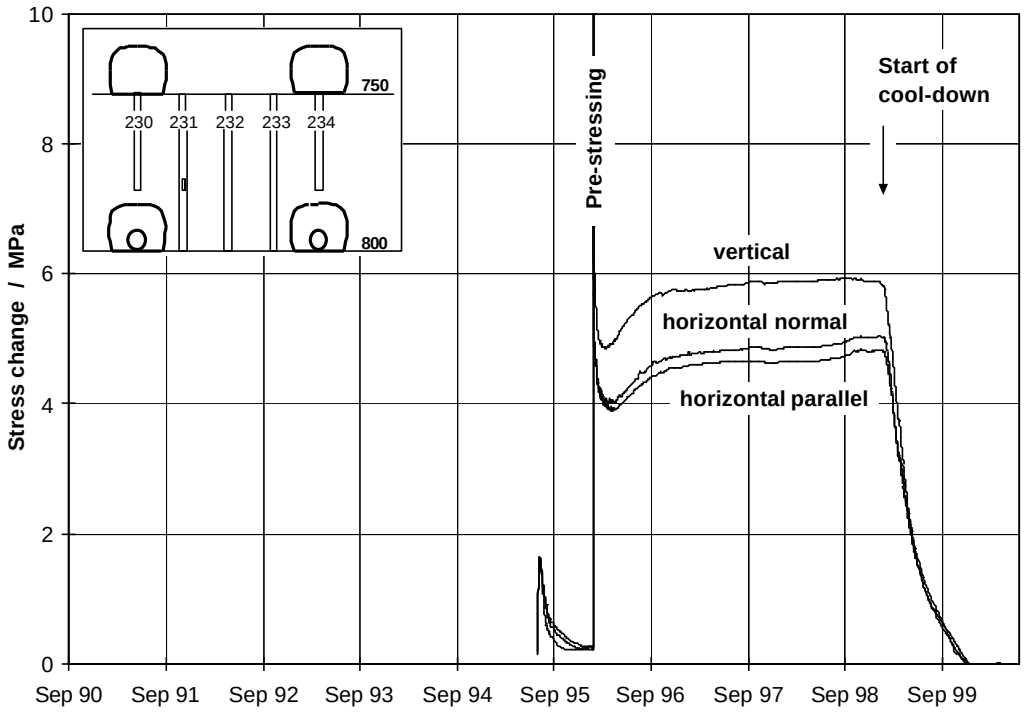

Fig. 5.5.10 Rock stress between the heated drifts recorded by replaced monitoring probes (section B^{+1})

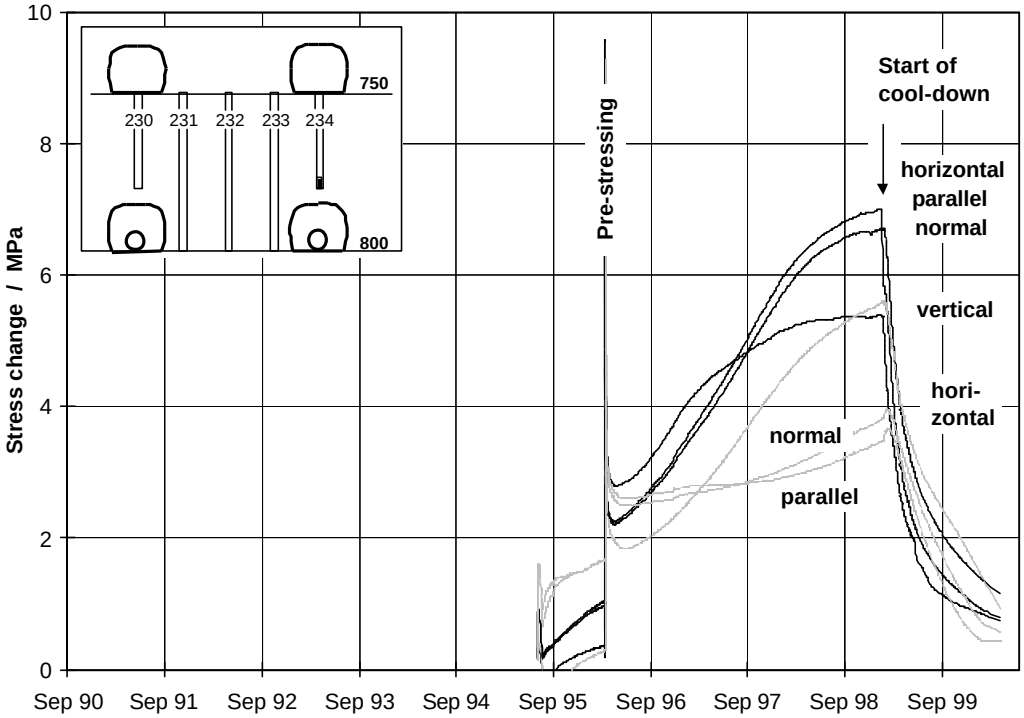

Fig. 5.5.11 Rock stress 1.5 – 2 m (solid curves) and 3 – 4 m (dotted curves) above the heated drifts recorded by replaced monitoring probes (section B^{+1})

After the heaters were switched off, all monitoring probes recorded a rapid pressure decrease due to relaxation of the thermally induced stress. In the pillar, the stresses dropped below 1 MPa within half a year (Fig. 5.5.10). Above the test drifts, the stresses decreased to 1 – 1.5 MPa within one year (Fig. 5.5.11). Higher above the drifts, a temporary stress increase of 0.1 – 0.2 MPa was recorded immediately after the heaters were switched off, but subsequently, the stresses decreased, too (Fig. 5.5.11).

5.6 Gas Generation and Transport

5.6.1 Gas Release

The primary objective of the gas measurements was to determine the chemical conditions near the corrosion samples which were located on the central heater cask and in the backfill. From these measurements, conclusions could be drawn, too, regarding gas generation and gas release. Gas sampling and analysis were described in /DRO 96/.

The most important gases analyzed in the backfilled drifts were hydrogen, methane, and carbon dioxide. Hydrogen was generated by corrosion of the heater casks, whereas methane and carbon dioxide were released from the backfill due to thermal desorption and thermal decomposition of salt minerals.

Prior to heating, the major gas components hydrogen, methane, and carbon dioxide were detected in the backfill in concentrations of 28 to 44 vpm, $\leq$ 4 vpm and 35 to 75 vpm, respectively. Assuming that the pore volume of the backfill was initially filled with mine air, these results indicated that hydrogen had already been generated at the ambient temperature of 36°C by corrosion or chemical interaction. The concentration of carbon dioxide was considerably lower than in the mine air due to adsorption of carbon dioxide at the surface of the backfill pore space.

Significant gas release started immediately after the heaters had been switched on. Within six months, the gas concentration increased up to 600 vpm hydrogen, 40 vpm methane, and 3000 vpm carbon dioxide (Fig. 5.6.1). These results indicate that cask corrosion was accelerated by the temperature increase causing significantly higher hydrogen concentrations. The carbon dioxide adsorbed at the surface of the crushed salt was released again at higher temperatures. More carbon dioxide was generated by

oxidation of hydrocarbons and release from the crystal lattice. Methane was desorbed from the surface of the backfill and from the crystal lattice. Furthermore, methane was generated by thermal decomposition of higher hydrocarbons.

in 1992 and 1994, sudden drops in gas concentration were caused by the overcoring of boreholes /BEC 97/. Generally, the concentration of the components varied in a range of 20 % within comparatively short times. These fluctuations were directly correlating with the air pressure at the entrance of the backfilled drifts which varied in a range of 50 mbar as a result of atmospheric pressure changes and variations in the mine ventilation leading to a flushing of the backfill.

Therefore, the gas concentration was constantly reduced due to the high porosity and permeability of the backfill. Consequently, the gas concentration decreased after one year of heating, indicating that gas production was lower than the escaping amount of gases. In order to estimate the total amount of gas generated, the northern test drift was sealed gastight at its entrance in February 1996. Consequently, the gas concentration increased considerably (Fig. 5.6.1).

In the end of 1996, the gas measurements were affected by drilling two boreholes for the replacement of failed measuring gauges causing a decrease in carbon dioxide concentration as well as a temporarily increased hydrogen production due to the borehole cementation. Subsequently, the gas concentration increased continuously until the end of 1998 (Fig. 5.6.1). The last measurements showed no further increase. It seems that the gas production in the sealed test drift had reached a steady state at the end of the heating phase.

During the heating period, gas sampling had to be stopped at several sampling points probably due to crystallizations at the surface of the glass filters in the backfill impeding further gas sampling. But damaged Teflon tubes which had been squeezed might have been responsible, too.

In the cool-down phase, the gas measurements were not continued as the results would have had no relevance for a final repository. The residual gas content in the backfill material, however, is important for characterizing the chemical conditions in the test drifts. During the dismantling of the experiment, backfill samples will be taken from the heated area for the determination of the residual gas content in the laboratory.

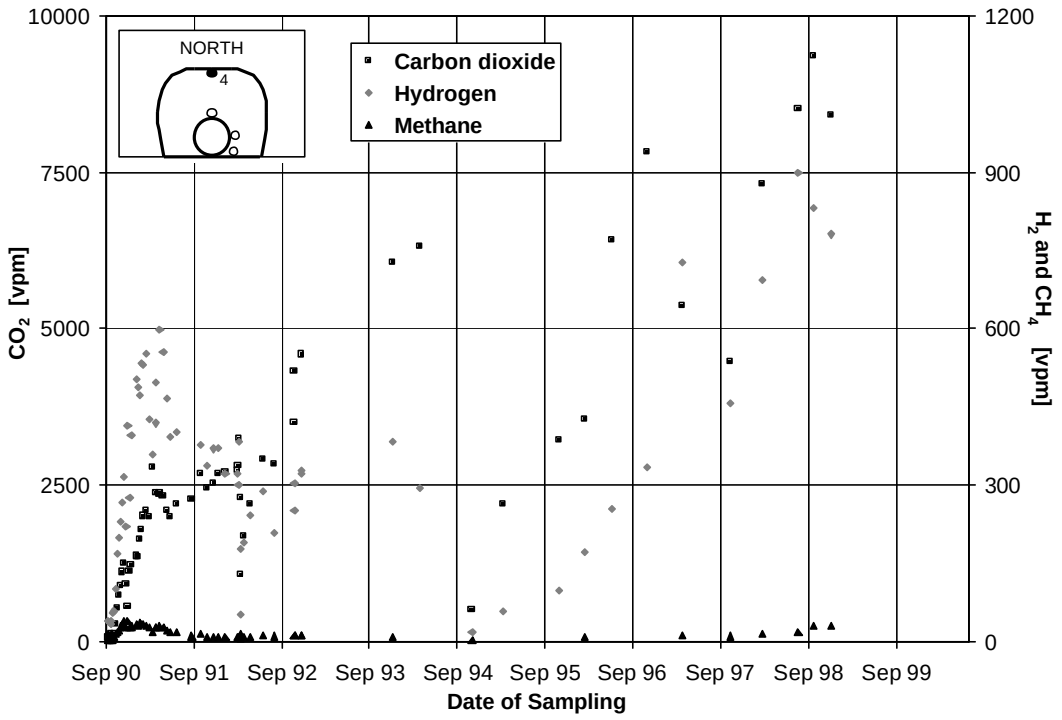

Fig. 5.6.1 Content of carbon dioxide, hydrogen, and methane in the backfill pore space at the roof of the northern test drift (section A: position B/A4)

In laboratory tests on crushed salt material, hydrochloric acid was released at temperatures over 80°C probably due to thermal decomposition of salt minerals like bischofite ($MgCl_2 \cdot 6\ H_2O$). In the test field, however, no hydrochloric acid was found. Obviously, all hydrochloric acid in the backfill reacted with the steel casks by generating hydrogen.

In conclusion, the gas generation in the test field was moderate. With the realized experimental set-up, however, it was not possible to quantify the total amount of gas which had been released.

5.6.2 Humidity

Cask corrosion and hydrogen generation were controlled by the water content in the backfill. Therefore, humidity was an important parameter for the chemical conditions in the backfill. Water was released from crystal surfaces and from hydrated minor minerals of rock salt. Samples from the backfill pore space were taken via the Teflon tubes of the gas sampling system.

First measurements were performed by means of a Binos gas analyzer device. Prior to heating, a water content of 15 - 20 g per m^3 air was determined in the pore volume of the backfill. After the start of heating, the humidity increased considerably due to dehydration of backfill and rock salt. After three months, the water content reached 42 - 50 g per m^3 air which is the saturation humidity at 40°C (Fig. 5.6.2). As the samples from the heated backfill were collected at the cold drift entrance, all values had to be corrected for temperature. The corrected humidity values are shown in Fig. 5.6.3. The corrected humidity values after three months of heating were 30 - 35 g water per m^3 air.

Subsequently, the water content exceeded the saturation humidity and water condensed inside the Teflon tubes. Though condensation stopped after one year, measurements were still not possible with the electronic gas analyzer device. In May 1995, another sampling technique was applied using a cooling trap. The measurements revealed that the water content had decreased to 20 - 25 g per m^3 air (Fig. 5.6.2) corresponding to corrected humidity values of 14 - 18 g water per m^3 air (Fig. 5.6.3). The water samples had a pH-value of 3.42.

Since the end of 1996, humidity measurements were carried out periodically using Dräger short-term tubes. In the access drifts, a humidity of 5- 12 g water per m^3 air was measured at 1096 hPa and 36°C ambient temperature (Fig. 5.6.2 and 5.6.3). In the heated backfill, the water content was between 28 - 38 g per m^3 air (20 - 30 g water per m^3 air corrected for temperature). Only in March 1997, a lower humidity of 23 - 28 g water per m^3 air was recorded (17 - 23 g water per m^3 air corrected for temperature).

Since the Dräger tube measurements revealed low molecular alcohols and further organic compounds, another method was applied since 1998, using Merck absorption tubes for water. By this gravimetric method, an absolute concentration in the same range of 27 - 34 g water per m^3 air was determined (21 - 27 g water per m^3 air corrected for temperature).

In the cool-down phase, the water content decreased from 23 - 28 g water per m^3 air in February 1999 to 13 - 25 g water per m^3 air in March 2000 (Fig. 5.6.2). But due to the temperature decrease in the backfill after the heaters had been switched off, the required temperature correction was lower. The corrected humidity values were 19 - 23 g water per m^3 air (February 1999) and 12 - 23 g water per m^3 air (March 2000) (Fig. 5.6.3).

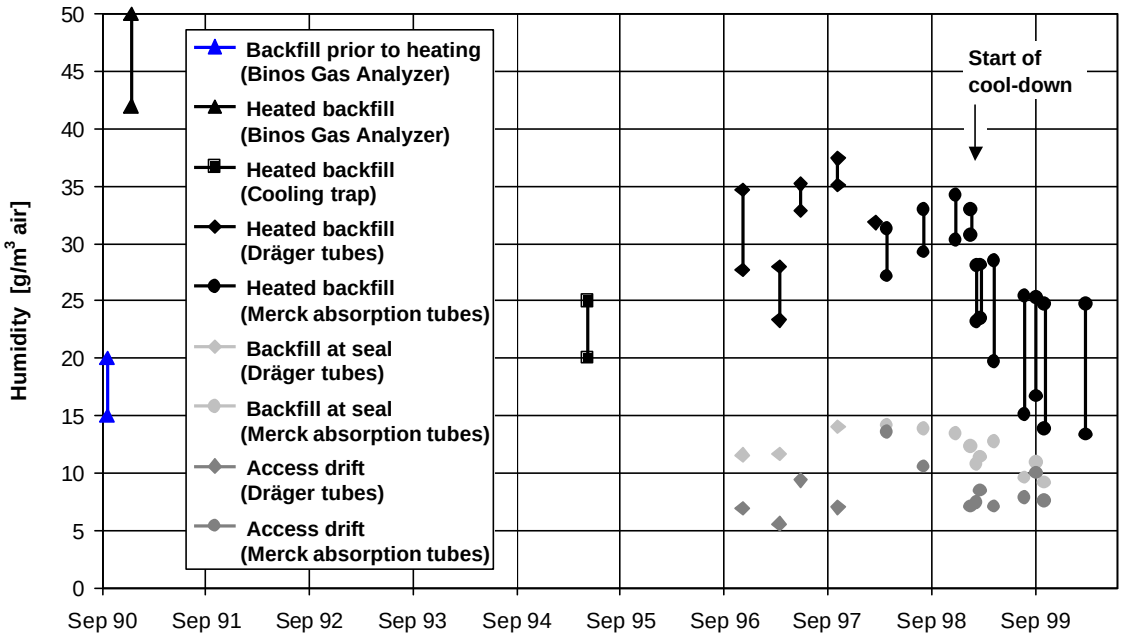

Fig. 5.6.2 Humidity in the backfill pore space (determination with different methods)

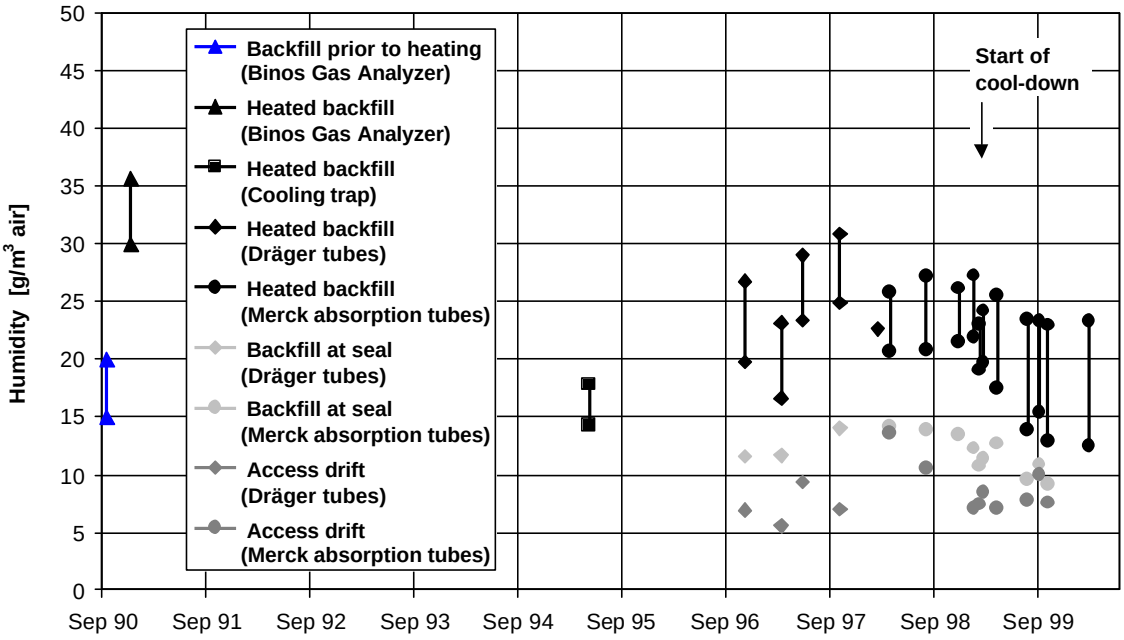

Fig. 5.6.3 Humidity in the backfill pore space: values corrected for temperature (determination with different methods)

From the humidity measurements, a total water content of 0.0003 – 0.0004 % (corrected for temperature and related to a backfill porosity of 25 %) was estimated for the heated backfill after eight years of heating. Considering the average water content of about 0.1 % in rock salt, the very low water content proved that the backfill had been dehydrated significantly by heating.

To confirm the humidity measurement results, backfill samples will be taken from the heated area during drift excavation for the determination of the residual water content in the laboratory.

5.6.3 Gas Diffusivity

Gas diffusivity of the heated backfill was determined by neon tracer gas injection. Neon was used because of its negligible content in the mine air. In a first attempt, the tracer gas was injected via a Teflon tube of a gas sampling point. By repeated gas sampling from the glass filters around and analyzing the neon content, the tracer gas migration within the pore volume of the backfill was supposed to be determined. However, the results could not be used for diffusivity calculation as the gas migration was not spherical.

Using another assumption, gas diffusivity could be successfully determined. Again, neon gas was injected at a glass filter which was located at the upper surface of a central cask. By subsequent gas sampling from the same glass filter, the resulting neon gas concentration was determined at the interface to the surrounding crushed salt. Thus, finite-difference calculations with a spherical model were possible assuming a theoretical distance of 0.1 m between injection and sampling. The calculated diffusivity ranged between $1.4 \cdot 10^{-5}$ m^2/s and $3.7 \cdot 10^{-5}$ m^2/s. From these values, the diffusivity for other gases in the backfill can be calculated.

5.6.4 Volatile Organic Compounds

During heating, volatile organic compounds were released by thermal disintegration of plastic materials from the installed measuring equipment. These compounds could affect working conditions during drift excavation. Therefore, the organic compounds and their concentration were determined in advance. The values were compared with the limits prescribed by law for working conditions according to safety regulations.

For sampling, a horizontal borehole was drilled into the heated backfill of the northern test drift. The work was carried out at the end of the cool-down phase in order to minimize interferences with the geotechnical measurements. Backfill samples were taken from different positions in the borehole. Sampling was also done from the air of the backfill pore space and the air in the access drifts. Sampling and analyses were carried out by the Institut für ökologische Chemie und Abfallanalytik of the Technische Universität Braunschweig.

In the samples taken from the backfill, a wide range of volatile organic compounds was detected comprising aliphatic and aromatic hydrocarbons, chlorinated and brominated hydrocarbons as well as oxygenated organic compounds like aldehydes, ketones or ester. High-volatile halogenated hydrocarbons were detected in the range of µg/m³. A maximum concentration of 1.04 mg/m³ was found for chloroform. In the ventilated access drifts, the concentration of all volatile organic compounds was below 0.005 mg/m³. All measured values were below the limits prescribed by law for working conditions (MAK-values and TRT-values).

During the dismantling of the experiment, acceptable working conditions can be assured if the excavated test drift is ventilated adequately. However, further measurements will be carried out on samples from the air and the backfill to check the working conditions regularly.

5.7 Excavation Disturbed Zone

Deviatoric stress situations around underground disposal rooms may lead to the development of excavation disturbed zones, the permeability of which being significantly higher than that of the undisturbed rock. These zones represent potential pathways for radionuclides released from waste canisters. Hence, healing of these zones after the installation of geotechnical barriers or the emplacement of backfill material would be advantageous. Therefore, the permeability in the rock around the test drifts was investigated at the end of the heating phase. These investigations will be continued and terminated within the framework of the project BAMBUS II.

For the measurements, two boreholes, P3 and P4, with a diameter of 86 mm were drilled parallel to the walls of the northern and the southern test drifts, at distances of 1.5 m and 0.5 m, respectively (Fig. 5.7.1). Measurements were carried out both in the

non-heated area and the heated area beside the test drifts. The measuring points were selected under consideration of a maximum packer temperature of the used probe of about 80°C. In borehole P3, measurements were performed at depths of 13 m at a temperature of 44°C and 27.75 m at a temperature of 71°C. In borehole P4, measuring points were at depths of 9.8 m at a temperature of 43°C and 27.5 m at a temperature of 80°C.

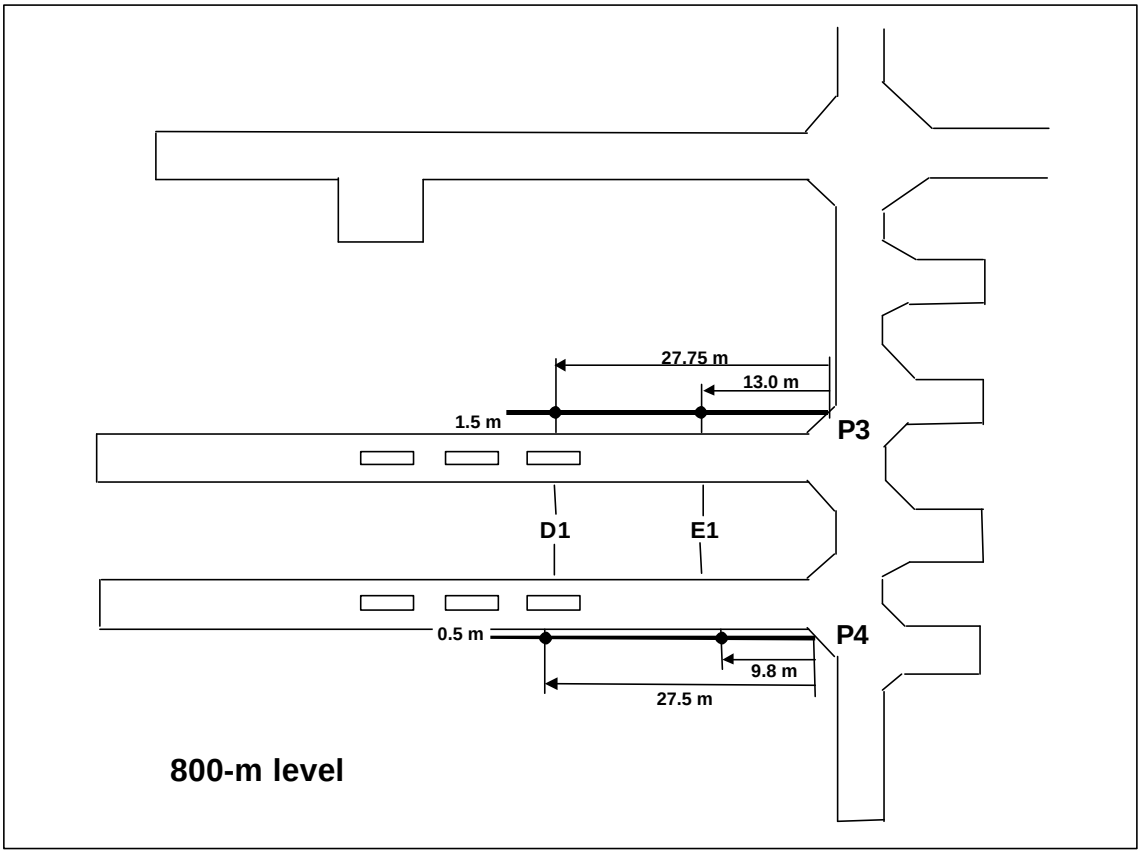

Fig. 5.7.1 Location of permeability measurement boreholes in the TSDE test field

For the permeability measurements, a four-packer probe was used with a 0.8-m-long central test interval and two control intervals of 0.3 m length each at both sides of the test interval. The packers had a length of 0.4 m and were pressurized individually with hydraulic oil up to about 8 MPa. Test fluid was nitrogen gas which was injected into the test interval with a maximum injection pressure between 1.6 and 2.1 MPa. Further details about the measuring equipment and the performance of permeability measurements are described in /WIE 98/.

Because low permeability values were expected, pulse injection tests were performed in all cases. During the injection phase, a constant nitrogen gas flow of 500 to 550 ml/min was applied. During the injection phases, no measurable gas flow into the surrounding rock was detected. The following shut-in phases lasted up to fourteen days.

In Figures 5.7.2 to 5.7.5, the measured and calculated pressure decay curves are shown. The calculations were performed with the commercial code Weltest 200 /SGE 97/ which was originally developed for oilfield reservoir engineering. The calculations yield optimum formation parameters, among them permeability, on the basis of a chosen "reservoir model". The following model assumptions were made:

- The formation is homogeneous and infinite and has a porosity of 0.2 %.
- Partial water saturation in the pore space is neglected.
- The borehole has a finite radius and a respective storage capacity.

All permeability values determined from the four measurements in the excavation disturbed zone were in the order of 10^{-22} m^2. In all cases, the measured pressure decay rates showed a linear trend after some hours indicating that packer leakage rates were higher than gas flow rates into the surrounding rock. From this fact it can be concluded that real permeability values were even smaller than the determined values which represented the limit.

Permeability values of less than 10^{-22} m^2 correspond to non-disturbed rock salt, thus indicating that if an excavation disturbed zone had existed after drift excavation, it was healed during heating. Healing is also indicated by recrystallization of the rock salt in the heated area resulting in very large salt crystals which were observed in the cores from both boreholes.

However, the zone directly at the drift walls could not be examined in these tests. But during the post-test investigations, permeability measurements and chemical-mineralogical analyses of the excavation disturbed zone directly around the dismantled test drift will be performed to verify if healing took place.

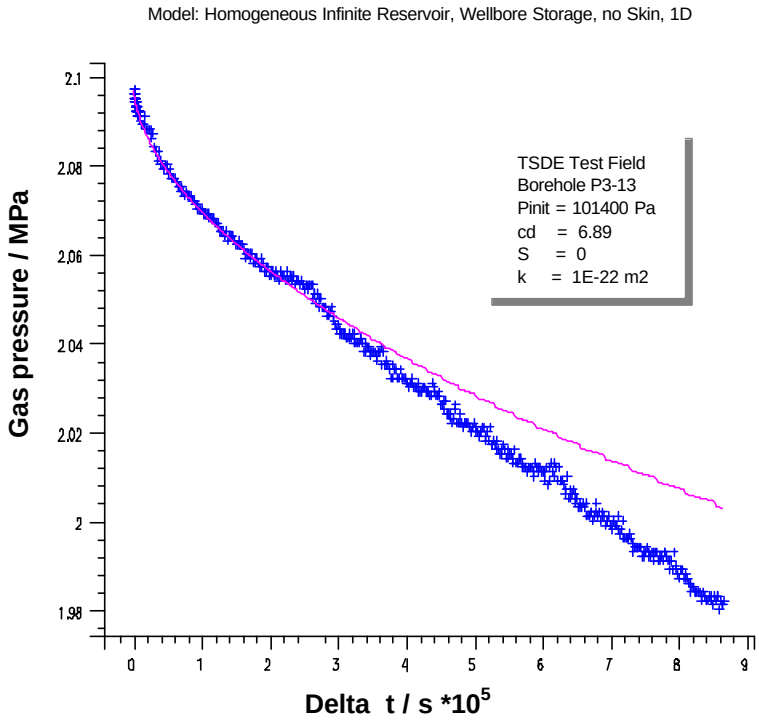

Fig. 5.7.2 Measured and calculated pressure decay in borehole P3 at 13 m depth

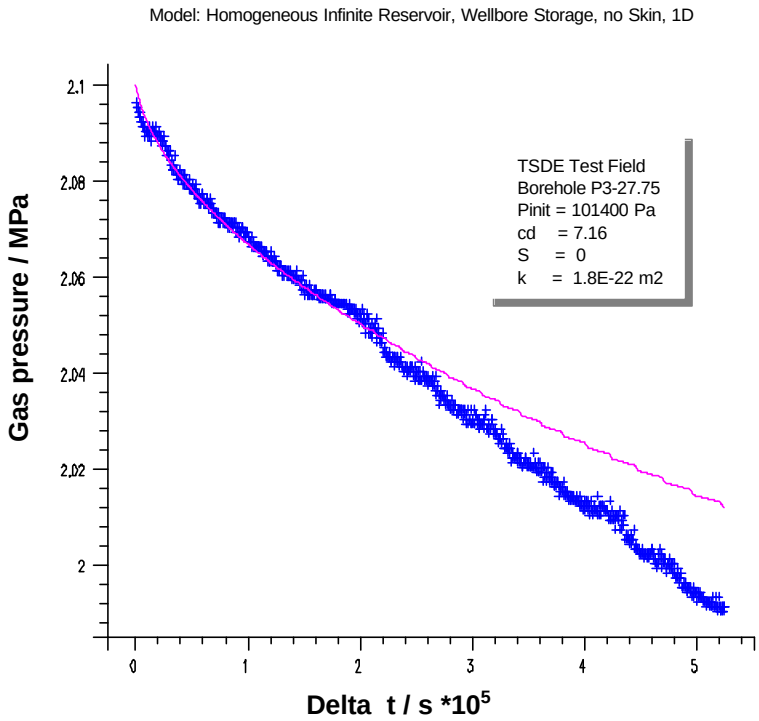

Fig. 5.7.3 Measured and calculated pressure decay in borehole P3 at 27.75 m depth

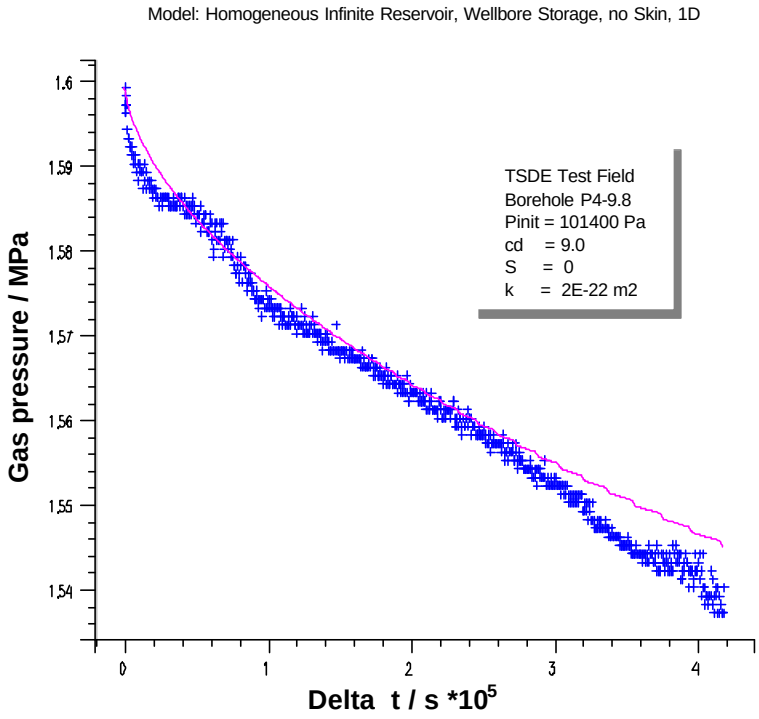

Fig. 5.7.4 Measured and calculated pressure decay in borehole P4 at 9.8 m depth

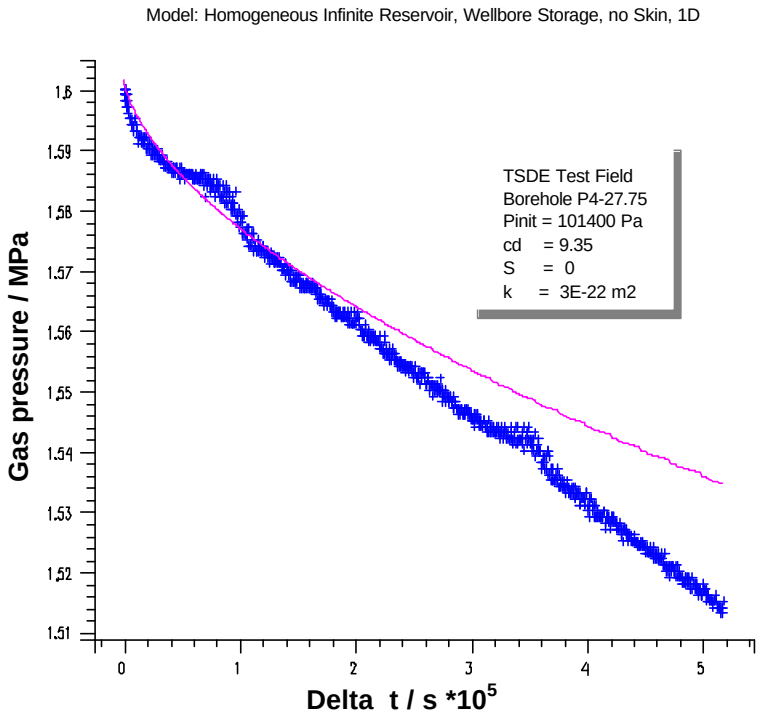

Fig. 5.7.5 Measured and calculated pressure decay in borehole P4 at 27.5 m depth

6 Comparison of Measurements and Modelling Results

Thermal and thermomechanical modelling of the TSDE test was not part of the GRS work, but was performed and improved by the other project partners since the beginning of the experiment /KOR 91/, /HEU 96/, /PUD 97/, /PUD 98/, /PUD 99/. In the frame of the BAMBUS project, different modelling teams (FZK-INE, ENRESA-CIMNE / Spain) were involved in the numerical analysis, too /BEC 99/. These investigations were aimed to validate and further refine the models by comparing numerical results with experimental data in order to predict the thermomechanical processes in a repository for heat generating waste in rock salt. In this chapter, some representative results of the model calculations are presented together with the experimental data to enable an adequate assessment of the in-situ measurements.

6.1 Thermal Modelling

Thermal analyses were performed by FZK-INE basing on a three-dimensional model of the test field geometry /KOR 91/, /PUD 97/. The thermal conductivity of crushed salt was described as a function of temperature and porosity.

The calculated temperatures corresponded quite well with the measurements in the test drifts. Typical results of calculated and measured temperature developments at different positions are presented in Figures 6.1 to 6.4. In the heated area, the calculations predicted the rapid temperature increase after the start of heating with a peak temperature of 212°C at the surface of the central cask. The following temperature decrease due to the increasing thermal conductivity of the compacting backfill was also well simulated by the calculations.

Further calculations were carried out to predict the temperature development in the cool-down phase /PUD 99/. The comparison of these values with the data measured since the heaters had been switched off showed a good agreement, too (Fig. 6.1 to 6.4). Taking into account the offset between calculated and measured values at the end of the heating phase, the conformity in the cool-down phase was even excellent.

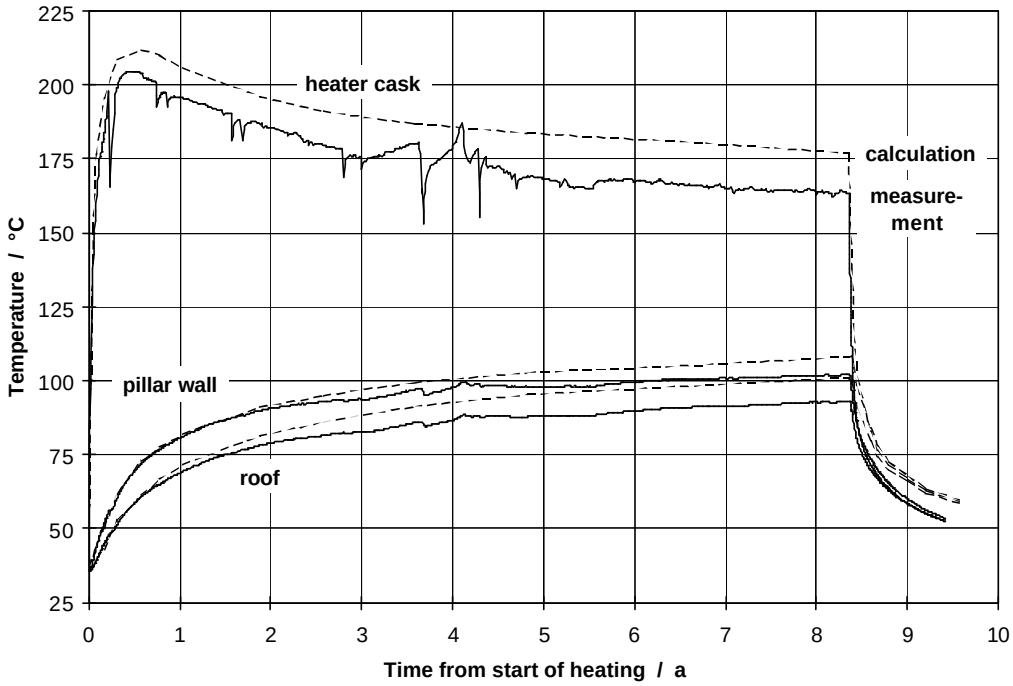

Fig. 6.1 Comparison of calculated (dashed curves) and measured (solid curves) temperatures around the central heater cask and at its surface (section A)

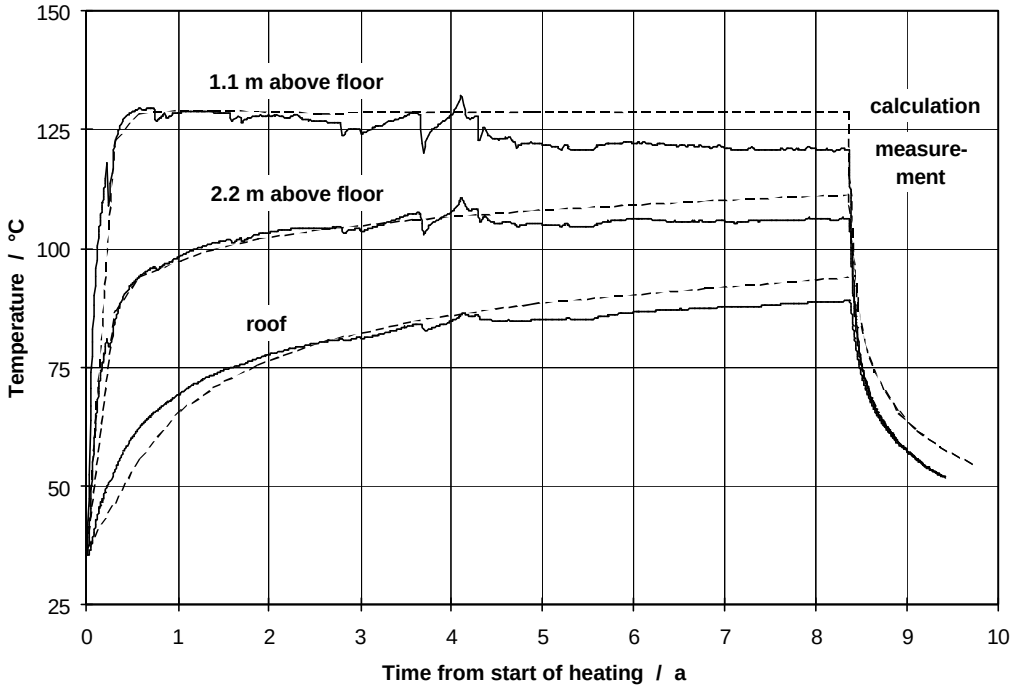

Fig. 6.2 Comparison of calculated (dashed curves) and measured (solid curves) backfill temperatures between the heater casks (section G2)

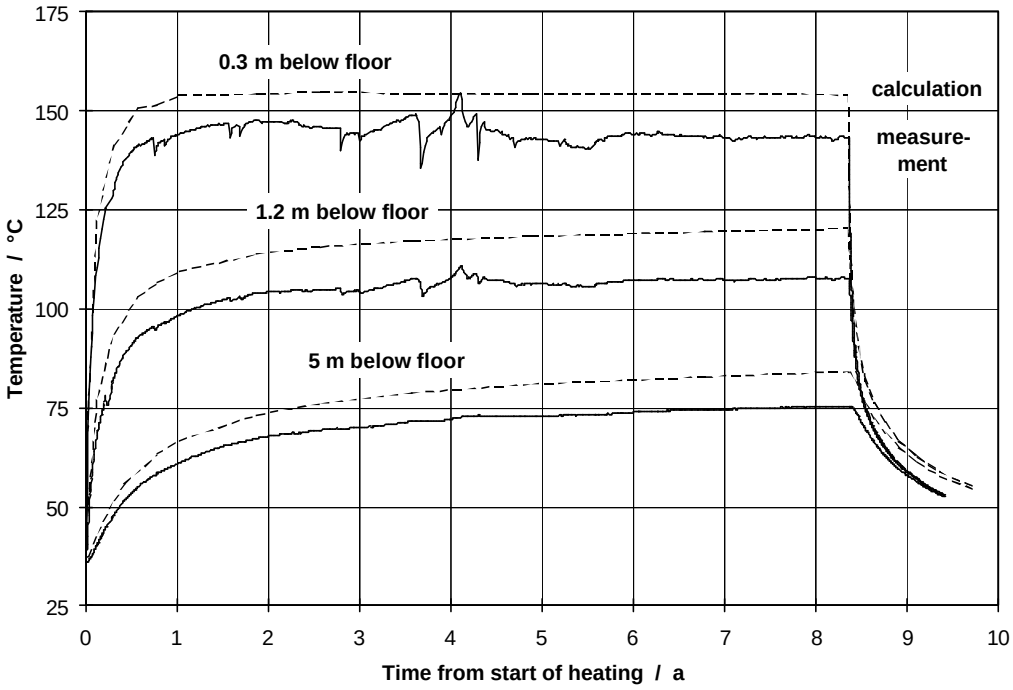

Fig. 6.3 Comparison of calculated (dashed curves) and measured (solid curves) rock temperatures below the central heater cask (section A)

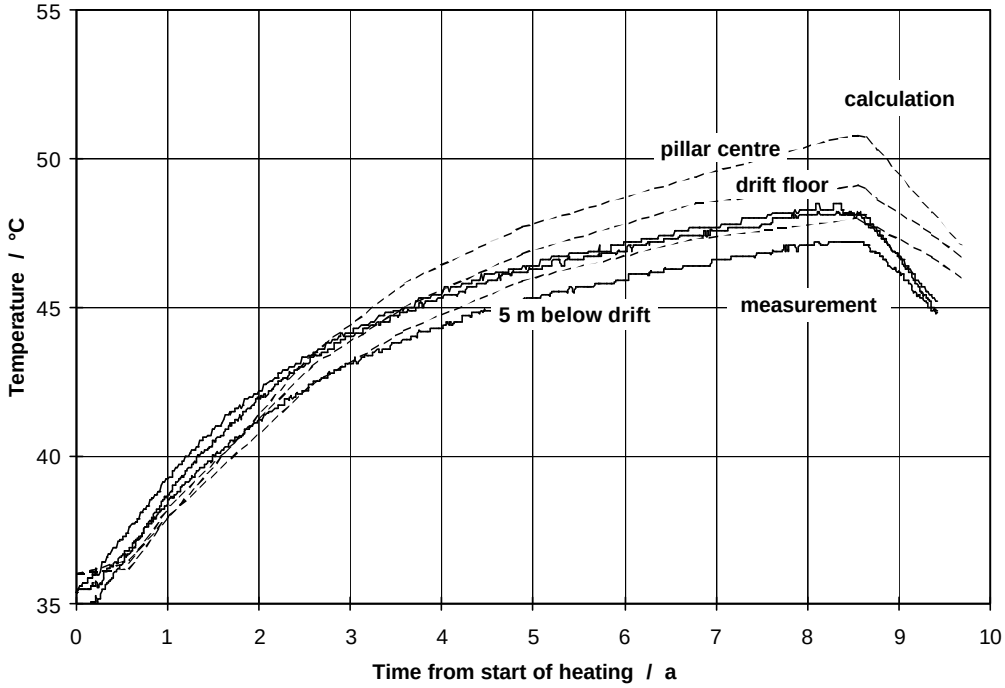

Fig. 6.4 Comparison of calculated (dashed curves) and measured (solid curves) temperatures in the non-heated area (section E2)

ENRESA-CIMNE computed thermal fields, too, using two-dimensional coupled thermomechanical calculations. By neglecting the temperature dependence of thermal conductivity and selecting a reduced constant value, the overestimation of the temperatures caused by the two-dimensional approximation was compensated /BEC 99/.

In summary, the temperature field was well reproduced by thermal modelling as proved by the coincidence of experimental and calculation results. Temperatures can be predicted adequately for repository performance assessments. Actually, the development of computer codes for temperature calculations simulating repository conditions is considered completed.

6.2 Thermomechanical Modelling

Basing on the temperature field obtained by thermal modelling, thermomechanical analyses were carried out by FZK-INE. To perform the analyses with reasonable numerical effort, a two-dimensional finite element model was used assuming generalized plane-strain conditions /PUD 98/, /PUD 99/. Two different constitutive models were applied for the backfill material. The earlier calculations based on a hydrostatic model for crushed salt /KOR 91/, /PUD 98/. Recently, additional numerical analyses have been performed using a deviatoric constitutive model /KOR 99/ which had been developed in the benchmarking exercise "Comparative Study on Crushed Salt" /BEC 99/.

Results from these thermomechanical calculations in comparison with in-situ measurements are shown in Figures 6.5 to 6.8. The development of drift closure in the non-heated area revealed a good correspondence with the calculated values (Fig. 6.5). In the heated area, however, drift closure was considerably lower than expected being overestimated by the calculation with the hydrostatic model by about 40 % (Fig. 6.6). With the deviatoric model, the deviations in drift closure were even larger /PUD 99/. As a result of the lower convergence rates, the decrease of backfill porosity in the heated area was also much slower than predicted (Fig. 6.7). The backfill pressure in the heated area was significantly lower than calculated by the hydrostatic model (Fig. 6.8), but comparison is problematical as deviatoric backfill behaviour cannot be calculated with the hydrostatic model /PUD 98/. The deviatoric model developed in the BAMBUS benchmark showed a much better agreement of backfill pressure values /PUD 99/.

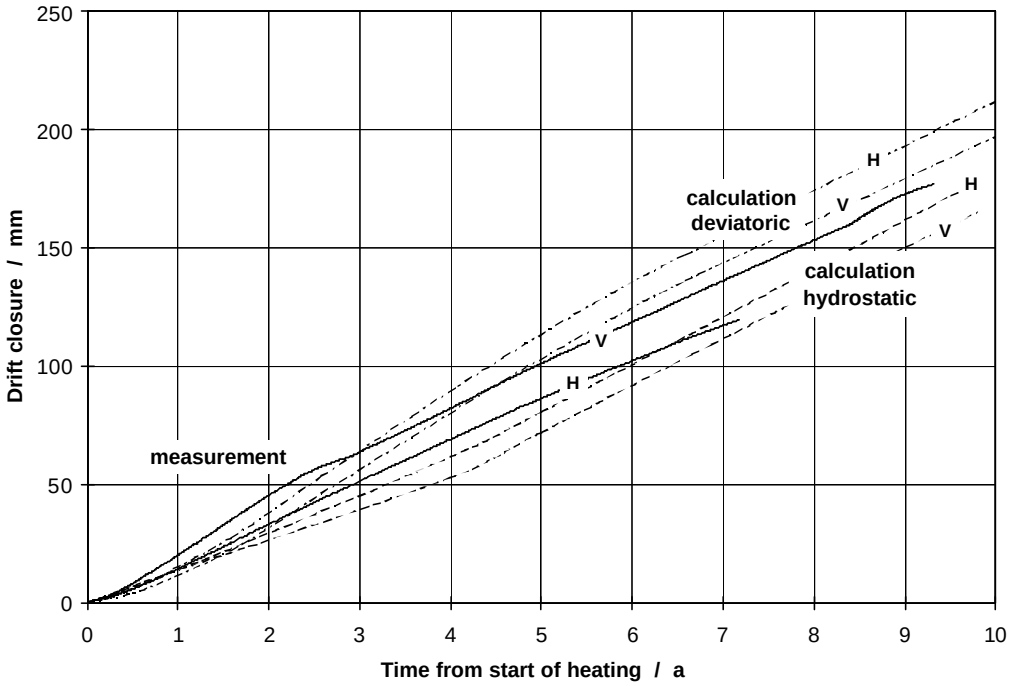

Fig. 6.5 Comparison of calculated (dashed curves) and measured (solid curves) drift closure in the non-heated area (V – vertical, H – horizontal closure)

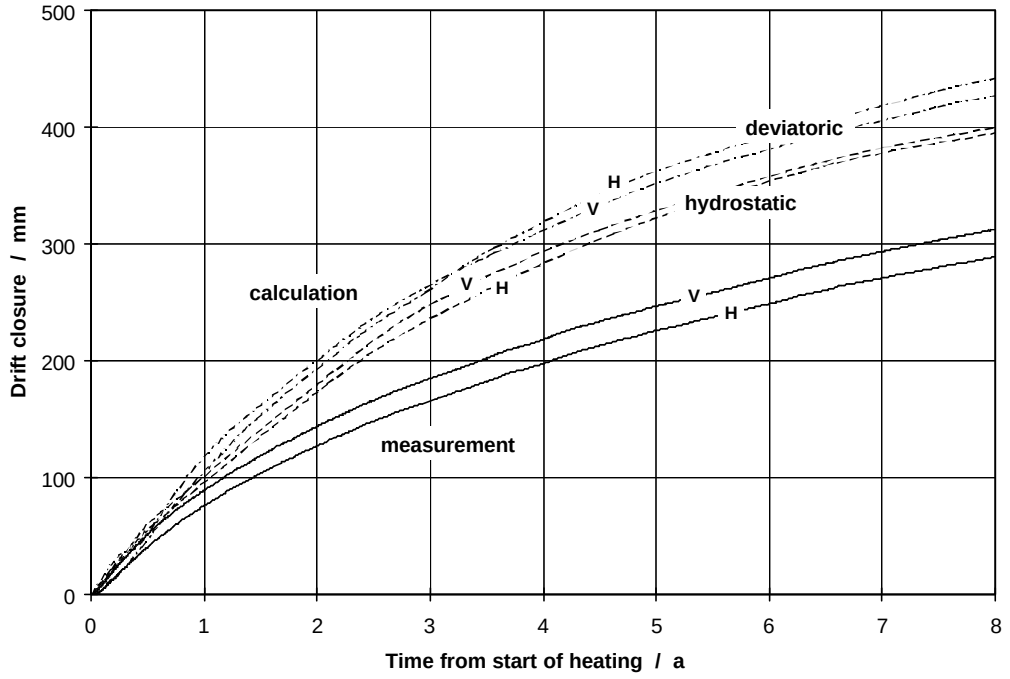

Fig. 6.6 Comparison of calculated (dashed curves) and measured (solid curves) drift closure in the heated area (V – vertical, H – horizontal closure)

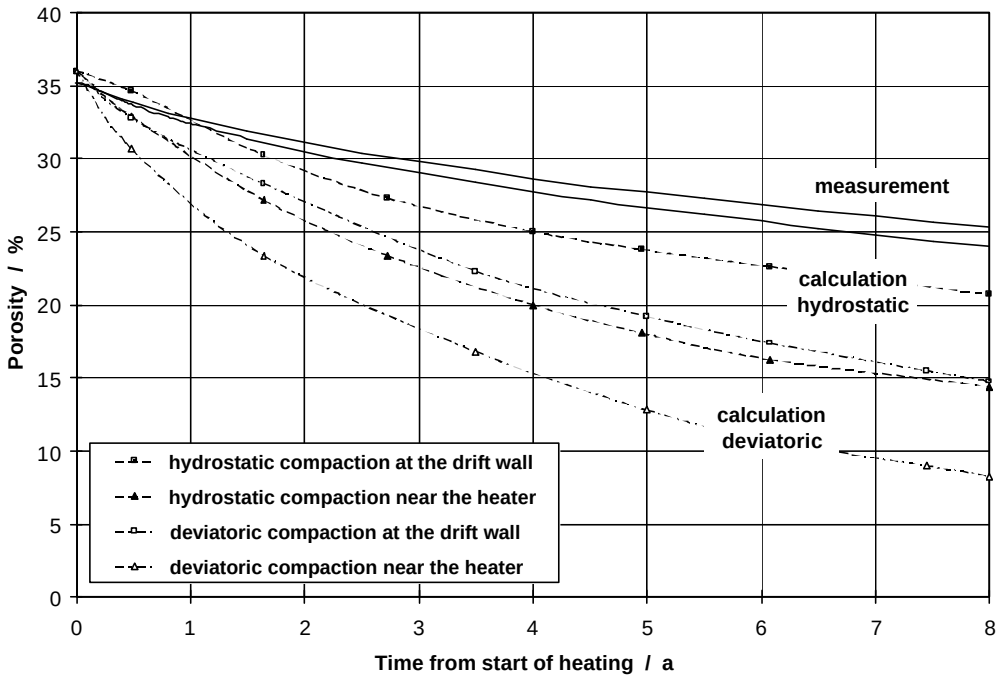

Fig. 6.7 Comparison of calculated (dashed curves) and measured (solid curves) backfill porosity in the heated area

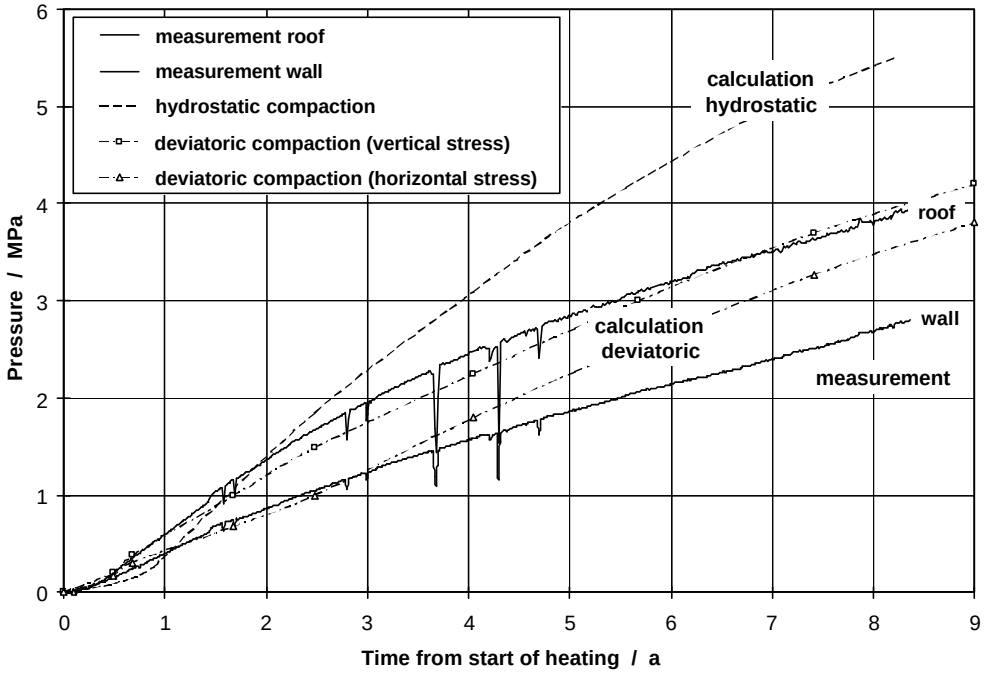

Fig. 6.8 Comparison of calculated (dashed curves) and measured (solid curves) backfill pressure in the heated area

ENRESA-CIMNE performed fully coupled thermomechanical analyses using a two-dimensional model /BEC 99/. Assuming a lower value of lithostatic stress (10 MPa), drift closure was well predicted. Calculated backfill stresses, however, were below the measured values.

Further model calculations were performed by BGR to prove the reliability of long-term stress measurements. The thermomechanical response of the host rock around the test drifts was calculated with the finite-element code ANSALT /HEU 96/. The initial state of stress in the test field was assumed to be 12 MPa. Modelling of the borehole inclusion technique, which was used for long-term stress measurements, showed that not only time-dependent stress conditions around the test drifts (i.e., stress relaxation due to creep of the rock salt), but also stress conditions around the borehole and in the borehole grout (i.e., continuous stress increase caused by borehole closure) had to be taken into account. After eliminating the borehole closure-induced stress increment, the model calculations were in good agreement with the measured data.

Generally, the results of thermomechanical modelling in the heated area were not as satisfactory as the thermal analyses. Drift closure and backfill compaction were much slower than predicted. Several reasons have been identified resulting in deviations between measurements and calculations /BEC 99/.

- In the thermomechanical calculations, two-dimensional numerical models were used which could not fully simulate the three-dimensional experimental conditions. An overestimation of stress and drift closure in the heated area is to be expected. Though available, three-dimensional codes could not be used because of their excessive computation time requirements.

- In a final repository, a higher lithostatic rock stress is being assumed. The in-situ experiment was carried out in a part of the Asse mine that was supposed to be not significantly disturbed by former mining activities. According to in-situ measurements, however, the lithostatic stress in the test field was considerably lower than expected due to the large excavations remaining from former salt mining /HEU 95/. Consequently, the creep rate of the surrounding rock salt was significantly lower than predicted, resulting in lower drift closure and backfill compaction rates.

- The material parameter values used in the numerical analyses were obtained from small-scale laboratory tests. By transferring these values to large-scale in-situ conditions, again the creep rate of rock salt is being overestimated by the calculations.

- The constitutive laws for crushed salt, which are basing on laboratory tests, cannot fully describe the complex backfill behaviour in situ. Especially, the temperature dependence of the constitutive models both for crushed salt and rock salt is not yet fully understood as indicated by the deviations in the heated area, while experimental and calculation results agreed well in the non-heated sections /PUD 99/. Thermomechanical calculations using a deviatoric constitutive model instead of the hydrostatic model showed a much better agreement of the backfill pressure values, but the deviations in drift closure were even larger /KOR 99/.

- The dimensions of the in-situ experiment were not large enough. Though the test field had been designed as far as possible like a real repository, the limited size of the experiment could not fully simulate complex repository conditions.

- Backfill compaction pressure was not as homogeneous as assumed by earlier modelling. For the deviatoric model of crushed salt, however, the calculated compaction pressures matched the measured pressure values. Due to temperature dependence, large thermal gradients, and also deviatoric load, non-homogeneous crushed salt compaction has to be expected both in axial and radial direction of the test drifts, but could not be determined in situ with the available measuring equipment. A detailed examination of the porosity distribution in the backfill will be performed during drift excavation in the post-test investigation phase.

- Most measurement data were obtained remotely without the possibility to check instrument accuracy and reliability during the experiment. Deviations due to instrument drifts or systematic measurement errors cannot be ruled out. Therefore, actual conditions in the test drifts will be determined during the dismantling of the experiment to confirm the measurement results. Recovered instruments will be re-calibrated both for quality control and evaluation of the experimental data.

In summary, numerical modelling was able to simulate adequately the thermomechanical behaviour of backfill and host rock under representative repository conditions. With the available codes, all basic phenomena in the in-situ experiment

were described without contradictions. The relevant physical processes are qualitatively well understood allowing further extrapolations in space and time for repository performance assessments.

Deviations between experimental and calculation results were mostly quantitative, but indicated the requirement of further improvements. Basically, a precise determination of in-situ stresses is indispensable. Progress is possible by using three-dimensional fully coupled thermomechanical analysis and by the development of improved constitutive laws for rock salt and crushed salt, especially regarding temperature dependence.

7 Benchmarking Exercise "Comparative Study on Crushed Salt" $(CS)^2$

The benchmarking exercise "Comparative Study on Crushed Salt" $(CS)^2$ was performed within the BAMBUS project to improve the knowledge about the numerical behaviour of crushed salt backfill under the thermomechanical conditions in a repository for high-level radioactive waste in rock salt /BEC 99/. Therefore, the constitutive laws had to be investigated and to be improved concerning the functional dependence of the essential thermomechanical effects.

The benchmarking exercise was divided into an experimental part and a numerical part. Experimental investigations with crushed salt were carried out by BGR, FZK-INE and GRS. The numerical calculations were performed by BGR, FZK-INE, GRS, ENRESA-CIMNE / Spain, G.3S / France and NRG / Netherlands. As subcontractor of GRS, the numerical calculations were performed by DBE. The numerical results achieved by DBE are summarized in the following chapter.

7.1 Benchmarking Calculations

7.1.1 Constitutive Models

Some of the benchmarking exercises comprised backfill material together with the surrounding rock salt. According to the particular requirements from benchmark specifications regarding the thermomechanical behaviour of the comprehensive system, the constitutive laws of both materials could be made up of two parts: a thermal part and a mechanical part. The thermal part of the rock salt model was described by a constant for thermal expansion, a temperature depending cubic polynomial for heat conductivity, and a linear function of temperature for heat capacity /BEC 99/. For crushed salt, the only modified thermal parameter was heat conductivity. A multiplicative decomposition into the heat conductivity of rock salt and a porosity depending linear function was used. The mechanical part of the rock salt model was described by an elastic-viscoplastic constitutive law. The state of stress $\underline{\underline{s}}$ within the elastic part is given by Hooke's law

$$\underline{\underline{\sigma}} = K\underline{\underline{\varepsilon}}_{el}^{vol} + 2G\underline{\underline{\varepsilon}}_{el}^{dev} \qquad (1)$$

with K, G: elastic coefficients

where $\underline{\underline{\varepsilon}}_{el} = \underline{\underline{\varepsilon}}_{el}^{vol} + \underline{\underline{\varepsilon}}_{el}^{dev}$ with $\underline{\underline{\varepsilon}}_{el}^{vol} = \frac{1}{3}\varepsilon_{ii,el}\underline{\underline{I}}$ and $\underline{\underline{\varepsilon}}_{el} = \underline{\underline{\varepsilon}} - \underline{\underline{\varepsilon}}_{vpl}$ (2)

is the decomposition of the elastic strain tensor $\underline{\underline{\varepsilon}}_{el}$ into a volumetric $\underline{\underline{\varepsilon}}_{el}^{vol}$ and a deviatoric $\underline{\underline{\varepsilon}}_{el}^{dev}$ part. The additive decomposition of the total strain tensor $\underline{\underline{\varepsilon}}$ into an elastic part and a viscoplastic part $\underline{\underline{\varepsilon}}_{vpl}$ is based on the small deformation theory.

The current viscoplastic strain tensor was calculated by an incremental update

$$\underline{\underline{\varepsilon}}_{vpl}(t+\Delta t) = \underline{\underline{\varepsilon}}_{vpl}(t) + \dot{\underline{\underline{\varepsilon}}}_{vpl}\Delta t \tag{3}$$

where the viscoplastic strain rate tensor is described by an associated flow rule of the yield criterion F

$$\dot{\underline{\underline{\varepsilon}}}_{vpl} = G(F)\frac{\partial F}{\partial \underline{\underline{\sigma}}} \quad \text{with} \quad G(F) = \frac{A}{2}e^{-\frac{Q}{RT}}(F)^n. \tag{4}$$

The temperature depending function is the Arrhenius-function with flow intensity A, activation energy Q, universal gas constant R and absolute temperature T.

This power law was used for rock salt where the yield criterion is the von-Mises equivalent stress $\overline{\sigma}$

$$\dot{\underline{\underline{\varepsilon}}}_{vpl} = A e^{-\frac{Q}{RT}}\left(\frac{\overline{\sigma}}{\hat{\sigma}}\right)^n \frac{\partial \overline{\sigma}}{\partial \underline{\underline{\sigma}}} \tag{5}$$

with n: stress exponent

$\hat{\sigma}$: reference stress $\hat{\sigma} = 1\,MPa$

For crushed salt there were two different constitutive laws for the viscoplastic part: a pure hydrostatic constitutive law according to Korthaus /KOR 91/ and a combined hydrostatic-deviatoric law in the original form of Hein /HEI 91/.

In case of the pure hydrostatic law /KOR 91/, the viscoplastic strain rate tensor is

$$\dot{\underline{\underline{\varepsilon}}}_{vpl} = A\, e^{-\frac{Q}{RT}} \frac{\phi^{c_2}}{\left(c_3 e^{c_4 \varepsilon^{vol}} - 1\right)^{c_5}} \left(\frac{p}{\hat{p}}\right)^{c_6} \tag{6}$$

and in case of the hydrostatic-deviatoric law /HEI 91/

$$\dot{\underline{\underline{\varepsilon}}}_{vpl} = A\, e^{-\frac{Q}{RT}} \left(h_1 p^2 + h_2 q^2\right)^2 \left(\frac{1}{3} h_1\, p\, \underline{\underline{I}} + h_2\, \underline{\underline{S}}\right) \tag{7}$$

with $$h_1 = \frac{1 - c_1 e^{c_2 \phi}\, c_3^2}{\left(\frac{c_4}{c_5}\left(\left(\frac{1-\phi}{1-\phi_0}\right)^{c_5} - 1\right) + c_8\right)^2} \quad \text{and} \quad h_2 = c_6 + c_7\, h_1 \tag{8}$$

where

c_i: material parameter

$\underline{\underline{S}}$: stress deviator; $\underline{\underline{S}} = \underline{\underline{\sigma}} - 1/3\, \sigma_{ii}\, \underline{\underline{I}}$

p: hydrostatic pressure; $p = -1/3\, \sigma_{ii}$

ε^{vol}: volumetric compaction

$\hat{p}$: reference pressure; $\hat{p} = 1\,MPa$

ϕ: porosity

q: norm of stress deviator $\underline{\underline{S}}$;

ϕ_0: initial porosity

$$q = \sqrt{\underline{\underline{S}} \cdot \underline{\underline{S}}} = \sqrt{2}\, J_2$$

In case of Hein's model, the elastic behaviour is described by a porosity depending function which leads to low elastic properties for bulk and shear modulus at the beginning of compaction and reaches the values of rock salt at total compaction

$$K = K_0\, e^{-c_k \phi \left(\frac{1-\phi_0}{1-\phi}\right)} \tag{9}$$

with K_0: bulk modulus of rock salt

c_k: material parameter

7.1.2 Benchmarking Exercises

The benchmarking exercises were performed in three stages with each stage comprising two exercises. The complexity of the benchmark problem increased from stage to stage. Borehole and drift disposal were considered under isothermal conditions as well as under varying temperatures.

Some general aspects were:

- The crushed salt was assumed to be dry; no moisture was taken into account.
- The initial porosity of the crushed salt was assumed to be 0.31.
- Two different sets of experimental data were available: BGR-data and FZK-data; in the following figures, the numerical results are marked in case of BGR-data by K-BGR for using the Korthaus model and by H-BGR for the Hein model, respectively by K-FZK and H-FZK in case of FZK-data.
- A weak coupling between the thermal and mechanical problem class was used in case of thermomechanically coupled problems only.
- All benchmarking exercises were performed by two-dimensional representations.
- Both problem classes were calculated by finite-element codes with the code MAUS ("Mechanical Analysis of Underground Storage") being used for mechanical calculations and the code TAUS ("Temperature Analysis of Underground Storage") for thermal calculations.
- 8-node elements were used for discretization in case of the mechanical problem class and 4-node elements for the thermal class.
- The geometric linear theory was assumed in case of the mechanical problem class.

- In the framework of a geometric full linearized theory, porosity is an internal quantity and therefore described by the deformation gradient.

For comparison reasons, the results of FZK-INE are also shown in the following figures and marked by FZK(K). FZK-INE also used the finite-element code MAUS for mechanical calculations, but the FAST-code for thermal calculations. The constitutive law was a modified Hein model with the new material functions

$$h_1 = \frac{a}{\left(\phi^c - \phi_0^c\right)\frac{1}{\phi_0^{2c}} + d} \quad \text{and} \quad h_2 = 1 + b\,h_1 \tag{10}$$

with a, b, c, d: material parameters

Stage 1

The objective of the first stage of benchmarking (BM 1) was to verify the constitutive laws and codes. In BM 1.1, the accuracy of the parameter identification process was examined by re-calculation of an existing oedometer test (Fig. 7.1). The oedometer test had been carried out as a deformation driven process with an initial strain rate of $6.9 \cdot 10^{-9}\ s^{-1}$. In a first step, an isotropic stress state was assumed. In a second step, the deviatoric component was considered, too, by constraints calculated from FZK-data. Figure 7.1 shows the stresses in axial and radial direction versus time. All calculation results corresponded with the given data.

From the numerical point of view it must be remarked that the stresses were almost zero at the beginning of the deformation driven process. During this period, only very small time steps could be used.

The identification process led to a stress exponent in the range of 10 to 22 depending on temperature and strain rate which had been taken into account by the BGR-data. Such values, however, made no physical sense. It was assumed that friction had been underestimated. Thus, the data base was changed at stage 2 applying another set of experimental data introduced by FZK. For comparison reasons, however, all benchmarking exercises during stage 2 were also calculated with the parameter set basing on the BGR-data.

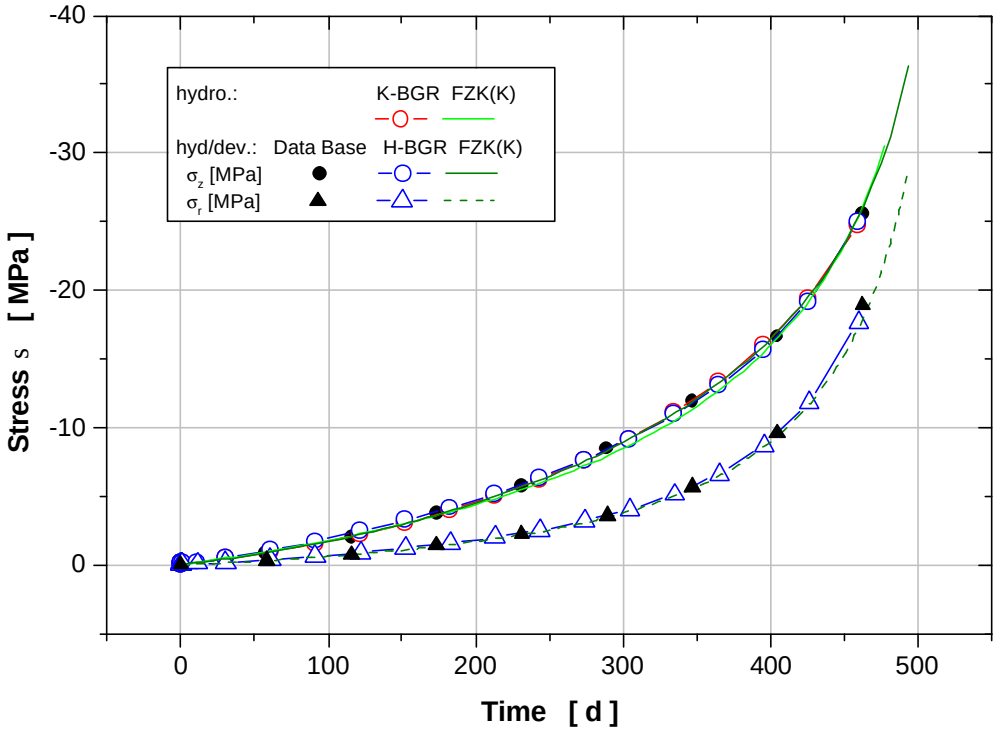

Fig. 7.1 BM 1.1 - Simulation of an oedometer test using BGR-data

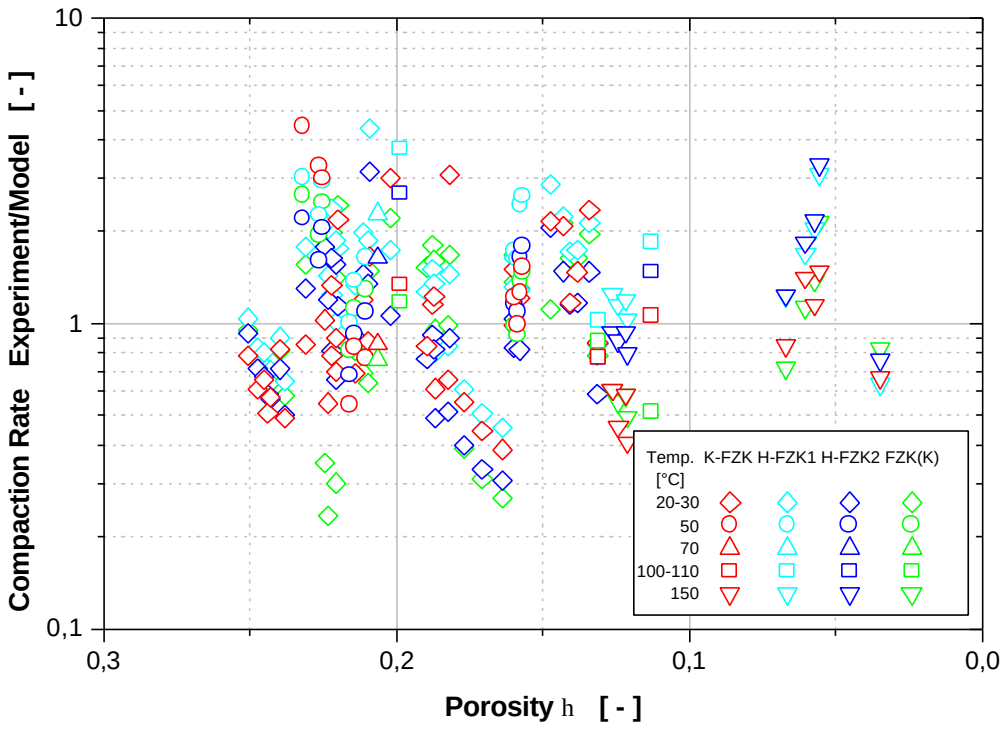

Fig. 7.2 Comparison of calculated and measured compaction rates for FZK-data

In Figure 7.2, the compaction rates obtained from the experimental data of FZK and from numerical identification are compared. During parameter optimization with the Hein model, activation energy, stress exponent, and material parameter c_3 were excluded from parameter variation. For these parameters, the values of rock salt were taken. As anticipation to BM 3.2, the estimated overall error F, which is shown in Table 7.1, is determined by

$$F^2 = \frac{\left(\ln\dot{\varepsilon}^{vol}_{Ident} - \ln\dot{\varepsilon}^{vol}_{Exp}\right)^2 + \left(\ln\dot{\varepsilon}^{dev}_{Ident} - \ln\dot{\varepsilon}^{dev}_{Exp}\right)^2}{n^{vol} + n^{dev}} \qquad (11)$$

Tab. 7.1 BM 3.2 - Overall error from the identification process with FZK-data

parameter set	K-FZK	H-FZK 1	H-FZK 2	FZK(K)
$\left(\ln\dot{\varepsilon}^{vol}_{Ident} - \ln\dot{\varepsilon}^{vol}_{Exp}\right)^2$	18.84	22.51	16.09	21.08
$\left(\ln\dot{\varepsilon}^{dev}_{Ident} - \ln\dot{\varepsilon}^{dev}_{Exp}\right)^2$	-	15.06	12.77	19.88
F	0.556	0.650	0.569	0.678

In BM 1.2, a backfilled borehole with free convergence was simulated. The borehole diameter was 2 m. Initial and boundary conditions were described by a homogeneous thermal field at 100°C and an isotropic stress state of 20 MPa. Borehole displacements in radial direction were the same for the deviatoric model H-BGR1 and FZK(K), but convergence of the borehole wall was lower in case of the pure hydrostatic constitutive law, as compaction was overestimated during the identification process due to the isotropic stress assumption.

Stage 2

The exercises of stage 2 aimed at small-scale laboratory tests in order to validate the models for essential physical parameters. BM 2.1 was a simulation of a multistage

laboratory test under isothermal hydrostatic conditions in a triaxial testing device. The deformation process was driven by a given stress path (Fig. 7.3). In case of the BGR-data, the difference between the hydrostatic and the deviatoric model was probably caused by the isotropic stress assumption of the experimental data. Due to their very high stress exponent, the region of low compaction and low stresses seemed to be reproduced inaccurately. But by a simple parallel shift at the beginning of compaction, a correspondence between the different numerical calculations could be achieved. The differences between the calculations using FZK-data were less, regardless whether the hydrostatic or the deviatoric law were used.

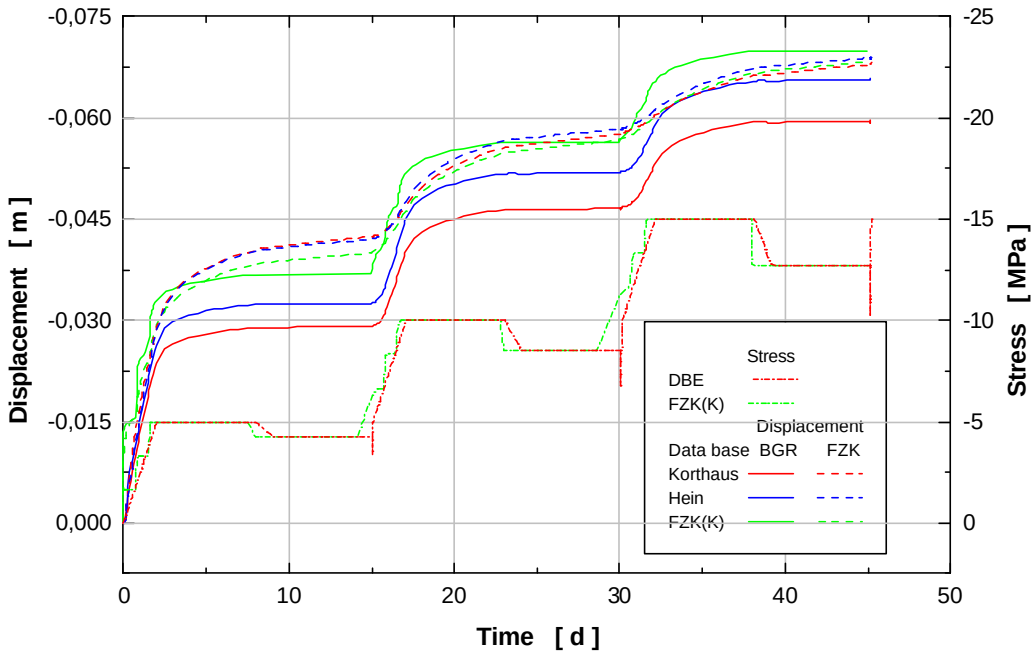

Fig. 7.3 BM 2.1 - Stress path and cell wall displacement versus time

BM 2.2 was an extended version of BM 1.2. A heater with a constant surface temperature of 200°C was assumed in the borehole. The borehole diameter was enlarged to 3 m and the initial stress lowered to 15 MPa. Similar to the earlier benchmarking exercises there were greater differences in borehole convergence using the BGR-data. Due to different geometric quantities there were some differences in heat transport.

Stage 3

BM 3.1 was a first attempt of calculating the TSDE test in the Asse salt mine. The numerical calculation was a two-dimensional representation of the real three-dimensional situation. Especially, thermal calculation was concerned by this restriction. The different thermal calculations were all comparable (Fig. 7.4), but large differences existed compared to the temperatures measured in situ /BEC 99/. Only small differences were found between the geometric quantities (Fig. 7.5).

The objective of BM 3.2 was to estimate different physical effects on equivalent values like the compaction rate. For a number of vectors describing stress state, temperature and porosity, the volumetric and deviatoric compaction rates were calculated. Only some differences occurred which reached more than one order of magnitude in case of deviatoric effects (Fig. 7.6 and 7.7).

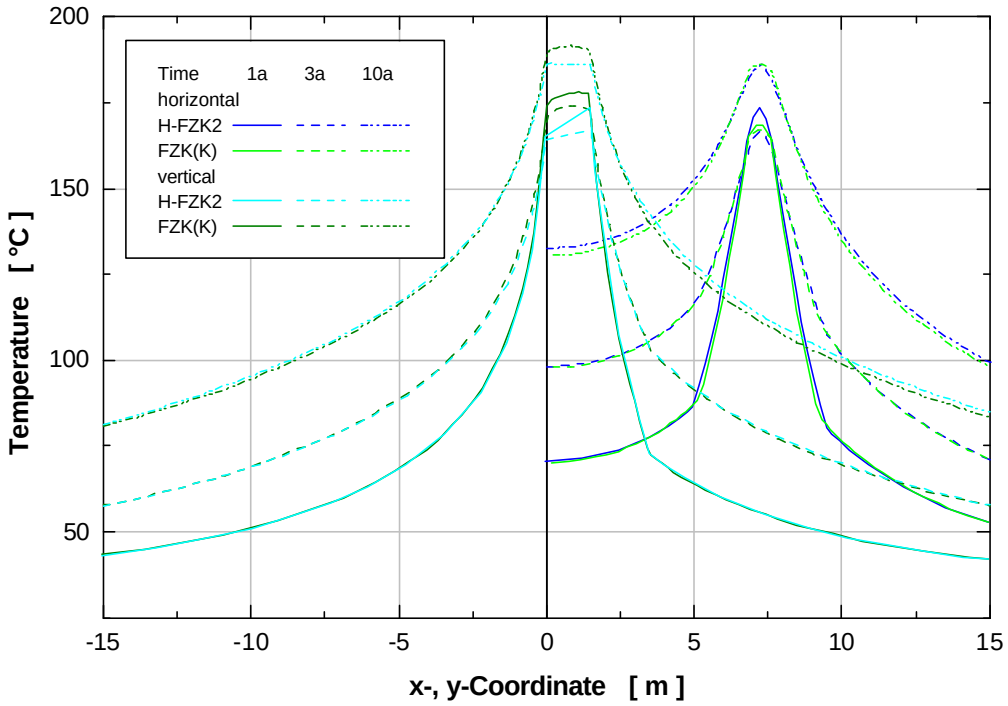

Fig. 7.4 BM 3.1 - Temperatures along a horizontal and a vertical line for different times after the start of heating

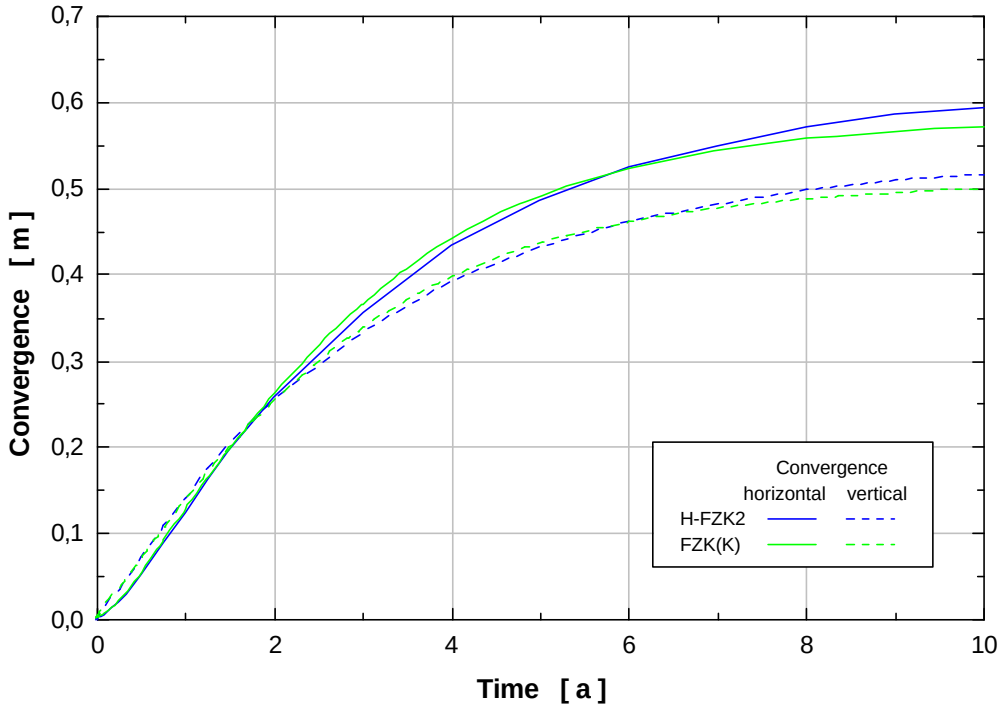

Fig. 7.5 BM 3.1 - Horizontal and vertical drift convergence over time

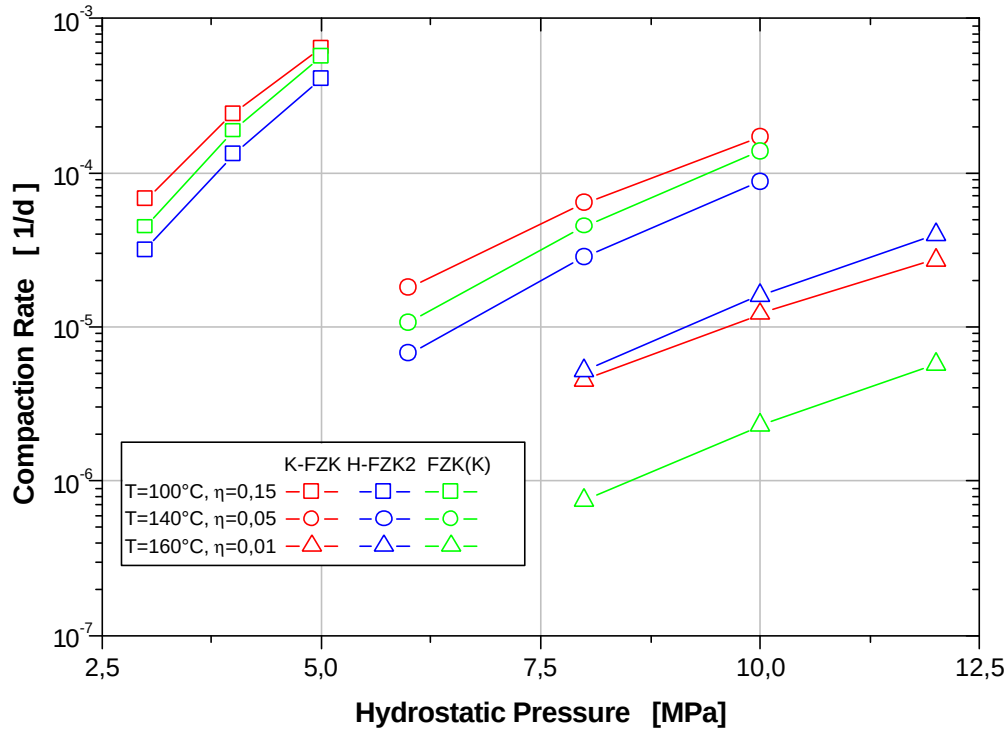

Fig. 7.6 BM 3.2 - Influence of hydrostatic pressure on the compaction rate

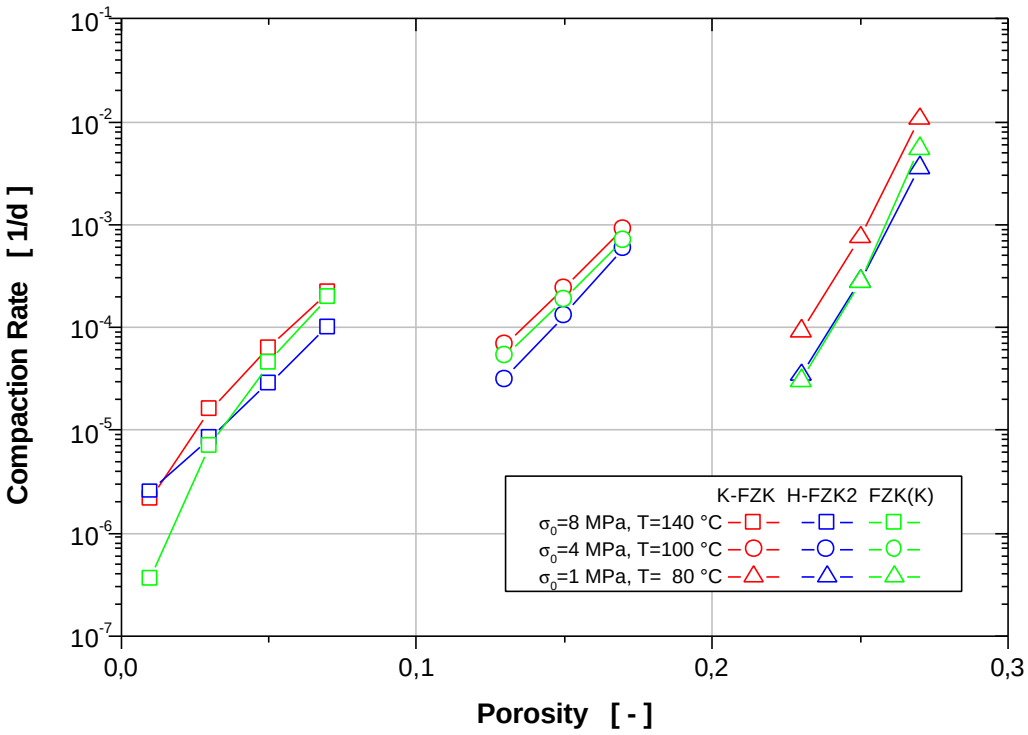

Fig. 7.7 BM 3.2 - Influence of current porosity on the compaction rate

7.2 Laboratory Analyses

Besides BGR and FZK, GRS contributed to the laboratory benchmarking exercise BM 2.1. The test was a multistage hydrostatic consolidation experiment which was performed at ambient temperature in a triaxial testing device with six creeping periods under constant load and a total duration of 45 days.

Further experiments on backfill compaction were performed at the GRS laboratory with the major objective to investigate the compaction behaviour of the coarse-grained crushed salt backfill in the TSDE experiment. The aim was to obtain the specific parameters required for the viscoplastic constitutive model of Hein /HEI 91/ which considers both volumetric and deviatoric strain rates under hydrostatic and shear stress conditions.

7.2.1 Benchmarking Experiment BM 2.1

The testing material for this experiment already mentioned in chapter 7.1.2 (stage 2) was crushed salt from the Asse salt mine which was prepared by sieving to reach a controlled grain size distribution. The same prepared crushed salt material was delivered to the other participants of the experiment. The adsorbed water content of the granular salt was less than 0.1 wt %. For determining initial and current porosities, the grain density of the used salt material was required which was determined in the laboratory to 2184.8 kg/m^3.

For the protection of the testing device jacket, the coarse grained crushed salt material was filled into an inlet of Perbunan NBR which had an inner diameter of 0.276 m, an outer diameter of 0.280 m and a wall thickness of 4 mm. The inlet was set into the jacket between the upper piston and the lower hydraulic cylinder of the testing device. In this way, the confining pressure fluid (hydraulic oil) was prevented from penetrating into the crushed salt sample. The initial length of the sample was 0.7033 m and the initial radius 0.138 m.

The multistage consolidation experiment at the GRS laboratory was performed under hydrostatic stress conditions in a MTS rock mechanic testing system (MTS Systems Corporation, Minnesota/USA). In the triaxial cell of the Karman type, the cylindrical specimen was emplaced in a pressure-tight vessel. The stress was applied axially at the bottom and the top of the specimen. The confining oil pressure was imposed radially. The test was conducted basically in accordance with the prescribed stress history (Fig. 7.8).

As no in-vessel measurement of the radial deformation was possible at that time, an indirect method was applied by measuring the oil volume which had been displaced from the pressure intensifier into the vessel. In this case, the compressibility of the hydraulic fluid is required for corrections.

The compaction histories of samples of all three participants are shown in Figure 7.8. Void ratios of the samples and hydrostatic pressures are given as a function of time. For the GRS-sample, the final void ratio was calculated from the displaced oil volume (corrected) and the axial displacement of the loading rod. A value of 0.21 was determined corresponding to a porosity of 17.2 %. At the end of the experiment, the compacted sample was retrieved and several diameter measurements were performed

along the sample resulting in a mean diameter of 0.259 m. The mean length of the compacted sample was 0.6605 m. Basing on these results, a void ratio of 0.16 was calculated corresponding to a porosity of 13.9 %.

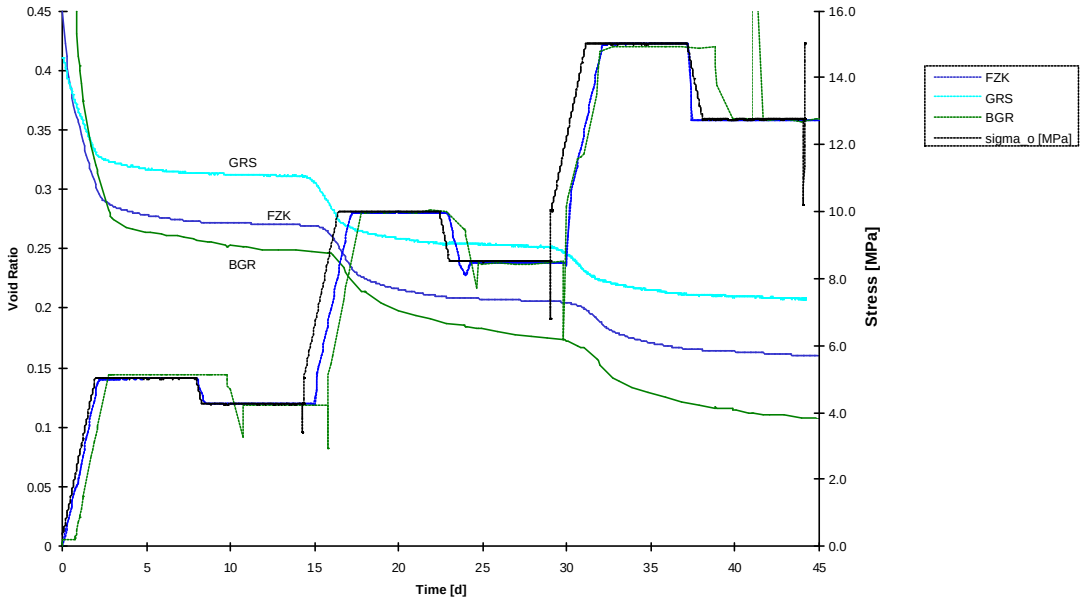

Fig. 7.8 Results of the hydrostatic tests performed in the framework of (CS)²-benchmark

The initial void ratio of the sample had been 0.41 corresponding to a porosity 29.1 %. This value was lower than the initial void ratio of the FZK-sample and even much lower than the void ratio of the BGR-sample. Furthermore, the sample of GRS appeared to be stiffer in the initial loading phase (from 0 to 5 MPa). Despite of the technical problems, however, the results of all participants showed an adequate agreement.

7.2.2 Backfill Compaction

As already described in chapter 7.1.1, the constitutive law of Hein /HEI 91/ was applied for predicting the compaction behaviour of the crushed salt in the TSDE experiment. The parameters h_1 and h_2 (see chapter 7.1.1) are dependent on the porosity ϕ as follows:

$$h_1(\phi) = \frac{1 - d(\phi) \cdot c_3^2}{\left(\frac{c_4}{c_5} \left(\left(\frac{1-\phi}{1-\phi_0} \right)^{c_5} - 1 \right) \right)^2}, \qquad h_2(\phi) = c_6 + c_7 \cdot h_1(\phi) \tag{12}$$

with $d(\phi) = c_1 \cdot \exp(c_2 \cdot \phi)$ being a further porosity dependent material parameter, c_3 being $\tan\varphi$, the coefficient of internal friction (φ = angle of internal friction), and ϕ_0 being the initial porosity of the crushed salt.

The flow condition for crushed salt as given by Hein including grain displacement, too, is presented in equation (13).

$$d\left(\frac{p}{q} - n\right)^2 + h_1 \cdot p^2 + h_2 \cdot q^2 = 1 \tag{13}$$

In order to determine the porosity dependent parameters h_1, h_2, and d, pairs of p, q-values and the dilatancy factor n are determined by compaction tests in which the transition from elastic to irreversible plastic behaviour is reached. By performing three independent tests, three linearly independent equations are obtained permitting to solve equation (13) for a defined porosity. The coefficient of internal friction, which is explicitly contained in the factor of dilatancy, must be determined in a separate test. For the case of n= 0, the irreversible volumetric strain is solely caused by viscoplastic deformations of the granular material.

For the experimental determination of the material parameters for coarse-grained crushed salt, several compaction tests were conducted. The parameters h_1, h_2, and d were determined at ambient temperature in a triaxial pressure cell (Karman type) which is designed for accepting samples with a diameter up to 280 mm and a height up to 700 mm. The grain size of the coarse-grained crushed salt material used was less than 32 mm. Thus, the ratio of the load piston diameter to the largest grain size was about 10. This ratio was sufficient to minimize interfering effects of cell limitations on the investigated sample material. The grain size distribution is plotted in Figure 7.9 and summarized in Table 7.2.

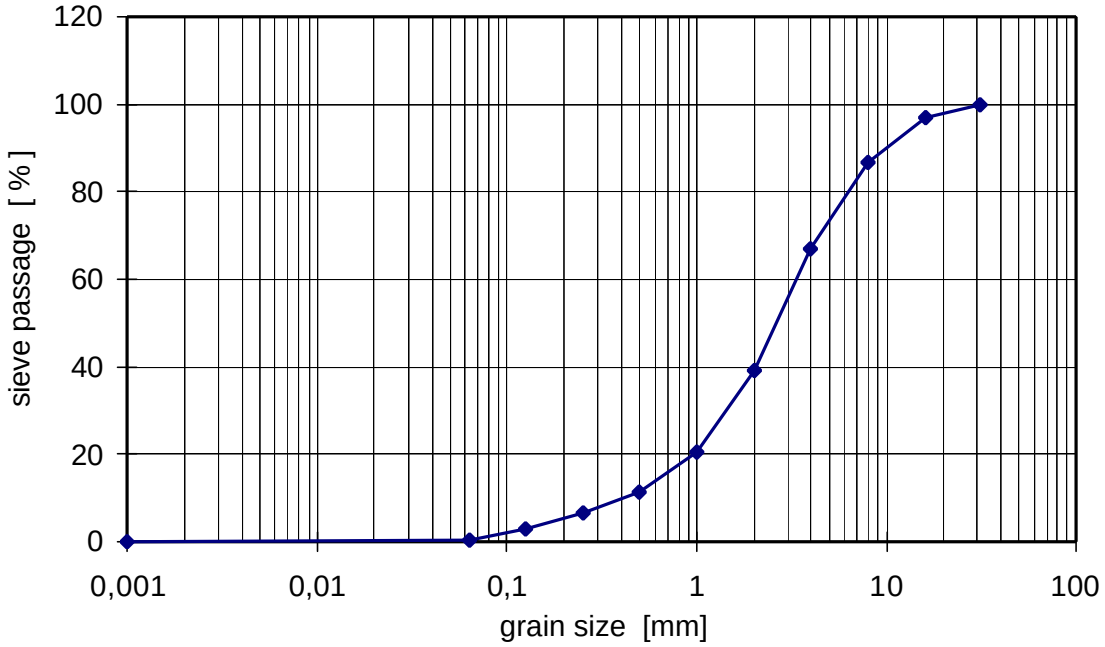

Fig. 7.9 Characteristic screening curve of the coarse-grained crushed salt used for the compaction tests

Tab. 7.2 Results from sieve analysis of the coarse-grained crushed salt used for the compaction tests

Grain size	Sieve passage
mm	%
31.5	100
16	97.1
8	86.89
4	66.79
2	39.29
1	20.53
0.5	11.26
0.25	6.49
0.125	2.97
0.063	0.49
0.001	0.07

For determining the porosity, the grain density was measured according to the specifications in DIN 18124 with the use of a Beckman air pycnometer. An important requirement for these tests is the determination of the water content which was performed by furnace drying according to DIN 18121. For this purpose, a part of the sample was dried at 105°C for about 72 hours, and the adsorbed water content was determined by weighing.

The axial deformation of the test specimen was measured with a displacement gauge. The volumetric compressive strain was determined by a measuring device which permitted the measurement of the sample diameter during the test by a gauge ring which was installed in the annulus of the cell (in-vessel measurement). The large triaxial cell is shown in Figure 7.10.

Fig. 7.10 MTS large triaxial cell with inserted jacketed cylindrical crushed salt sample; the vessel is uplifted. In the mid-height of the sample, a device for the measurement of the sample diameter is shown

In the large triaxial cell, the samples were compacted under hydrostatic pressure at a rate of 1 MPa/min. Subsequently, the crushed salt specimen remained under the given compaction pressure for about 17 hours. The envisaged porosity values were 18 %, 14 %, and 10 %; the corresponding compaction pressures required for preparation were 10 MPa, 24 MPa, and 30 MPa, respectively. After the consolidation time, the compacted crushed salt test specimen were deformed at a strain-controlled rate of 1 mm/min from an initial hydrostatic stress in axial direction. For this purpose, the confining pressure on the samples with given porosity values was maintained at the initial hydrostatic stress level with values of 10 MPa, 5 MPa, and 1 MPa. The transition from elastic-reversible to plastic-irreversible deformation was recognizable from the variation in deviatoric stress with increasing axial compressive strain. At least three identical test specimen are also necessary for determining the three parameters h_1, h_2, and d for the respective porosity.

In the Hein flow condition, the material-specific coefficient of internal friction is explicitly included in the dilatancy factor. The coefficient of internal friction of the coarse-grained crushed salt material was determined under triaxial test conditions at ambient temperature. For this purpose, three backfill samples were exposed to an initial hydrostatic pressure of 2 MPa, 5 MPa, and 10 MPa and subsequently to an axial deformation at a rate of 1.5 mm/min. The respective confining pressure was being held constant at 2 MPa, 5 MPa and 10 MPa. After maximum compaction was reached, further axial loading resulted in de-consolidation of the sample material. The transition between these two states marks zero-dilatancy where no volume change occurs. By means of the three Mohr circles, the angle of internal friction or the coefficient of internal friction can be determined in the τ, σ-plot after Mohr-Coulomb /LEI 68/.

For the compaction of backfill samples with defined porosity values, certain preparation pressures were necessary for short-term compacting. A functional relationship, which depends on the initial porosity, is existing between the irreversible volumetric compressive strain and the applied pressure. The material parameters c_4 and c_5, which describe this relationship, were determined in the laboratory.

During hydrostatic tests in the large triaxial cell, samples with porosity values of about 18 % and confining pressures of 5 MPa and 10 MPa showed an anomalous behaviour in the p-q plane (Fig. 7.11). The samples lost their internal coherence at an axial stress of 9 MPa and 13 MPa, respectively.

Generally, the solutions of the flow condition equation (13) were unrealistic in the present case. The results were probably influenced by inhomogeneities caused by segregation of different grain fractions when the sample material was filled into the rubber jacket. For a representative crushed salt sample with an initial porosity of 27 %, the material parameters c_4 and c_5 were determined to 62.47 MPa and 11.10 [-]. The coefficient of internal friction was determined to c_3 = 0.87 and the resulting angle of internal friction to φ = 41°.

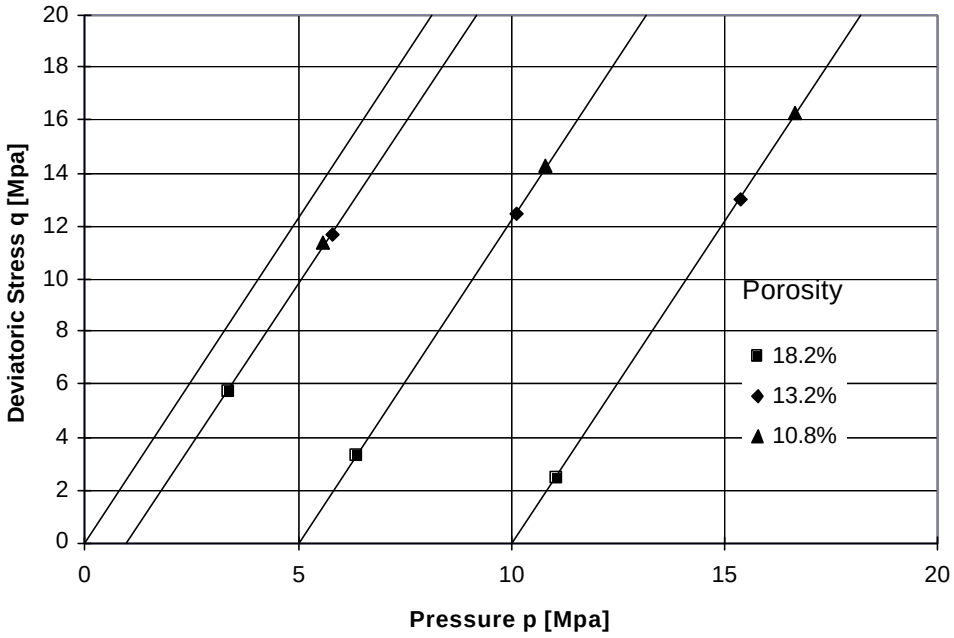

Fig. 7.11 p, q-values indicating the transition from elastic-reversible to plastic-irreversible material behaviour of coarse-grained salt samples

7.3 Conclusions from the Benchmarking Studies

For the benchmarking studies, numerical calculations were performed with regard to six different tasks dealing with simple laboratory investigations as well as the TSDE test. For the calculations, the finite element method (FEM) was used. The numerical models were two-dimensional representations. The calculations of DBE were performed with the combined hydrostatic-deviatoric law by Hein and for most tasks also with the pure hydrostatic constitutive law by Korthaus.

There was a good correspondence between the results from both constitutive laws regarding to temperature. The stress results differed slightly due to the ignored deviatoric stress in the Korthaus model. The pure hydrostatic law led to adequate results if only the main effect of volumetric compaction was taken into account. The Hein model is appropriate for more detailed investigations, i.e., considering shear stresses.

As the general situation in a final repository is dominated by hydrostatic behaviour, the Korthaus model is sufficient. From a numerical point of view, this constitutive law is preferred because of its stability and its numerical costs. If deviatoric stresses are important for system behaviour or details in the general system, the more complex constitutive law by Hein should be used.

To validate the experimental results and to check the plausibility of the stress exponent, a common experimental task was performed by some project partners. This test was used for numerical prediction, too. Differences from experimental investigations were in the same order as differences from numerical calculations with different constitutive laws. Experimental difficulties especially with the coarse-grained material which had been investigated can possibly be attributed to inhomogeneities caused by segregation of granular fractions when the material was poured into the testing devices.

Obviously, there is a need for more experimental work using a carefully controlled starting material to investigate the mechanisms which control the compaction process. Additionally, consideration of more experimental data, e.g., initial porosity and grain size or additional physical effects like moisture and stratigraphic units, could be useful for improving the constitutive laws.

8 Evaluation of the In-situ Experiment

8.1 Experimental Results

Large-scale in-situ experiments are indispensable to understand the complex processes in a final repository and provide valuable experience for repository construction and operation, too.

In the TSDE test, the behaviour of backfill and surrounding rock salt was studied under almost representative repository conditions. The agreement of experimental data and results of numerical modelling proved that relevant processes can be predicted adequately for repository performance assessments. However, quantitative differences in thermomechanical predictions indicated the requirement of further studies as discussed in chapter 6. Especially, the constitutive model for crushed salt has to be improved. Fully coupled three-dimensional thermomechanical analyses are necessary to simulate the three-dimensional experimental conditions.

The investigation of the compaction behaviour of crushed salt backfill was a main objective of the in-situ test. At the end of the experiment, backfill porosity decreased only slowly and was still significantly higher than expected. Backfill compaction had not reached the values expected in a repository, but further decrease in porosity would have required a much longer heating period. A residual porosity down to 1 % cannot be reached in situ within a reasonable time. Thus, the porosity range between the compaction state reached in the TSDE experiment and the remaining porosity in a repository could not be validated by the in-situ test. To confirm extrapolations of model calculations, the final stages of backfill compaction have to be investigated by laboratory tests. Sampling of compacted backfill from the test drifts will be done during the test drift dismantling to perform further compaction tests in the laboratory.

For the determination of backfill density, different methods were used. The most reliable results were achieved by drift closure measurements. The obtained density values, however, were only mean values over the respective cross sections basing on a limited number of measuring gauges. Non-homogeneous backfill compaction could not be determined with this measuring equipment. For future experiments, a more extensive instrumentation of the backfill is being recommended to enable measurement of local inhomogeneities in situ.

Density measurements using the radiometric γ-γ-method were successful, too, even if absolute density values could not be determined. But measured density changes were in the same range as the results from drift closure measurements. The radiometric borehole measurements showed a non-homogeneous vertical density distribution in the backfilled drifts with an increasing density towards the roof. This initial density distribution, which was attributed to the slinger technique, was conserved during ongoing compaction.

Non-homogeneous backfill compaction was probably also caused by thermal gradients within the backfill leading to deviations between thermomechanical model calculations and experimental results. For a final assessment of the density distribution, the backfill will be recovered from one test drift during the post-test investigation phase in the project BAMBUS II and samples will be taken to determine the local porosity in different areas.

Lithostatic rock stress is the most important parameter for the creep behaviour of rock salt and has to be determined precisely in a site characterization programme. In the test field, the lithostatic rock stress was considerably lower than expected due to the large excavations from former salt mining resulting in lower drift closure and backfill compaction rates. In an undisturbed salt dome, a lithostatic rock stress of 18 MPa can be assumed at the same depth which is significantly higher than the measured value of 12 MPa in the TSDE test field /HEU 95/. Therefore, drift closure would be considerably faster in a repository in undisturbed rock salt.

Although the TSDE experiment had been designed to simulate reference repository conditions, its results cannot be directly transferred to potential repository sites. The test drifts represented only a small section of an emplacement panel which will consist of a large number of drifts being about 200 m long with pillars of 13.5 m width between /BEC 99/. In a repository, a much larger rock volume will be heated resulting in a higher creep rate of the surrounding rock salt. Consequently, drift closure and backfill compaction rates will be significantly higher. These different boundary conditions have to be taken into account when the experimental results of the TSDE test are extrapolated for repository performance assessments.

In the post-test investigation phase, one test drift will be dismantled within the framework of the project BAMBUS II. A validation programme will be performed which is an integral part of the in-situ test for a final evaluation of all experimental data. The

backfill will be examined carefully during dismantling and the results will be compared with in-situ measurements. Backfill samples will be taken for laboratory tests to investigate the final stages of backfill compaction and the homogeneity of backfill density distribution. In future in-situ experiments, a post-test validation programme should be adopted already in the design phase to improve the experimental results.

8.2 Instrument Performance

The measuring equipment in the TSDE test field had been designed for a three to five years testing period, but was operated over almost ten years under conditions similar to a final repository in rock salt. These extraordinary conditions, i. e., high temperatures, stresses, and deformations were very demanding on gauges and measuring lines. As expected, an increasing part of the measuring equipment was damaged and failed during the long testing period. Therefore, the layout of the measuring systems had been designed redundantly allowing for failures of measuring devices. Additionally, several replacement measures were carried out during the heating phase to compensate for failed gauges. In the following, instrument performance and failure reasons are discussed for the different types of gauges.

8.2.1 Temperature Gauges

The temperatures were recorded by resistance thermometers which operated very successfully. During installation and in the preliminary phase, about 2 % of the gauges had been damaged until heating started in September 1990 (Fig. 8.1). Up to the end of March 2000, about 14 % of the temperature gauges failed. Considering the large number of redundantly installed thermometers, the failure quota of the gauges was low. 80 % of the failures occured in the heated area. Detailed examinations revealed that 80 % of the failures in the heated sections were caused by damaged measuring cables which had been squeezed leading to short-circuited or broken cables. About 20 % of the failures in the heated area were due to gauge defects. In the non-heated sections, all failures were caused by damaged measuring cables.

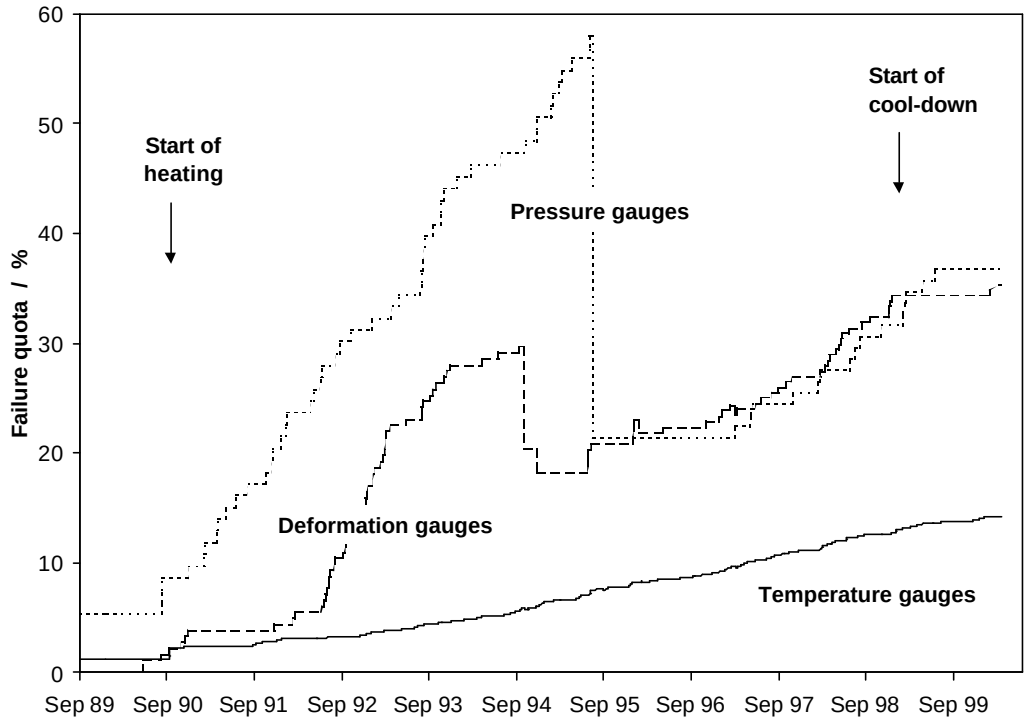

Fig. 8.1 Failure of measuring gauges

8.2.2 Deformation Gauges

The gauge design of the different deformation measuring systems proved to be successful as no gauges were damaged since the start of heating. But the measuring cables were the weak component of the measuring systems. Especially, the multicore cables were affected by the deformations leading to a large number of failures.

Due to these cable damages, the failure quota of the deformation measuring systems increased considerably since 1992 reaching 30 % in 1994 (Fig. 8.1). The extensometers in the heated area were the most concerned with their failure quota reaching up to 58 % (Fig. 8.2). To avoid problems in the deformation assessment around the heated drifts, replacement measures were carried out successfully in 1994 and early 1996. Thus, the total failure quota was reduced to 18 % (Fig. 8.1). The failure quota of extensometers in the heated area was lowered to 26 %, but increased again slightly to 31 % up to March 2000 (Fig. 8.2).

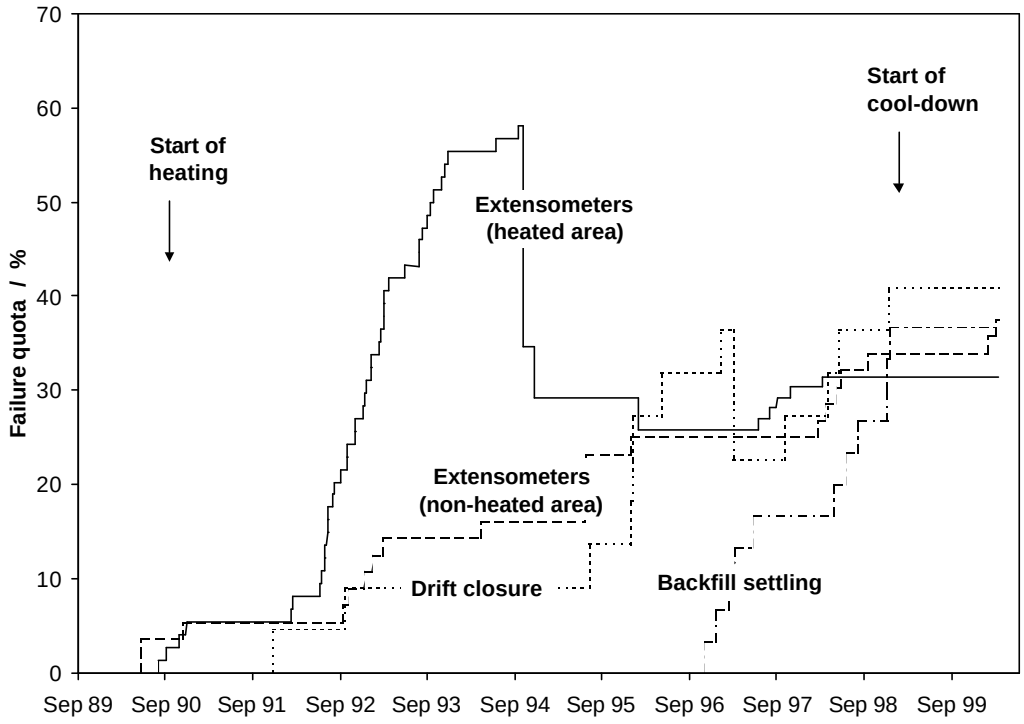

Fig. 8.2 Failure of different types of deformation gauges

The extensometer array in the cold area was less concerned by failures. The failure quota increased continuously up to 37 % at the end of March 2000 (Fig. 8.2).

The number of failed drift closure measuring gauges was tolerable in the beginning, but increased considerably in 1996 (Fig. 8.2). In the end of 1996, four failed convergence measuring gauges in horizontal direction were replaced reducing their failure quota temporarily. Since 1997, the failure quota increased again up to 41 % at the end of March 2000 (Fig. 8.2).

The equipment measuring the backfill settling operated completely until the end of 1996. Subsequently, the failure quota increased more and more up to 37 % at the end of March 2000 (Fig. 8.2). A replacement of failed gauges in the backfill was not feasible.

An investigation of the damaged measuring cables revealed that 80 % of the failures in the heated area were caused by squeezing which led to short-circuited or broken cores inside the multicore cables. About 20 % of the failures were due to the intrusion of electrolytes into the cables, gradually setting out of order all gauges which were

connected to the same multicore cable. In the cold sections, only 30 % of the failures were due to squeezing, while 70 % were caused by the intrusion of electrolytes. Over 50 % of the failures were located in the cable ducts, almost 20 % in the cable slots, and about 30 % inside of boreholes /DRO 96/.

In conclusion, the multicore cable design with diameters of up to 16.6 mm cannot be recommended for in-situ measurements in the heated area. The single cables with diameters of 4.4 mm, which were used for the temperature gauges, were less sensitive to deformations. For future experiments or the safety monitoring of a repository, the protection of the cables has to be improved. Furthermore, the realized cable duct design is not recommendable neither. As all measuring lines are enclosed in these ducts near the roof, local deformations of the cable duct may cause severe problems. A better protection of the measuring lines could be achieved by cable slots along the drift walls or near the roof in regions with low rock deformation.

8.2.3 Pressure Gauges

The determination of rock stress and backfill pressure is very important, but in-situ measurements are difficult. For the measurements in the test field, Glötzl type hydraulic pressure cells were used.

To observe long-term stress changes in the rock, stress monitoring probes were installed in different boreholes. The pressure gauges in these monitoring probes, however, were considerably affected by the accelerated rock deformations after the start of heating. The stress monitoring probes in the boreholes directly below the heater casks failed rather early (Fig. 8.3: 800-m level). Most of the monitoring probes above and between the test drifts, which had been installed from the observation drifts on the 750-m level, failed, too, until 1995 (Fig. 8.3: 750-m level). In July 1995, these gauges were replaced by probes of the same type. Thus, the stress monitoring array from the 750-m level was completed again (Fig. 8.3) and the total failure quota of the pressure gauges was reduced to 21 % (Fig. 8.1). A replacement of the probes below the heater casks was not feasible. Since 1998, first failures were observed at the replaced monitoring probes, too. Up to the end of March 2000, their failure quota increased to 20 % (Fig. 8.3).

Detailed investigations of the defects revealed that most of the stress monitoring probes had failed due to damages at the pressure gauges. Only 15 % of the failures were caused by defects at the hydraulic measuring lines. In the beginning of the experiment, the single pressure gauges of each stress monitoring probe were equipped with common return lines. But for a detailed investigation of failed gauges as well as for the continuation of pressure measurements in case of damaged pressure lines, separate return lines are recommended for each gauge. The common use of return lines by several gauges should be avoided.

The backfill pressure was measured by single pressure gauges. Unlike the probes in the boreholes, most gauges operated over a long time. Up to the end of March 2000, their failure quota reached 32 % (Fig. 8.3). Almost all failures occured in the heated area and could be attributed to damages at the hydraulic measuring lines, particularly inside the cable slots.

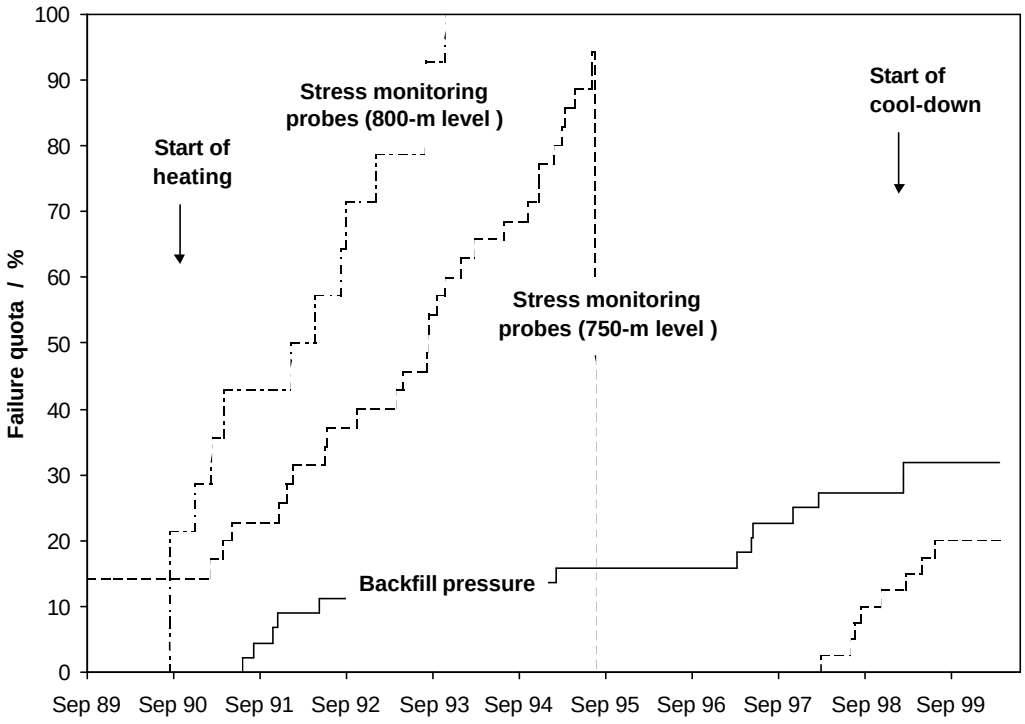

Fig. 8.3 Failure of different types of pressure gauges

8.3 Measurement Accuracy and Reliability

The geotechnical investigation programme carried out in the TSDE test has been described in chapter 3.2 together with specifications of the instruments' accuracy. In the design of the instrumentation programme, redundancy, diversity, and symmetry had been allowed for to reach a high consistency of the measured results. Most data had to be obtained remotely as the measuring equipment in the boreholes and the backfilled drifts was not accessible any more after backfilling. As no maintenance or re-calibration services were possible during the experiment, instrument accuracy and reliability could not be checked at site. Thus, deviations due to sensor drifts or systematic measurement errors cannot be excluded.

Quality control and confirmation of the measurement results are only possible by the dismantling of the experiment. Post-test examinations of the instruments are also fundamental for repository safety assessments. As similar equipments will be used for the safety monitoring of a repository, the long-term stability of the sensors and the corrosion behaviour of the material are important features.

During drift excavation, the measuring equipment will be recovered as far as possible. The correct function of the different measuring devices will be checked at site. By additional investigations, the actual conditions in and around the excavated drift will be determined as far as possible. These results will be compared with the data of the installed measuring devices. Failed gauges will be checked carefully with regard to their failure reason. As probably most gauges failed due to damages at the measuring lines, these investigations will comprise both function of the measuring devices and control of the measuring lines.

From the recovered measuring equipment, representative gauges will be selected for re-calibration. The calibration work will be carried out by the respective gauge manufacturer and an authorized laboratory of the German Calibration Service (Deutscher Kalibrierdienst). The re-calibration results will be compared with the original calibration certificates. Basing on the investigations on instrument accuracy and reliability and the re-calibration results, a final evaluation of all experimental data will be performed. From this evaluation, and taking into account instrument performance and failure reasons, recommendations will be developed for improvements of the instrumentation for the monitoring of a repository.

8.4 Testing of Measuring Techniques

Another objective of the TSDE test was the testing of measuring techniques for the safety monitoring of a repository. For this purpose, the long-term behaviour of drift closure measuring systems under different temperature conditions was studied by DBE. In each test drift, the cross sections G2 in the heated zone and $E1^{-1}$ in the non-heated area were equipped with test devices (Fig. 8.4). The examinations were carried out by means of three stationary drift closure measuring equipments and six temperature sensors per drift section which were of the same type as the gauges used for the geotechnical investigation programme.

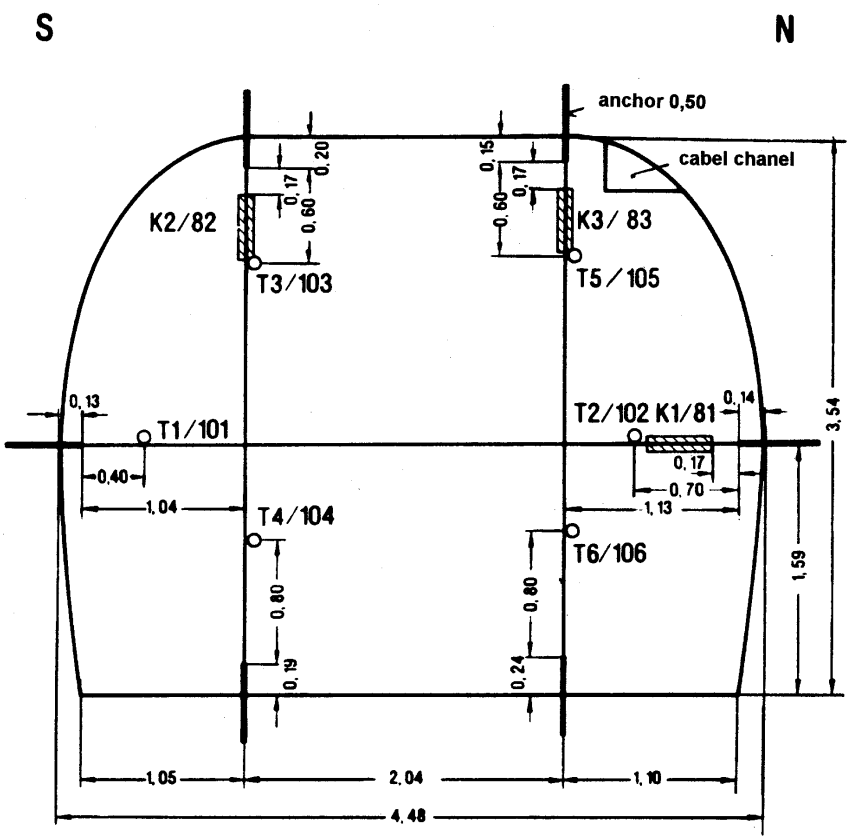

Fig. 8.4 General view of monitoring cross section G2 with drift closure measuring devices K1 - K3 and temperature measuring sensors T1 - T6

The drift closure measuring devices had been designed for drift convergences up to 270 mm at temperatures up to 200°C. Considering the temperature influence on the curve characteristics of the displacement transducer, the uncertainty of measured

values amounted to 3 mm in the heated section G2 and to 1 mm in the non-heated section $E1^{-1}$. At each drift closure measuring device, two temperature sensors were installed along the telescopic protection tube of the measuring rod. The sensor measuring range was from -55°C to +200°C. The maximum measuring uncertainty was 0.6°C at 200°C.

During the testing period until the end of 1998, a different instrument performance was observed in the heated and the non-heated sections. In the heated section G2, only three temperature sensors operated until the end of 1998, while all other gauges had failed. Examinations of the failure reasons showed that 14 sensors probably failed due to short-circuited or broken cables in the backfilled drifts. One of the gauges reached the end of it's measuring range (270 mm) after seven years of operation. Within the testing time of over eight years, the sensors in the heated area failed as follows:

- 1 sensor after 3 years measuring time
- 2 sensors after 4 years measuring time
- 6 sensors after 5 years measuring time
- 3 sensors after 6 years measuring time
- 2 sensors after 7 years measuring time.

In the non-heated section $E1^{-1}$, 16 of a total of 18 installed sensors operated until the end of 1998. Only two sensors failed in 1997 due to damaged measuring cables. All operating sensors provided plausible data until the end of the testing period.

The results of the temperature measurements are summarized in Fig. 8.5 showing the average temperature changing rates quarterly. In the heated area, the rates decreased distinctly since the start of heating, but in 1994, temperature changes due to the mentioned heater power deviations are evident. Drift closure measurement results are summarized in Fig 8.6. The rates reflected the temperature development including the deviations in the heated area in 1994. In the end of 1996, higher rates were caused by the drilling of boreholes for the replacement of failed drift closure measuring gauges. The results corresponded to the measurements in other cross sections and have already been discussed in chapter 5.2.

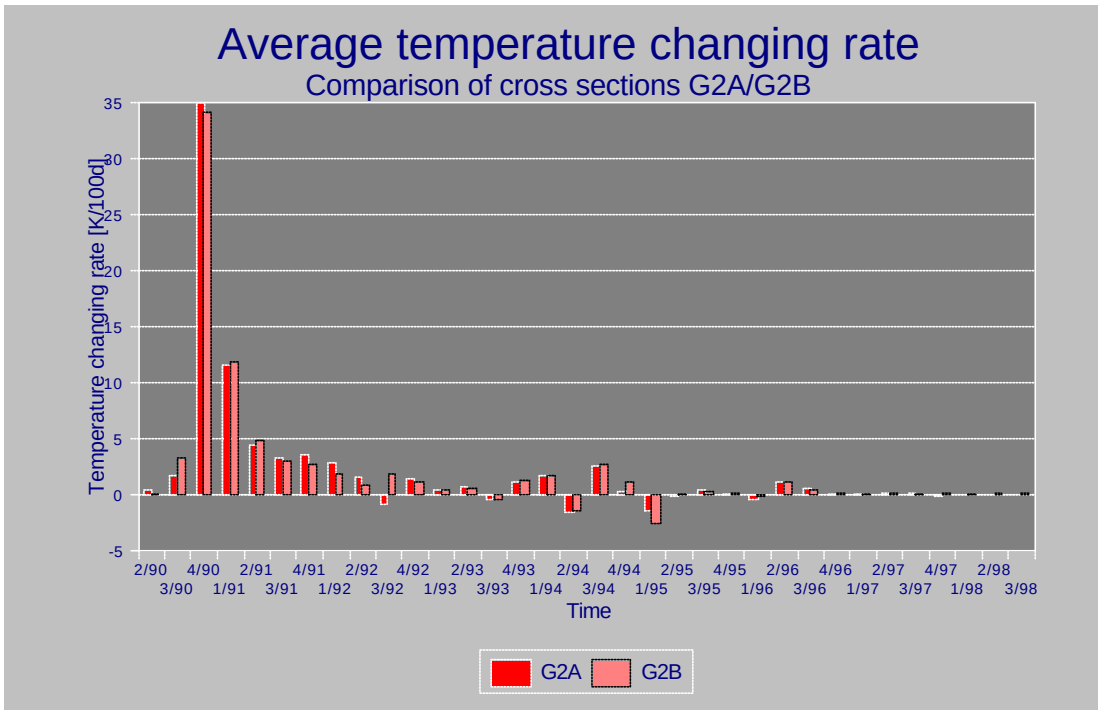

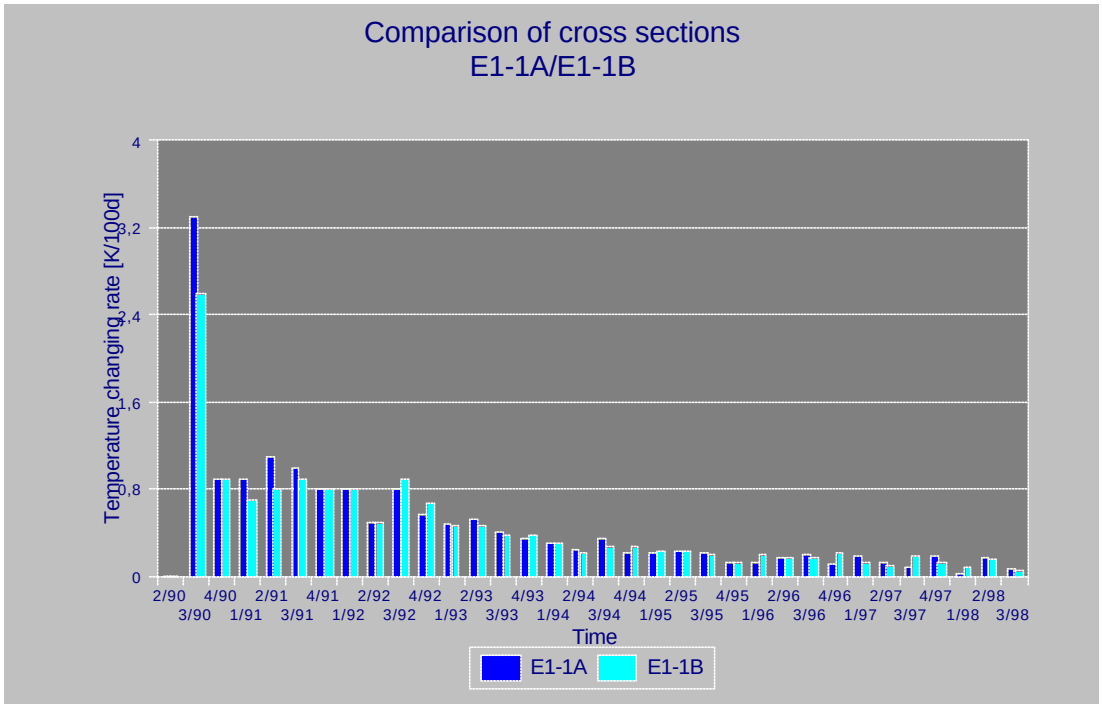

Fig. 8.5 Average temperature changing rates in the heated section G2 and the non-heated section E1[-1]

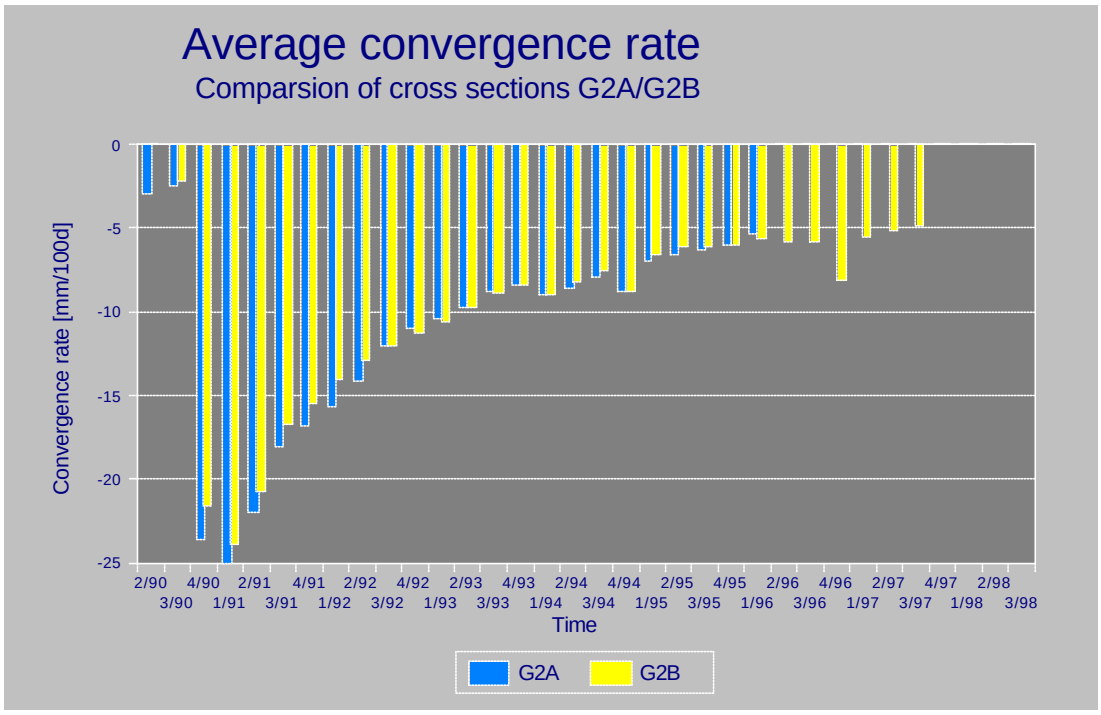

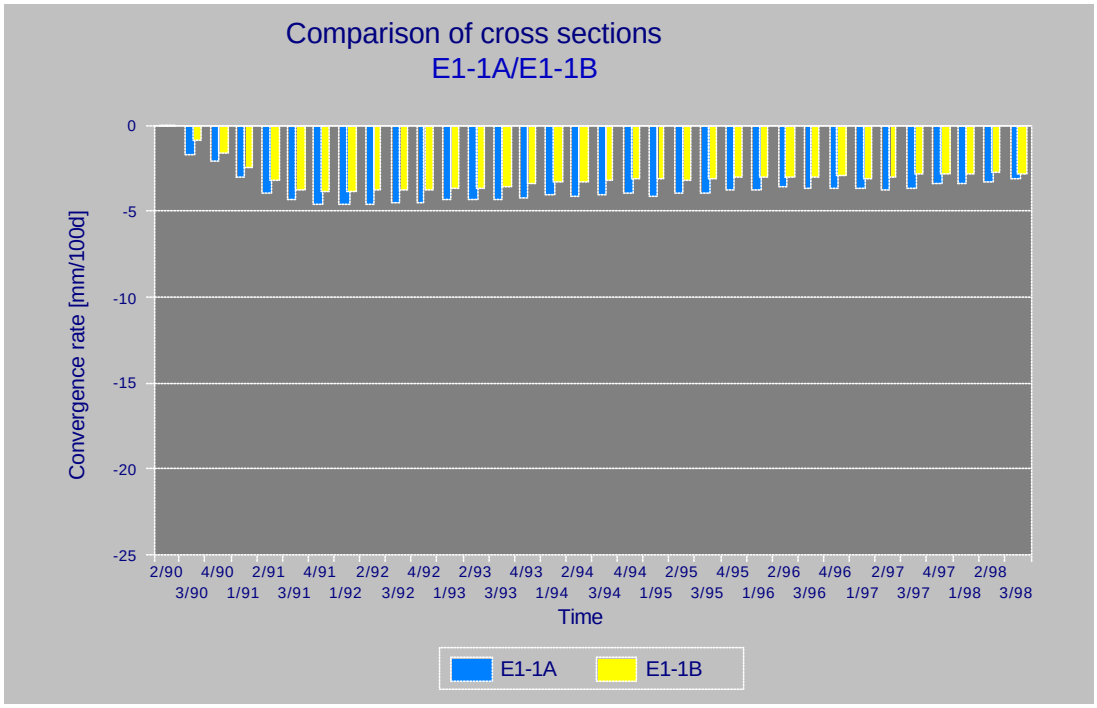

Fig. 8.6 Average convergence rates in the heated section G2 and the non-heated section E1[-1]

It can be stated that the measuring equipment was successfully tested under representative repository conditions. Neither the backfilling procedure nor temperatures up to 106°C had an impact on the tested sensors. But increasing backfill compaction caused damages at the measuring cables in the backfill and finally the failure of measuring systems. The data acquisition system operated without significant interruptions. Only some faulty multiplexer relays for pressure measurements at the front end processor MFA interfered with the tested sensors temporarily.

9 Summary

In the TSDE experiment, the thermomechanical processes in backfilled emplacement drifts and the surrounding rock salt were investigated under repository conditions. The in-situ test provided a lot of data regarding the temperature, deformation, and stress fields in a repository and the compaction behaviour of crushed salt backfill. Measurement results are available from a heating phase of over eight years followed by a cool-down phase of more than a year. The experimental data were compared with the numerical results of model calculations which were performed by the project partners (BGR, DBE, FZK-INE, ENRESA-CIMNE) to validate and further refine the existing thermal and thermomechanical computer codes. With these studies, the capability for predicting the long-term performance of a repository in rock salt was further improved.

Since the start of heating on September 25, 1990, the test performance was very satisfying. The electrical heaters operated more than 73,000 hours until the end of the heating phase on February 1, 1999 without the failing of a heating circuit. Several short power failures had no significant impact on the thermomechanical behaviour of rock and backfill.

Despite some equipment failures, the designed measuring gauges proved to be successful under extraordinary conditions and are recommended for the safety monitoring of a repository in rock salt. The data acquisition systems fitted the requirements as well. Most failures of measuring systems were caused by damaged measuring cables implying that the protection of the cables has to be improved. Furthermore, the realized multicore cables and the cable duct design are not recommended for in-situ measurements in the heated area.

At the surface of the heater casks, a maximum temperature of 210°C was reached after a few months. Because of the increasing thermal conductivity of the backfill, the temperatures decreased subsequently approaching steady state conditions around the heaters after three to five years of heating. With increasing distance from the heaters, a steady state was not reached until the end of the heating phase. After the heaters had been switched off, the temperatures decreased rapidly. At the end of March 2000, an almost uniform temperature distribution was recorded in the test field ranging from about 50°C in the heated area to about 45°C in the non-heated sections.

The temperature development in the test field was well predicted by thermal modelling as proved by the coincidence of experimental and calculation results.

Drift closure was accelerated considerably by heating, but drift closure rates and backfill compaction were lower than expected. Backfill porosity decreased from initially 35 % to 23 % in the heated area and to about 30 % in the non-heated regions. In 1998, a backfill permeability of at least 10^{-11} m^2 was determined by finite-difference calculations basing on the actual porosity of 25 %.

Primary settling of the backfill due to gravity induced the opening of a gap between the roof and the top of the backfill. In the heated area, the gap was closed very rapidly due to accelerated drift closure. In a final repository, the roof gap will probably not appear as primary settling of the backfill will be exceeded immediately by accelerated drift closure. After the closing of the gap in the heated area, mainly the upper part of the backfill was compacted at first. Subsequently, the lower part was increasingly involved, until the vertical distribution of backfill compaction was approximately balanced after two years of heating.

Rock displacements towards the test drifts were accelerated significantly by heating with the first and largest deformations occurring in the rock below the heater casks. From these measurements, it was concluded that vertical drift closure in the heated area was by two thirds composed of floor uplifting and only by one third of roof sinking. In horizontal direction, an approximately uniform closure can be assumed from both sides of the test drifts.

Backfill pressure increased continuously after the start of heating. At the roof, the average backfill pressure reached 3.3 MPa at the end of the heating phase, but this were only 27.5 % of the initial vertical stress which had been estimated at about 12 MPa in the test field region.

Long-term stress measurements in the heated area showed a significant increase in rock stress by up to 7 MPa after the start of heating. In the vicinity of the heater casks, these thermo-elastic stress changes reached maximum values after a few months, but then decreased continuously due to relaxation of the thermally induced stress by creeping of the rock salt. In the pillar, a steady stress state was observed since 1994. Farther away, the stresses increased slowly over a longer time reaching a maximum after a couple of years. Since 1996, the stresses were more or less constant until the end of the heating phase.

In 1997, the actual total stress in the heated host rock was determined by hydrofracturing measurements of BGR. The minimum principal rock stress was between 16 and 17 MPa which was considerably higher than the initial rock stress due to the significant increase in thermally induced stress during heating.

The most important gases analyzed in the backfilled drifts were hydrogen, methane, and carbon dioxide. Hydrogen was generated by corrosion of the heater casks, whereas methane and carbon dioxide were released from the backfill. Gas generation in the test field was moderate. However, it was not possible to quantify the total amount of gas which had been released as the gas was constantly diluted into the open access drift due to the high permeability of the backfill.

From humidity measurements, a total water content of 0.0003 – 0.0004 % (related to a backfill porosity of 25 %) was estimated for the heated backfill after eight years of heating. Considering the average water content in rock salt of about 0.1 %, the very low water content proved that the backfill had been dehydrated significantly by heating.

During heating, volatile organic compounds were released by thermal disintegration from the installed measuring equipment. A wide range of organic compounds was detected, but all values were below the limits prescribed by law for working conditions (MAK-values and TRT-values). During the dismantling of the experiment, acceptable working conditions can be assured if the excavated test drift is ventilated adequately.

The permeability of the excavation disturbed zone around the test drifts was determined at the end of the heating phase. The permeability values were in the order of 10^{-22} m^2 which corresponded to non-disturbed rock salt, thus indicating the healing of the excavation disturbed zone.

In summary, the data base on relevant processes in a final repository was significantly increased. The basic phenomena are qualitatively well understood allowing further extrapolations in space and time for repository performance assessments. Valuable experience for repository construction and operation was obtained, too. Nevertheless, the predicted degree of backfill compaction was not achieved. Deviations between experimental and calculation results were mostly quantitative, but indicated the requirement of further studies. The constitutive models for crushed salt and rock salt have to be improved. Furthermore, fully coupled three-dimensional thermomechanical analyses are necessary to simulate three-dimensional experimental conditions.

For a final assessment of its density distribution, the backfill will be recovered. Dismantling of the experiment will also allow to confirm the measurement results and to recover the measuring equipment for quality control. In a validation programme, instrument accuracy and reliability will be checked and representative sensors will be re-calibrated for a final evaluation of all experimental data. In future in-situ experiments, a post-test validation programme should be adopted already in the design phase for the necessary post-test confirmation of the experimental results.

List of References

/BEC 97/ Bechthold, W., Heusermann, S., Koß, S., Bollingerfehr, W., Manthee, F., Korthaus, E., Pudewills, A., Droste, J., Rothfuchs, T.: Thermal Simulation of Drift Emplacement (TSS), Summary of Interim Results. FZKA-PTE Nr. 4, Forschungszentrum Karlsruhe, 1997

/BEC 99/ Bechthold, W., Rothfuchs, T., Poley, A., Ghoreychi, M., Heusermann, S., Gens, A., Olivella, S.: Backfilling and Sealing of Underground Repositories for Radioactive Waste in Salt (BAMBUS Project), Final Report. EUR 19124 EN, CEC, Brussels, 1999

/CAL 95/ Callahan, G.D., Loken, M.C., Van Sambeek, L.L., Chen, R., Pfeifle, T.W., Nieland, J.D., Hansen, F.D.: Evaluation of Potential Crushed-Salt Constitutive Models. SAND95-2143, Albuquerque, 1995

/DRO 96/ Droste, J., Feddersen, H.-K., Rothfuchs, T., Zimmer, U.: The TSS Project: Thermal Simulation of Drift Emplacement, Final Report Phase 2. GRS-127, 128 S., GRS Braunschweig, 1996

/HEI 91/ Hein, H.-J.: Ein Stoffgesetz zur Beschreibung des thermomechanischen Verhaltens von Salzgranulat. Thesis, RWTH Aachen, 1991

/HEU 95/ Heusermann, S.: Analysis of Initial Rock Stress Measurements in Salt. Proc. 5th Int. Symp. on Numerical Models in Geomechanics, 669 – 674, Balkema, Rotterdam, 1995

/HEU 96/ Heusermann, S., Koss, S., Sönnke, J.: Analysis of Stress Measurements carried out in the TSDE test at the Asse Salt Mine. Proc. 4th Conference on the Mechanical Behaviour of Salt, Montreal, June 17-18, 1996

/HUN 94/ Hunsche, U., Schulze, O.: Das Kriechverhalten von Steinsalz. Kali und Steinsalz, Band 11, Heft 8 / 9, 238 - 255, Verlag Glückauf, Essen, 1994

/KOR 91/ Korthaus, E.: Thermische und thermomechanische Prognose-rechnungen zum TSS-Versuch (Thermische Simulation der Strecken-lagerung). Primärbericht KfK, 19.03.03 P 04A, 1991

/KOR 96/ Korthaus, E.: Consolidation and Deviatoric Deformation Behaviour of Dry Crushed Salt at Temperatures up to 150°C. Proc. 4th Conference on the Mechanical Behaviour of Salt, Montreal, June 17-18, 1996

/KOR 99/ Korthaus, E.: Consolidation Behaviour of Dry Crushed Salt: Triaxial Tests, Benchmark Exercise, and in situ Validation. Proc. 5th Conference on the Mechanical Behaviour of Salt, Bucharest, August 9-11, 1999

/LEI 68/ Leibholz, H.: Einführung in die Elastizitätstheorie. Reihe Wissenschaft und Technik, Verlag G. Braun, Karlsruhe, 1968

/MLY 97/ Müller-Lyda, I. (Ed.): Erzeugung und Verbleib von Gasen in einem Endlager für radioaktive Abfälle, GRS-Workshop vom 29 – 30. Mai 1996 in Braunschweig. GRS-129, GRS Braunschweig, 1997

/MLY 99/ Müller-Lyda, I., Birthler, H., Fein, E.: Ableitung von Permeabilitäts-Porositätsrelationen für Salgrus. GRS-148, 74 S., GRS Braunschweig, 1999

/OLI 93/ Olivella, S., Gens, A., Carrera, J., Alonso, E.: Behaviour of Porous Salt Aggregates. Constitutive and Field Equations for a Coupled Deformation, Brine, Gas and Heat Transport Model. Proc. 3rd Conference on the Mechanical Behaviour of Salt, Trans Tech. Pub., 1993

/PUD 97/ Pudewills, A.: Thermal Simulation of Drift Emplacement: Temperature Analyses. Topical Report, FZKA 5955, Forschungszentrum Karlsruhe, 1997

/PUD 98/ Pudewills, A.: Thermomechanical analysis of the TSS experiment. Proc. Int. Conference on Underground Construction in Modern Infrastructure, Stockholm, June 7-9, 1998 (Eds.: Franzén, Bergdahl & Nordmark), 317 – 323, Balkema, Rotterdam, 1998

/PUD 99/ Pudewills, A., Rothfuchs, T.: Thermomechanical Analyses for the TSS-Experiment and Comparison with in situ Measurements. Proc. 5th Conference on the Mechanical Behaviour of Salt, Bucharest, August 9-11, 1999

/ROT 99/ Rothfuchs, T., Feddersen, H.-K., Kröhn, K.-P., Miehe, R., Wieczorek, K., Poley, A.: The DEBORA-Project: Development of Borehole Seals for High-Level Radioactive Waste – Phase II, Final Report. GRS-161, 109 S., GRS Braunschweig, 1999

/SGE 97/ Schlumberger-Geoquest: Weltest 200 Technical Description, Longined BV, 1997

/SPI 88/ Spiers, C.J., Peach, C.J., Breskowsky, R.H., Schutjens, P.M.T.M., Liezenberg, J.L., Zwart, H.J.: Long-Term Rheological and Transport Properties of Dry and Wet Salt Rocks. EUR 11848 EN, CEC, Luxembourg, 1988

/STÜ 95/ Stührenberg, D., Zhang, C.: Results of Experiments on the Compaction and Permeability Behaviour of Crushed Salt. Proc. 5th Conference on Radioactive Waste Management and Environmental Remediation, Berlin, 1995

/TEST 93/ Testplan zum Demonstrationsversuch “Thermische Simulation der Streckenlagerung” im Salzbergwerk Asse (Revidierte Fassung). Hauptband Direkte Endlagerung, Kernforschungszentrum Karlsruhe, 1993

/WIE 98/ Wieczorek, K., Zimmer, U.: Untersuchungen zur Auflockerungszone um Hohlräume im Steinsalzgebirge, Abschlußbericht. GRS-A-2651, 86 S., GRS Braunschweig, 1998

/ZHA 93/ Zhang, C., Heemann, U., Schmidt, M.W., Staupendahl, G.: Constitutive Model for Description of the Compaction Behaviour of Crushed Salt Backfill. Proc. ISRM International Symposium, EUROCK 93, Lissabon, 1993

List of Figures

List of Tables

Gesellschaft für Anlagen- und Reaktorsicherheit (GRS) mbH

Schwertnergasse 1
50667 Köln
Telefon +49 221 2068-0
Telefax +49 221 2068-888

Forschungsinstitute
85748 Garching b. München
Telefon +49 89 32004-0
Telefax +49 89 32004-300

Kurfürstendamm 200
10719 Berlin
Telefon +49 30 88589-0
Telefax +49 30 88589-111

Theodor-Heuss-Straße 4
38122 Braunschweig
Telefon +49 531 8012-0
Telefax +49 531 8012-200

www.grs.de

ISBN 3-931995-40-2